

# THE QUANTUM HALL PROBLEM IN LATTICES

A Dissertation

Presented to the Faculty of the Graduate School  
of Cornell University

in Partial Fulfillment of the Requirements for the Degree of  
Doctor of Philosophy

by

Eliot Kapit

August 2012

© 2012 Eliot Kapit  
ALL RIGHTS RESERVED

# THE QUANTUM HALL PROBLEM IN LATTICES

Eliot Kapit, Ph.D.

Cornell University 2012

This thesis represents a body of work investigating the physics of strongly interacting quantum particles, confined to a two-dimensional plane in a nontrivial vector potential (such as a transverse magnetic field), commonly referred to as quantum Hall physics. The result which anchors these studies is my discovery, reported in 2010 (PRL **105**, 215303), of a lattice model in which there is a degenerate manifold of single-particle states, with wavefunctions matching those of the lowest Landau level of continuum particles, providing a bridge between continuum and lattice physics. Within this model anyonic states are robust and thus amenable to observation. Building on this result, I numerically demonstrate the braiding of anyons in many-body quantum Hall states of bosons, confirming their anyonic statistics. I also study the equation of state of quantum Hall bosons for various flux densities and choices of hopping parameters, with the goal of quantifying the effects of finite temperature and examining the feasibility of observing these states in a system of cold atoms. I then propose a new architecture for superconducting qubits, where flux states of circulating current combined with superconducting transformers and tuned voltage offsets mimic the physics of charged particles in a magnetic field, allowing boson quantum Hall physics to be studied in an environment free of charge noise. Finally, I review the work presented here and speculate on its possible applications to topological quantum computing.

## **BIOGRAPHICAL SKETCH**

Eliot Kapit graduated from Reed College in May of 2005 with a B.A. in physics. He was a finalist for the Apker award of the American Physical Society in 2005 and the Hertz Foundation graduate fellowship in 2006. He subsequently attended the University of Chicago from 2006-2007, where he was awarded a M.S. in physics. From there, he was admitted to the physics Ph.D. program at Cornell University. In 2008, he was awarded both the National Defense Science and Engineering and National Science Foundation graduate fellowships. He will receive his Ph.D. in Physics from Cornell in August of 2012, and from there he will move to Oxford University, where he will be a fellow of Worcester College and a postdoctoral researcher in the physics department.

## ACKNOWLEDGEMENTS

I would first like to thank the agencies which have supported me in my path through graduate school: the American Society of Engineering Education through the National Defense Science and Engineering Graduate Fellowship, the National Science Foundation through the NSF Graduate Fellowship Program, and of course, Cornell University. Without their support I could never have achieved the things that I did. I would also like to thank quite a few members of the Cornell Physics faculty. Piet Brouwer, Paul Ginsparg, Chris Henley, Andre LeClair, Kyle Shen, and most of all my advisor, Erich Mueller, I owe you all a great debt of gratitude for your guidance over the past five years. As well, to many of my friends in physics— alphabetically, Melina Blee, David Marsh, Gordan Krnjaic, Kendra Letchworth Weaver, Stefan Natu, Mike Schmidt, Nate Tompkins and Kassie Wells— you gave graduate school much of its color. To A. M. and J. T. M., I thank you for your support. And of course, I would not be here without twenty-nine years of love and support from my parents, Wynn and Laurie, and my brother Neil. Nor would life have been nearly as enjoyable without the company of close friends outside physics— Jane Calder, Danielle Cudmore, Ada Kurkowski, Tom and Abby McSweeney, and Zach Yuzwa. My time here was far more interesting for having known all of you.

Finally, I would like to thank my wife Eliza, who has loved and put up with me from the beginning of all this. There are no joys greater than you.

## TABLE OF CONTENTS

Biographical Sketch . . . . .	iii
Acknowledgements . . . . .	iv
Table of Contents . . . . .	v
List of Tables . . . . .	vii
List of Figures . . . . .	viii
<b>1 Introduction</b>	<b>1</b>
1.1 Quantum Hall Physics . . . . .	1
1.1.1 The Lowest Landau Level . . . . .	2
1.1.2 Towards a Quantum Hall State of Bosons . . . . .	9
1.1.3 Quantum Hall Bosons and the Lattice . . . . .	10
1.2 Artificial Gauge Fields in Cold Atoms . . . . .	11
1.2.1 Rotation . . . . .	12
1.2.2 Light-Assisted Hopping . . . . .	14
1.3 Superconducting Device Arrays . . . . .	16
1.3.1 Charge Qubit Lattice . . . . .	17
1.3.2 Flux Qubits . . . . .	20
1.4 Outline of this Dissertation . . . . .	20
<b>2 Parent Hamiltonian for the Quantum Hall States in a Lattice</b>	<b>22</b>
<b>3 Non-Abelian Braiding of Lattice Bosons</b>	<b>32</b>
3.1 Introduction . . . . .	32
3.2 Model . . . . .	33
3.3 Results . . . . .	36
3.4 Summary and Conclusions . . . . .	42
3.5 Acknowledgments . . . . .	43
<b>4 Equation of State of Quantum Hall Bosons in a Lattice</b>	<b>44</b>
4.1 Introduction . . . . .	44
4.2 Methods and Hamiltonian . . . . .	47
4.2.1 System Hamiltonian . . . . .	47
4.2.2 Local Density Approximation . . . . .	49
4.2.3 Many-Body States . . . . .	51
4.3 Results and Discussion . . . . .	54
4.3.1 Equation of State . . . . .	54
4.3.2 Total Entropy of the Trapped System . . . . .	59
4.4 Conclusions and Outlook . . . . .	62
4.5 Acknowledgments . . . . .	63

<b>5</b>	<b>A Vector Potential for Flux Qubits</b>	<b>64</b>
5.1	Introduction . . . . .	64
5.2	Three-Junction Flux Qubits . . . . .	66
5.3	Many-Ring Hamiltonian . . . . .	72
5.3.1	Transformer-Capacitor Coupling . . . . .	72
5.3.2	Interactions . . . . .	76
5.3.3	Constraints on $M$ . . . . .	77
5.3.4	Charge Noise . . . . .	80
5.3.5	Difference from the Aharonov-Casher Effect . . . . .	81
5.3.6	Two Dimensional Arrays and the Lowest Landau level . . . . .	84
5.4	Conclusion . . . . .	87
5.5	Acknowledgments . . . . .	87
<b>6</b>	<b>Conclusion</b>	<b>88</b>
6.1	Anyon Qubits . . . . .	88
6.1.1	Anyon Fusion and Ising Anyons . . . . .	88
6.1.2	Fibonacci Anyons . . . . .	92
6.1.3	Measuring a Non-Abelian Anyon Qubit . . . . .	94
6.2	Towards a <i>Quantum Loom</i> . . . . .	100
	<b>Bibliography</b>	<b>103</b>

## LIST OF TABLES

3.1	<p>The results of our numerical braiding studies. Here, <math>N</math> is the total particle number, <math>N_\phi</math> is the total number of flux quanta, and <math>N_{\text{imp}}</math> impurity sites have a repulsive potential applied. “GFS” refers to whether the degenerate pair of eigenstates are the ground (G), first excited (F) or second excited (S) states. The braids are each characterized by a unitary matrix with eigenvalues <math>e^{i\pi p_1}, e^{i\pi p_2} \rightarrow (p_1, p_2)</math>. The exchange paths are shown in Fig. 1, with <math>R_{ij}</math> denoting the exchange of impurities <math>i</math> and <math>j</math>. The algebras in the non-abelian cases approximate those described in the text [38, 50]; cases labeled as ambiguous contain non-commuting paths but the transformations associated with these paths depended on the details of the path and/or did not match the analytical predictions. Due to finite size splitting, not all paths were accessible on all lattices; only paths which led to a sensible braid and which were stable against small changes in the impurity strength <math>V_j</math> are quoted here. Hard core interactions (<math>U_2 = \infty</math>) were used in all cases except <math>4 \times 4^*</math>, where we also used (<math>U_2 = 0, U_3 = \infty</math>). These two interactions gave nearly identical results. . . . .</p>	39
5.1	<p>Hopping phases for different choices of contacts and offset voltages when a fluxon tunnels from ring <math>j</math> to ring <math>k</math> for a given <math> G </math>. The magnitude of each hopping term is identical. <math>G</math> is linearly proportional to the offset voltage <math>V_E</math>. A phase of zero corresponds to a hopping matrix element which is real and negative. .</p>	77

## LIST OF FIGURES

1.1	Schematic picture of light-assisted hopping as a source of an artificial vector potential. Through a 2-photon Raman process (black arrows), a pair of lasers promote particles to an excited hyperfine state $ e\rangle$ and then back down to the ground state with a net energy and momentum boost of $\pm V$ and $\pm \mathbf{k}_l$ . This allows the particle to hop along $x$ , and due to the energetic gain and loss from the Raman process, the tilt vanishes in the low-energy Hamiltonian. Since the momentum boost along $y$ depends on $x$ , the Raman process acts as an artificial magnetic field on the neutral atoms in the lattice. For visual clarity, the sinusoidal variation of the lattice potential along $y$ is not shown. . . . .	16
1.2	Unit cell for a charge qubit array. The superconducting grains (red) are small enough that their charging energy $E_C$ is larger than the Josephson coupling energies $E_J$ and $E'_J$ . If this is the case, fluctuations in the Cooper pair density $n_i$ are strongly suppressed, and occupation at each site is restricted to $n$ and $n + 1$ Cooper pairs. Since the states created and annihilated by $a_i^\dagger$ and $a_i$ are real Cooper pairs, the system's conductivity can be measured directly through standard methods. . . . .	19
2.1	(Color Online) All single particle eigenvalues for the hopping Hamiltonian in Eq. (2.1) with $\phi = 1/3$ on a $12 \times 12$ lattice with periodic boundary conditions. The index $n$ labels eigenvalues from smallest to largest. The dark blue points use hopping matrix elements given by Eq. (2.2), the light green points are the same model with only nearest and next nearest neighbor hopping, and the medium red points have only nearest neighbor hopping (the Hofstadter Hamiltonian). Energies are all measured in units of $t$ . The blue and green points are nearly indistinguishable. The lowest $1/3$ of the dark blue points are all degenerate. . . . .	27
2.2	First 100 eigenvalues for 4 particles on a $4 \times 4$ lattice with periodic boundary conditions, $\phi = 1/2$ , and hard core repulsion. The two states at $\epsilon = -4$ are Laughlin states (2.10); the degeneracy stems from the toroidal geometry. There is a distinct energy gap of $0.566t_{nn}$ to the lowest excited states, where $t_{nn}$ is the nearest neighbor hopping amplitude. . . . .	30

2.3	Schematic plot of $\langle n \rangle$ vs. $\mu$ , for lattice bosons described by the model given in Eqs. (2.1,2.2), with hard core interactions added. The steps correspond to incompressible fractional quantum Hall states commensurate to $\nu = 1/2$ . This structure will be visible in the density profile of a trapped gas. In the presence of finite (but large) local repulsion this same structure will repeat between each of the Mott plateaus. Similar structure will be seen with Fermions, but with plateaus at fillings with odd denominators. . . . .	31
3.1	(Color online) (a)–(c) Exchange paths used to braid quasiparticles on various lattices. In each path, the impurities (shaded red) are incrementally moved along the segments (1,2,3...) until they return to their starting positions, exchanged. The dashed box represents the periodic lattice boundary. (d)–(i) show the initial configurations of the impurities for the 3- and 4- impurity braids.	38
4.1	Eigenvalues of the Gaussian hopping model (4.4) as a function of $\phi$ for $J_{NN} = t$ . The energies diverge as $\phi$ approaches 1 since the hopping amplitudes become infinite-ranged in this limit. The lower band is an exactly degenerate LLL and contains $\phi L_x L_y$ degenerate states on an $L_x \times L_y$ lattice. The excited bands are qualitatively similar to the fractal bands of the nearest neighbor (Hofstadter) model, and are analogous to the excited Landau levels of the continuum problem, albeit without the exact degeneracy of the continuum Landau levels. The gap from the lowest Landau level to the first excited band scales linearly with $\phi$ for small $\phi$ , but by $\phi = 1/4$ it is approximately constant, increasing by only $\sim 14\%$ from $\phi = 1/4$ to $\phi = 1/2$ . Beyond $\phi = 1/2$ , it increases and eventually diverges as the hopping becomes infinite ranged. . . . .	50
4.2	(Color online) The effect of temperature on the equation of state for a $4 \times 4$ lattice with 8 fluxes using Gaussian hopping parameters. The curves for the $4 \times 4$ lattice were calculated for the Gaussian hopping model for $T = \{0.01, 0.05, 0.25\} J_{NN}$ (blue, purple, gold) and demonstrate the effect of temperature on the observability of the plateaus in $\partial \langle n \rangle / \partial \mu$ . While the signatures of the plateaus at $T = 0.25 J_{NN}$ are difficult to discern by eye, traces of the $\nu = 1/2$ plateaus are visible as weak local minima in $\partial n / \partial \mu$ . . . . .	55

- 4.3 (Color online) The effect of hopping parameter choices on the equation of state, demonstrated in a  $5 \times 4$  lattice with 6 fluxes for  $T \rightarrow 0$ . The three choices of hopping parameters are Gaussian (blue), NN and NNN (purple), and NN only (gold). The increased plateau width for longer-ranged hopping is clearly apparent. For larger fluxes ( $\phi \sim 1/2$ ) additional terms beyond NNN hopping must be included to match the Gaussian model results. 55
- 4.4 (Color online) (a,b) Plateau widths vs  $\phi$  at  $\nu = 1/2$  (a) and  $\nu = 1$  (b) vs  $N_\phi$  for various lattice sizes. Blue circles correspond to the Gaussian hopping model, purple squares to NN and NNN hopping, and gold diamonds to the Hofstadter model. These widths are extracted by finding the width in  $\mu$  for which  $\partial n/\partial\mu$  vanishes as  $T \rightarrow 0$ . Anomalously large gaps at  $\nu = 1$  occurred when the flux was commensurate and could indicate competition from charge density wave order. Due to the small system sizes studied, density correlations are insufficient to separate charge density wave states with long-range order from fractional quantum Hall liquids with short-ranged antiferromagnetic correlations. Longer ranged hopping increases  $W$  in every case at  $\nu = 1/2$  and in most cases at  $\nu = 1$ . At lower fluxes, the NNN and Gaussian results were nearly identical. (c) Scatter plot of all plateaus observed in our calculations, as a function of  $\nu$ . Gaps tend to decrease with increasing  $\nu$ . Most of the filling fractions shown (such as  $\nu = 3/4$  or  $5/4$ ) are likely to be abelian composite fermion states [97]; the states at  $\nu = 1$  and  $3/2$  are likely to be non-abelian. . . . . 57
- 4.5 (Color online) (a,b) Trap-averaged entropy per particle as a function of  $k_B T$  for  $\phi = 3/10$  (a, calculated on a  $5 \times 4$  lattice) and  $\phi = 4/9$  (b, calculated on a  $6 \times 3$  lattice). The blue curve corresponds to the Gaussian hopping model, the purple to NN and NNN hopping, and the gold to the Hofstadter model. (c) Radial density (blue), compressibility ( $\partial n/\partial\mu$ , purple) and entropy density (gold) as a function of radial coordinate  $r$  for the Gaussian hopping model with  $\mu(r) = (3.3 - 0.0028r^2)J_{NN}$  and  $k_B T = 0.15J_{NN}$ . Due to the finite system temperature,  $\partial n/\partial\mu$  does not vanish, but it does exhibit local minima at the appropriate rational filling fractions. . . 61

- 5.1 Single flux qubit, without any circuitry to connect it to its neighbors. The center Josephson junction has its Josephson energy and capacitance scaled by the parameter  $\alpha$  relative to the equivalent parameters in the other two junctions;  $\alpha$  is typically in the range of 0.6-0.8. The capacitances  $\kappa C$  are used to apply an external voltage  $V_E$  to generate phases when the rings are coupled, and  $\kappa$  is  $O(1)$ . The capacitances  $\gamma C$ , on the other hand, represent the passive coupling to stray charge noise in the environment, and in a typical flux qubit,  $\gamma \sim 10^{-2}$ . Since  $\gamma \ll \kappa$  we neglect these terms in our calculations. A magnetic flux  $f\Phi_0$  penetrates the ring, and if  $f \neq 1/2$  or zero time-reversal symmetry is broken. The phases  $\phi_1$  and  $\phi_2$  of the superconducting regions (1) and (2) are the two degrees of freedom of the qubit, and the bottom of the ring is chosen to be  $\phi = 0$  and held at voltage  $V_0$ . . . . . 68
- 5.2 Eigenstates of (5.4), with plots of the potential in the bottom row. In the top row,  $|\psi(\phi_1, \phi_2)|^2$  is plotted for the ground state  $|0\rangle$  (left) and the first excited state  $|1\rangle$  (right) for  $E_J = 40E_C$ ,  $\alpha = 0.75$ ,  $\kappa = 1$  and  $f = 0.515$ . In this regime the potential has two minima (with different energies, since  $f \neq 1/2$ ), and  $|0\rangle$  and  $|1\rangle$  are concentrated in them with little overlap. Due to the large potential barrier separating them, the tunneling matrix elements in this regime are exponentially suppressed with  $J_{jk} \propto \exp -c\sqrt{E_J/E_C}$  for some  $c$  dependent on  $f$  and  $\alpha$ . In contrast, in the middle row the same quantities are plotted for  $|0\rangle$  and  $|1\rangle$  when  $f = 0.54$  and the potential has a single (asymmetric) minimum and the overlap in  $|\psi(\phi_1, \phi_2)|^2$  between the wavefunctions is appreciable.  $J_{jk}$  is no longer exponentially suppressed and is 2 orders of magnitude larger in this regime, but it is difficult measure the state of the qubit by measuring the current  $I_c \sin \phi_1$ . On the bottom row, the potential terms in (5.4) are plotted for  $f = 0.515$  on the left and  $f = 0.54$  on the right. . . . . 69

5.3	<p>Flux qubit array. (a) Schematic circuit diagram. The lattice unit cell consists of a single superconducting ring interrupted by three Josephson junctions, with <math>E_J</math> and <math>C</math> labeled in the figure. The phases of regions in (1) and (2) are taken to be the two degrees of freedom in each ring, and each is broken up by a transformer <math>M</math>, which is shorted across the top so the voltage at the coupling capacitors <math>gC</math> is given by <math>V_i - M\partial I_i/\partial t</math>, where <math>I_i</math> is the current through the Josephson junction to the bottom half of the ring. The applied voltages <math>V_E</math> alternate down the array. The rings discussed in the text are labeled <math>j</math> and <math>k</math>. (b) One possible arrangement of wires which realizes the transformer-capacitor coupling. This scheme can be generalized to 2d arrays as well, provided that the voltages and geometries of the contacts are chosen appropriately. If <math>r \ll a</math> and <math>r \ll r'</math>, the mutual inductance <math>M</math> is given by <math>M = (\mu_0/2\pi) \left( r - \sqrt{a^2 + r^2} + a \tanh^{-1} \frac{a}{\sqrt{a^2 + r^2}} \right)</math>. The phase generated in this arrangement will be <math>\varphi + \pi</math> as detailed in table 5.1. . . . .</p>	71
5.4	<p>Clockwise from top: <math>\omega</math> in GHz, <math>\delta I = \langle 1   \sin \phi_1   1 \rangle - \langle 0   \sin \phi_1   0 \rangle</math> and <math>\delta \phi^2</math> for state <math> 1\rangle</math>, as functions of <math>\alpha</math> and <math>f</math>. These values were calculated for <math>E_J = 200\text{GHz}</math>, <math>E_C = 5\text{GHz}</math> and <math>\kappa = 1</math>. Note that most of the plot range falls outside of the double minimum regime in the potential. . . . .</p>	78
5.5	<p>Left to right: <math>J_{jk}</math> and the nearest neighbor energy shift <math>U_{jk} = 8gE_C (1 + \kappa)^2 (1 + 2\alpha + \kappa)^{-2} G^2 \times \langle 1   \cos \phi_1   1 \rangle (\langle 1   \cos \phi_1   1 \rangle - \langle 0   \cos \phi_1   0 \rangle)</math>, both in GHz, as functions of <math>f</math> and <math>\alpha</math> for <math>G = 0.8\pi</math>, <math>g = 0.1</math>, <math>E_J = 200\text{GHz}</math>, <math>E_C = 5\text{GHz}</math> and <math>\kappa = 1</math>. The hopping phase is approximately <math>\pi/4</math> for this choice of <math>G</math>. . . . .</p>	79
5.6	<p>Schematic arrangement of additional transformer-capacitor couplings which cancels the interaction term (5.14) generated by the primary coupling. The transformers on the lower right (between region 2 and the constant voltage source <math>V_0</math>) side of each ring are reversed relative to the other transformers in each ring, flipping the sign of their voltage shifts. Changing the magnitudes of <math>M</math> or <math>g</math> in the lower couplings, or changing the arrangement of the transformers, will produce different nearest neighbor interaction potentials. . . . .</p>	79

- 5.7 Analogy between the artificial vector potential in our flux qubit arrangement and the Aharonov-Casher effect. In (a) the flux qubits are arranged with identical applied voltages  $V_E$  so that tunneling a fluxon around the ring accumulates a nonzero phase  $\varphi$ . The voltage shifts are equivalent to placing a point charge in the center of the ring. In (b), a physical dipole  $\mathbf{m}$  pointing out of the page encircles a point charge  $q$ , also accumulating a phase  $\varphi$  in making a complete loop. It is important to note that, while the hopping phases in (5.13) are structurally similar to the Aharonov-Casher phases, they do not arise from that effect, as detailed in the text. . . . . 82
- 5.8 A 2d array configuration which would lead to a uniform effective gauge flux of  $1/4$  quanta per plaquette (a net phase of  $\pi/2$  accumulated for encircling a plaquette by moving counterclockwise). The links between rings above or below each other are connected to the inner side of each transformer so pick up no voltage shifts or complex phases. Here  $V_0 = 0$  and the applied voltage  $V_E$  alternates appropriately to ensure that a step to the right yields the phase indicated along the side of each row. By noting that  $\langle \psi | \exp iG \sin \phi_1 | \psi \rangle = \langle \psi | \exp -iG \sin \phi_2 | \psi \rangle$  and  $G \propto V_E$ , we see that  $\varphi = \pi/2$  for motion around any plaquette in this lattice. Next nearest neighbor contacts can also be added, but are not shown here for simplicity. . . . . 86

6.1 Schematic configuration for measuring the statistics of the anyons, adapted from [101, 13, 51, 14, 135, 121]. Particles are forbidden from hopping to the black sites (either due to the sites being physically removed from the array or due to large local repulsive potentials applied at them) and the gray triangles labeled 1-4 are external contacts; in the experiment, a “voltage” (real voltage for electrons and Cooper pairs, a magnetic field shift for fluxons) is applied between contacts 3 and 4 to induce a chiral edge current of quasiparticles from contact 4 to contact 3. The edge quasiparticles are able to tunnel through the narrow constrictions with amplitudes  $t_1$  and  $t_2$ , and as a consequence a voltage is induced between contacts 1 and 2, yielding a finite longitudinal conductivity  $\sigma_{xx}$  (which would be zero were the constrictions absent). The sites shaded red represent the path that ends with tunneling across the  $t_1$  constriction, the sites shaded blue represent the paths which either tunnel through  $t_2$  or exit the system at contact 3, and the sites shaded pink represent the path which includes interfering contributions from the red and blue paths. As argued in the text, one can determine the statistics of the anyons by studying the response of  $\sigma_{xx}$  to changes in the quasiparticle content or flux density of the region between the two constrictions. If the constrictions are removed, the longitudinal conductivity  $\sigma_{xx}$  vanishes and the quantization of the transverse conductivity  $\sigma_{xy}$  can be observed. . . . .

# CHAPTER 1

## INTRODUCTION

### 1.1 Quantum Hall Physics

This dissertation studies the quantum properties of identical particles confined to a plane in a transverse magnetic field, commonly known as quantum Hall physics. This nomenclature comes from the classical Hall effect, the generation of a transverse voltage in conductors in crossed electric and magnetic fields. It was discovered by Edwin Hall in 1879. This voltage, which arises from the accumulation of charges due to the bending of the charge carriers' paths from the magnetic field, can be used to define a transverse electrical conductivity,  $\sigma_{xy}$ , the ratio of the applied current to the generated transverse (Hall) voltage  $I/V_H$ .

First discovered by Klaus von Klitzing in 1980 (just after the hundredth anniversary of Edwin Hall's discovery) [130], the quantum Hall effect (QHE) is an exact quantization of this conductivity in clean, two-dimensional electron gases at extremely low temperatures, into integer or rational fractional multiples of  $e^2/h$  depending on the carrier density and magnetic field strength. The precise value of  $\sigma_{xy}$  is given by  $\nu e^2/h$ , where the coefficient  $\nu$  is referred to as the filling fraction and is the dimensionless ratio of the carrier density to the density of magnetic flux quanta penetrating the sample. This quantization is so exact that the QHE is used to define the international standard for electrical resistance from Planck's constant and the electron charge. Beyond this incredible precision, the quantum Hall states at fractional values of  $\nu$  exhibit a number of exotic properties, the most famous of which being that the fundamental excitations of these states are emergent *anyons*, collective vortices which carry an

exact fraction of an electron charge. These anyonic systems represent a state of matter profoundly unlike any others discovered previously, thus making them one of the most important areas of condensed matter research in the past three decades. As I shall describe below, they may turn out to be important from a practical and technological vantage point as well.

As background, I will begin with a brief overview of quantum Hall physics, focusing on important theoretical aspects of the problem and describing some of the methods used to study it. After that review, I will describe attempts to realize this physics in other systems (particularly bosonic ones), beginning with cold atoms and then moving to superconducting device arrays. I will then conclude this chapter with an outline of the four papers that make up the bulk of this dissertation.

### 1.1.1 The Lowest Landau Level

A truly remarkable fact about the quantum Hall effect is how strongly the *many*-particle physics of the interacting electrons depends on the *single* particle spectrum of two-dimensional charged particles in quantum mechanics, known as the Landau levels. Since the structure of the Landau levels is important to all of my subsequent work, we will quickly review it here before proceeding. We first consider a single particle, placed in a plane. The Hamiltonian for this particle is

$$H = \frac{1}{2m} (\mathbf{p} - e\mathbf{A}/c)^2, \quad (1.1)$$

where  $\mathbf{p} = -i\hbar\partial/\partial\mathbf{x}$  is the particle's momentum and  $\mathbf{A}$  is the magnetic vector potential, which satisfies  $\mathbf{B} = \nabla \times \mathbf{A}$ . Since this equation does not have a unique solution,  $\mathbf{A}$  is defined only up to a gauge transformation  $\mathbf{A} \rightarrow \mathbf{A} + \nabla f(\mathbf{r})$ , where

$f$  is any real, continuously differentiable scalar function of  $\mathbf{r}$ . Clever choice of this gauge can massively simplify the desired calculation, and for most of this work we will choose the “symmetric gauge” where

$$\mathbf{A} = \frac{B}{2} (y\hat{x} - x\hat{y}). \quad (1.2)$$

This vector potential describes a constant magnetic field  $\mathbf{B} = B\hat{z}$  which points normal to the plane, and will be the gauge of choice for this section.

We now define complex coordinates  $z = x + iy$  and  $z^* = x - iy$  and let  $l_B = \sqrt{\hbar c/eB}$  be the magnetic length scale.  $H$  can be decomposed as:

$$a = 2\frac{\partial}{\partial z^*} + \frac{z}{2l_B^2}; \quad b = 2\frac{\partial}{\partial z} - \frac{z^*}{2l_B^2}; \quad (1.3)$$

$$H = -\frac{\hbar^2}{2m}ba + \frac{1}{2}\hbar\omega_c, \quad (1.4)$$

where  $\omega_c = eB/m$  is the particle’s cyclotron frequency. We note that  $[H, b] = \hbar\omega_c b$ , so  $b$  can be regarded as a ladder operator. The ground states of  $H$  are thus any functions annihilated by the operator  $a$ , and (ignoring normalization) are given by

$$\psi_n(z) = z^n \exp\left(-\frac{|z|^2}{4l_B^2}\right). \quad (1.5)$$

The states  $\psi_n$  are the lowest Landau level (LLL) wavefunctions, and form an exact, massively degenerate level since any power of  $z$  multiplied by the gaussian factor is a ground state of  $H$ . The excited states can be found by simply acting with powers of  $b$  on the LLL wavefunctions, and each excited level has the same degeneracy as the LLL. For an infinite system this degeneracy is infinite, and for a finite system the degeneracy is equal to  $N_\phi$ , where  $N_\phi = 2^{-1}\Phi_0^{-1} \int \mathbf{B} \cdot d\mathbf{S}$  is the total magnetic flux penetrating the system divided by twice the magnetic flux quantum  $\Phi_0 = h/2e$ . We choose  $N_\phi$  to be an integer in all subsequent calcula-

tions, and in periodic systems  $N_\phi$  must be an integer for the boundary conditions to be well-defined. To avoid confusion, we specify the flux quantum as  $h/2e$  rather than  $h/e$  since we will be concerned with superconducting systems later in this work. For a finite disc geometry, this degeneracy sets the highest power of  $n$  of  $z^n$  as  $N_\phi - 1$ . In a toroidal geometry (periodic boundary conditions), the LLL is expressed in terms of Jacobi theta functions [45, 1], with the degeneracy unchanged. The reduction to 2 dimensions is typically accomplished in experiments through the use of quantum wells— ultrathin sheets of a material (typically gallium arsenide) sandwiched between two insulators with a large band gap. If the well width  $w$  is thin enough, the excitation frequency  $\omega_z = \hbar^2 \pi^2 / 2m^* w^2$  can be made much larger than the Landau level spacing, so the effect of the third dimension can be ignored outside of possible renormalization of the interaction matrix elements.

The structure of the LLL allows for a number of striking analytical predictions which would be nearly impossible to make for other single particle spectra. Firstly, given the finite integer spacing of the Landau levels and infinite density of states, one would expect the 2DEG to be a band insulator, except when the chemical potential is precisely equal to an integer multiple of  $\hbar\omega_c$ . While it is true that the bulk conductivity does vanish when  $\mu \neq \hbar\omega_c$ , the *edge* conductivity is nonzero, leading to an exactly quantized transverse conductivity  $\sigma_{xy} = \nu e^2/h$  from chiral edge states at zero temperature. First derived by Thouless [124], employing the Kubo formula to compute the transverse conductivity yields an expression proportional to

$$\sigma_{xy} \propto \frac{i}{2\pi} \int dk_1 dk_2 \left[ \left\langle \frac{\partial \psi}{\partial k_1} \left| \frac{\partial \psi}{\partial k_2} \right\rangle - \left\langle \frac{\partial \psi}{\partial k_2} \left| \frac{\partial \psi}{\partial k_1} \right\rangle \right]. \quad (1.6)$$

This is nothing more than the momentum space integral of the Berry curvature [137] over the entire Brillouin zone, and given that the system's wavefunc-

tion is single-valued, it must be an integer, called the Chern number. At finite temperature, there will be an exponentially small longitudinal conductivity  $\sigma_{xx} \propto \exp -\hbar\omega_c/k_B T$  as well, due to a nonzero population in the excited bands.

This result is also robust against impurities. Provided that enough available states remain in the LLL (see below), a quantum Hall system can always completely screen static, short-ranged repulsive impurity potentials at nearly zero energy cost. Consider an impurity placed at complex position  $w$ . We assume that the impurity interacts with the electrons through contact repulsion, so that the impurity potential is  $U_{\text{imp}}\delta^2(z-w)$ . To screen the impurity potential, we simply modify the many-body wavefunction by

$$\Psi(\{z_j\}) \rightarrow \prod_i (z_i - w) \Psi(\{z_j\}). \quad (1.7)$$

This wavefunction now vanishes whenever any particle contacts the impurity, and therefore has no energy shift from the impurity potential. Since it is constructed only from single particle states in the LLL, it is a valid ground state. The common terminology for these states is to say that the new state has a *quasihole* at position  $w$ . A quasihole is a quantized vortex which threads a single quantum of flux and has vanishing fluid density at its core. Generically, quasiholes (and their conjugates, quasiparticles) are a fundamental excitation of any many-body quantum Hall state, and for fractional states ( $\nu$  non-integer; see below) they are anyons with fractional statistics and charge [66]. In the many-body system with a random distribution of attractive and repulsive impurities, the Landau levels will be broadened slightly by the impurity scattering rate, but so long as the chemical potential  $\mu$  remains in the gap between them, the conductivity quantization argument of the previous paragraph still holds and the transverse conductivity is exactly quantized, up to exponentially small corrections from finite

temperature.<sup>1</sup> It is also important to note that if the impurity position  $w$  is controllable, quasiholes can be moved simply by changing  $w$ . This process, called braiding when multiple quasiholes are present, is the primary focus of chapter 3.

The exact degeneracy of the LLL also makes it easy to construct exact or variational ground states for the interacting many-body problem. Though our previous discussion mainly referred to fermionic states, let us now consider a quantum Hall system of bosons with mass  $m$  and charge  $q$ , interacting through a contact interaction. The grand canonical Hamiltonian is

$$H = \frac{1}{2m} \sum_i (\mathbf{p}_i - q\mathbf{A}_i/c)^2 + U \sum_{ij} \delta^2(\mathbf{r}_i - \mathbf{r}_j) - \mu N \quad (1.8)$$

Imagine that we have a group of  $N$  bosons in a circular region penetrated by a total of  $N_\phi$  flux quanta. Remarkably, if  $N \leq N_\phi/2$ , the ground states of this system are known exactly, and further, the system is compressible up to  $N = N_\phi/2 - 1$  but gapped when  $N = N_\phi/2$ . As proof, we first require all of the particles to occupy LLL states. Within this restriction, the ground state will be a polynomial in the complex particle coordinates  $z_j$ , and that the maximum degree of any coordinate in the polynomial is  $N_\phi - 1$ , as described in the discussion of the single particle LLL states earlier in the chapter. Further, we require that the polynomial is homogeneous, so that for any given component of the polynomial  $z_1^{n_1} z_2^{n_2} \dots z_N^{n_N}$  the sum of all powers  $n_i$  must be constant. With these requirements laid down, we consider the case of  $N = N_\phi/2$ , a filling fraction of  $\nu = 1/2$ . The ground state is

---

<sup>1</sup>It is important to note that a finite population of impurities is actually required to observe the QHE in an experiment, since the chemical potential would otherwise undergo discontinuous jumps and have an essentially zero probability of sitting between Landau levels. The impurities create a manifold of localized states in between the Landau levels, which allow the chemical potential to sit between Landau levels without contributing to conductivity. However, a large enough population of impurities will disrupt the formation of the more complicated fractional states discussed below, so ultrapure samples are required for most FQHE experiments.

unique and exactly given by the Laughlin state, which for bosons at  $\nu = 1/2$  is

$$\Psi(\{z_j\}) = \prod_{i < j} (z_i - z_j)^2 \exp -\frac{1}{4l_B^2} \sum_i |z_i|^2. \quad (1.9)$$

This wavefunction is a ground state of the system, since all of the particles are in the LLL and the wavefunction vanishes whenever two particles coincide, thus completely suppressing the contact interaction in (1.8). To see that it is the unique ground state, we note that any change in the wavefunction consistent with bose statistics must involve adding or removing even powers of  $(z_i - z_j)$ , since any terms involving  $z_i^*$  involve promotion into excited Landau levels and cost a finite energy  $\hbar\omega_c$ . Removing even powers of  $(z_i - z_j)$  costs energy, however, since the interaction energy no longer vanishes, but *adding* powers of  $(z_i - z_j)$  is also forbidden, since the highest allowed power of  $z_i$  in a LLL wavefunction is  $N_\phi - 1$ . The Laughlin state is therefore unique and gapped. Similarly, for  $N < N_\phi/2 - 1$  an exact ground state can be found by multiplying (1.9) by a symmetric polynomial in  $z_i$  of appropriate degree, so the wavefunction is no longer unique and particles can be added without any interaction energy cost. For longer ranged interactions, (1.9) is still an excellent variational ground state (for fermions interacting through Coulomb repulsion—the longest ranged interaction between fundamental particles—the fermionic Laughlin state at  $\nu = 1/3$  has better than 97% overlap with the numerical ground state [141]) and the system remains gapped. Note that a gapped state in bosons indicates strong correlation physics—since bosons cannot fill a Landau level, there will be no integer quantum Hall effect as in the fermionic 2DEG.

Much of the theoretical knowledge we have of many-body quantum Hall states comes from exact diagonalization studies, where the low-lying eigenvectors and eigenvalues of a many-body Hamiltonian such as (1.8) are computed numerically for small numbers of particles in a finite region. Exact diagonal-

ization is popular for two reasons: First, other techniques, such as perturbation theory or quantum Monte Carlo, are inapplicable; there is no small parameter to perturbatively expand in, and the gauge field leads to a sign problem in Monte Carlo. Second, the large spacing between Landau levels dramatically simplifies the exact diagonalization calculation. Provided that the particle density is not too large, one can assume that all particles are in the LLL (a technique referred to as lowest Landau level projection), which reduces the problem to one of finding the appropriate polynomial in  $z_i$  which minimizes the interaction potential. This is equivalent to finding the lowest eigenstates of the Hamiltonian:

$$H_{LLL} = \sum_{ijkl}^{N_\phi-1} V_{ijkl} a_i^\dagger a_j^\dagger a_k a_l, \quad V_{ijkl} = \langle ij | H_{int} | kl \rangle \quad (1.10)$$

where  $i, j, k, l$  are single particle eigenstates in the LLL. The interaction coefficients  $V_{ijkl}$  for arbitrary interactions must be found numerically, though by decomposing them into angular momentum channels analytical results can be employed to dramatically simplify the calculation. LLL projected exact diagonalization an ideal tool to test the validity of trial wavefunctions such as (1.9); these trial wavefunctions include complex paired states with non-abelian anyon excitations– the subject of my study in chapter 3. Though I do not use LLL projection in this work (it is less necessary in lattice systems, and many of the systems I study are strongly interacting and relatively dense), the analytical insights which have come from it have guided much of my work, and I will refer frequently to them throughout. Exact diagonalization is also my tool of choice for understanding many-body states when analytical methods have failed, and forms the bulk of my calculations in chapters 3 and 4.

Non-abelian anyons [82] are fractional excitations where the wavefunction for three or more anyons is degenerate, and adiabatic exchanges of two anyons

produces a nontrivial rotation in this degenerate subspace. Generically, different exchanges do not commute, so repeated exchanges of anyons (referred to as braids) can be used to construct complicated unitary transformations. Anyonic braiding is the subject of the third chapter of this work, so I won't discuss it in detail here, except to say that non-abelian anyons could be used to build a noise-tolerant topological quantum computer [61]. So long as the anyons are sufficiently far apart, the degeneracy associated with them will not be lifted by local perturbations unless those perturbations are strong enough to create additional anyon-antianyon pairs. If the ground state is gapped, this energy cost is finite and all noise below it is exponentially suppressed, providing a profound degree of protection against decoherence from external noise sources.

### **1.1.2 Towards a Quantum Hall State of Bosons**

The only experimentally observed examples of quantum Hall effects are two dimensional electron gases confined in ultrapure GaAs quantum wells or single layers of graphene. In particular, no bosonic quantum Hall system has yet been realized, for the simple reason that it is extremely difficult to construct a system of charged, planar bosons in a strong magnetic field. The bosonic quantum fluids studied in condensed matter experiments are either electrically neutral (Helium-4) or expel magnetic flux (Cooper pairs in a superconductor), and trapped ions are untenable since complex magnetic field configurations are necessary for the trap itself. This is an unfortunate state of affairs, since beyond natural academic interest, there is a deep technological reason to search for quantum Hall bosons: non-abelian anyons and topological quantum com-

puting.<sup>2</sup>

As I show in chapter 3, and as argued previously [95, 24, 82], the bosonic quantum Hall states at  $\nu = 1$  and  $\nu = 3/2$  exhibit non-abelian anyon excitations. Taking this as sufficient motivation to search for a bosonic quantum Hall system, I will now describe some of the most promising candidates. These include arrays of superconducting qubits (where two states of the qubit can act the presence or absence of a hard core boson) [131, 28, 85], “photon lattices” of coupled optical waveguides [42, 127] and neutral cold atoms, [10] where an effective magnetic field may be introduced through rotation [24, 100, 21, 120, 136, 36] or more exotic means [81, 43, 71, 109, 72, 22, 4, 25]. I will shortly describe some of these systems, focusing on cold atoms (studied in chapters 2, 3 and 4) and superconducting device arrays (chapters 3 and 5). I will detail the advantages and disadvantages of these systems for quantum Hall physics, and discuss the experimental challenges inherent in building them.

### 1.1.3 Quantum Hall Bosons and the Lattice

As I will describe, many of the most promising proposals for producing bosonic quantum Hall physics involve lattice Hamiltonians of the Bose-Hubbard form,

$$H = - \sum_{jk} \left( J_{jk} e^{i\phi_{jk}} a_j^\dagger a_k + H.C. \right) + \frac{U}{2} \sum_j n_j (n_j - 1). \quad (1.11)$$

Here,  $j$  and  $k$  denote lattice sites on a two-dimensional square lattice,  $J_{jk}$  is a real hopping amplitude, and  $U$  is a local repulsion term. The phases  $\phi_{jk}$  are

---

<sup>2</sup>There are also non-abelian anyon states in the 2DEG; there is good evidence to support their existence at  $\nu = 5/2$ , and they may also occur at  $\nu = 12/5$ . See the introduction to chapter 3 for a list of other candidate systems.

equivalent to the Peirels phases generated by a gauge field,

$$\phi_{jk} = \frac{q}{\hbar c} \int_{\mathbf{r}_j}^{\mathbf{r}_k} \mathbf{A} \cdot d\mathbf{l}. \quad (1.12)$$

The sum of  $\phi_{jk}$  around any closed path in the lattice is gauge invariant, and if the system is in a nonzero effective magnetic field, nonzero.

At first glance this Hamiltonian looks nothing like the continuum Hamiltonian (1.8), and aside from the dilute limit, there is no *a priori* reason to expect that the physics of its ground states should match that of the continuum. Building on previous studies [108, 43, 49], a central result of this dissertation is that the two systems share profound similarities; the (qualitative) gaps, quantized conductivities and the statistics of their anyonic excitations *are* the same. This relationship can be demonstrated analytically through the appropriate choice of hopping amplitudes  $J_{jk}$ . The direct equivalence of the lattice and the continuum is demonstrated in chapter 2, and the following chapters 3 and 4 build on that result to study the exchange statistics and thermodynamic properties of this system. To prepare for these theoretical discussions, I will now detail some of the physical systems described by (1.11), which represent the best opportunities to realize bosonic quantum Hall physics in the real world.

## 1.2 Artificial Gauge Fields in Cold Atoms

A particularly promising system to realize a bosonic QHE is trapped, cold, electrically neutral atoms.[10] At first glance, this is an extremely counterintuitive statement; neutral atoms do not experience a magnetic field except through the Zeeman interaction and shifts in the hyperfine levels, and the traditional definition of the QHE is a quantized, transverse conductivity, something which

is difficult or impossible to measure in a trapped cloud. Nonetheless, it is quite likely that QHE physics will be observed in cold atoms in the near future. While the loss of the simplest measurement (conductivity) is indeed an obstacle, other observational methods unique to cold atoms (time of flight and *in situ* density imaging) can be employed to study these systems in ways which are impossible in a 2DEG. The fourth chapter of this dissertation is devoted to a study of precisely this system, and shows how density imaging of trapped quantum Hall bosons can reveal a staircase of incompressible quantum Hall states, the signatures of which persist at temperatures high enough to be reached in the next generation of experiments.

The key to realizing a quantum Hall state in cold atoms is the generation of an artificial gauge field, a set of terms in the system's Hamiltonian which are structurally the same as the magnetic vector potential in (1.1). There are a number of ways to do this (see [25] for a review), and I will describe two in some detail here. The first, rotation [21], is the simplest to understand, but for technical reasons it is unlikely to scale to the field strengths necessary to reach the quantum Hall regime. The second, light assisted hopping in an optical lattice, is more exotic and inapplicable to the continuum system, but has already been used to generate extremely strong *staggered* effective magnetic fields [4], and can readily be generalized to the uniform fields considered in this work.

### 1.2.1 Rotation

We consider the Hamiltonian of a particle in an anisotropic Harmonic trap,

$$H = \frac{\mathbf{p}^2}{2m} + \frac{1}{2}m\omega_t^2(x^2 + y^2) + \frac{1}{2}m\omega_z^2z^2. \quad (1.13)$$

We let  $\omega_z \gg \omega_t$ , so that the confinement is much stronger along the  $z$  axis. In this limit, the Hamiltonian is approximately 2d, and we can ignore motion in  $z$ . We now imagine that a perturbation is introduced to set the particle rotating around the  $z$  axis, such as an elliptical deformation of the trap potential which rotates in the  $xy$  plane with angular frequency  $\Omega$ . We transform to the rotating frame, and obtain a new Hamiltonian:

$$H \rightarrow \frac{\mathbf{p}^2}{2m} + \frac{1}{2}m\omega_t^2(x^2 + y^2) - \Omega \mathbf{r} \times \mathbf{p}. \quad (1.14)$$

We now observe that we can pull the  $\mathbf{r} \times \mathbf{p}$  term into the Hamiltonian's kinetic term:

$$H \rightarrow \frac{(\mathbf{p} - m\Omega \widehat{z} \times \mathbf{r})^2}{2m} + \frac{1}{2}m(\omega_t^2 - \Omega^2)(x^2 + y^2). \quad (1.15)$$

This is nothing more than (1.1) with  $q\mathbf{A} = m\Omega\{y, -x, 0\}$  and an additional harmonic confinement term; the Hamiltonian of a harmonically trapped particle in a constant magnetic field (in  $z$ ) of strength  $B = 2m\Omega/q$ . Rotating atomic gases, both with and without optical lattices [100, 136, 120, 21] have been extremely successful in studying vortices and vortex lattice physics, but the (relatively) slow rotation in these experiments corresponds to  $\nu \sim 100$ , two orders of magnitude higher than the quantum Hall regime. Previous calculations have suggested that the transition from vortex lattice to quantum Hall physics occurs around  $\nu = 6$  [21], but the details of this transition are not well-understood.

The great drawback to rotation is that it turns static disorder sources into dynamic ones and can lead to rapid heating and particle loss. As described earlier in the discussion of quasiholes, quantum Hall states are surprisingly robust against static disorder, merely accumulating pinned quasiparticles or quasiholes at potential minima and maxima, Further, since the magnetic length is very short– the typical cloud would be hundreds of magnetic lengths wide in

the LLL regime— smooth inhomogeneous potentials should simply lead an inhomogeneous distribution of quantum Hall puddles across the trap, which can be readily distinguished from each other through *in situ* imaging.

In the rotating system, however, any inhomogeneities in the optical potential which do not co-rotate with the rest of the cloud will become time-dependent potentials in the rotating frame, and thus will cause heating, scattering and particle losses. These scattering rates should scale with the rotation frequency, and thus ensuring that they are small compared to the Landau level spacing (which is also proportional to  $\omega$ ) requires fine control over the magnetic and optical potentials. While this is primarily an engineering problem and not a theoretical one, it is difficult enough that the strongly correlated LLL regime [104] has only been reached for extremely small clouds ( $< 10$  particles) [36], where signatures of quantum Hall physics are murkier and far less conclusive than in the many-body limit.

## 1.2.2 Light-Assisted Hopping

An exciting alternative to rotation is to use 2-photon Raman transitions to create an effective gauge field in a tilted optical lattice. We begin with an anisotropic cubic lattice, with the barriers along the  $z$  direction strong enough that transitions between layers are essentially forbidden and the system can be treated as a set of independent planes. We then tune the optical potential to add a potential gradient to the system along the  $x$  direction, so that the atoms experience a position dependent chemical potential  $\mu \rightarrow \mu + Vx_i/a$ , where  $a$  is the lattice spacing and  $x_i$  are positions in the lattice. There is no potential gradient along the  $y$  di-

rection. If  $V$  is large compared to the hopping parameter  $J$ , energy conservation will freeze the atoms into lines of constant  $x_i$ , reducing the lattice to an array of 1d tubes.

To restore  $x$ -direction hopping and introduce an artificial gauge field, we now add two lasers as shown schematically in figure 1.1. These lasers, at momenta and frequencies  $\{\mathbf{k}_1, \omega_1\}$  and  $\{\mathbf{k}_2, \omega_2\}$ , are tuned so that  $\omega_1$  and  $\omega_2$  are near a resonance to drive a transition into one of the atom's hyperfine states. In the process shown in figure 1.1, the atom first absorbs a photon from laser 1 and then emits a photon from laser 2, acquiring a net energy  $\omega_1 - \omega_2$  and net momentum  $\mathbf{k}_1 - \mathbf{k}_2$ . If  $\omega_1 - \omega_2 = V$ , the atom can hop from row  $x_i$  to row  $x_i + 1$ , thus freeing the particles to move along the  $x$  direction. With each hop, however, the particle has gained a momentum boost of  $\mathbf{k}_1 - \mathbf{k}_2$ , and if the lasers are tilted so that  $\mathbf{k}_1 - \mathbf{k}_2 = k_l \widehat{y}$ , the canonical momentum  $\mathbf{p}$  of the hopping particle is shifted by

$$\mathbf{p} \rightarrow \mathbf{p} + k_l \frac{x}{a} \widehat{y}. \quad (1.16)$$

With the lasers turned on, the *scalar* potential tilt vanishes from the particle's Hamiltonian (the energy gained or lost to photons in the hopping process cancels it out), replaced instead by a *vector* potential equivalent to a constant magnetic field. The magnitude of the  $x$  direction hopping depends on the details of the optical potential and the Rabi frequencies of the atom-laser coupling. This technique has already been successful [4] in realizing strong staggered magnetic fields (using a staggered optical potential  $V(x) = V(-1)^{x_i/a}$ ), and I expect uniform fields to be obtained in the near future.

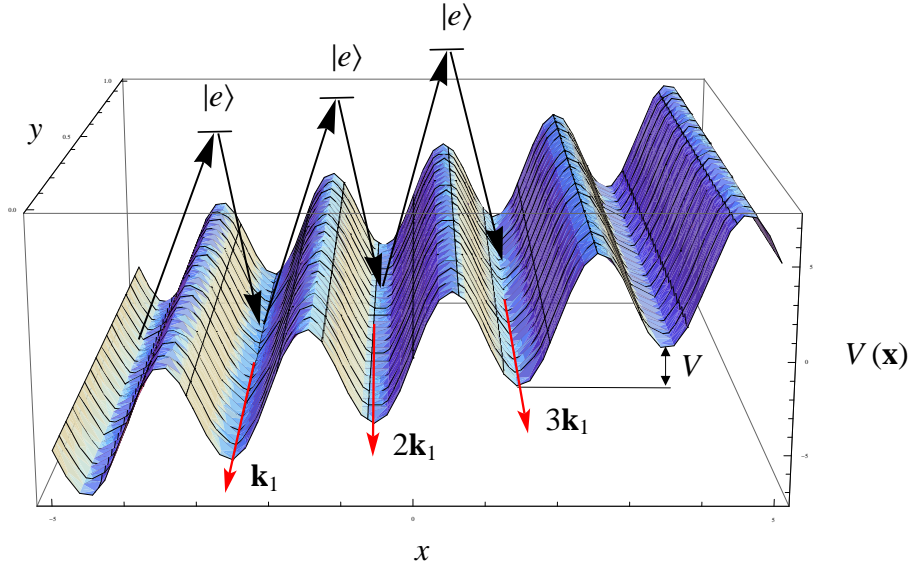


Figure 1.1: Schematic picture of light-assisted hopping as a source of an artificial vector potential. Through a 2-photon Raman process (black arrows), a pair of lasers promote particles to an excited hyperfine state  $|e\rangle$  and then back down to the ground state with a net energy and momentum boost of  $\pm V$  and  $\pm \mathbf{k}_l$ . This allows the particle to hop along  $x$ , and due to the energetic gain and loss from the Raman process, the tilt vanishes in the low-energy Hamiltonian. Since the momentum boost along  $y$  depends on  $x$ , the Raman process acts as an artificial magnetic field on the neutral atoms in the lattice. For visual clarity, the sinusoidal variation of the lattice potential along  $y$  is not shown.

### 1.3 Superconducting Device Arrays

An alternative set of systems which could mimic the physics of quantum Hall bosons are arrays of superconducting devices. Unlike cold atoms, only lattice quantum Hall systems are possible using superconductors, since the Meissner effect guarantees that bulk superconducting systems will expel magnetic flux and the Cooper pairs will not experience an external magnetic field until superconductivity is disrupted at the critical field  $H_c$ . With that restriction in mind,

multiple candidate devices remain for simulating the Bose Hubbard Hamiltonian (1.11) in an effective magnetic field. After all, formally any set of coupled 2-level systems can be reduced to (1.11) in the  $U \rightarrow \infty$  limit, and provided that the phase factors  $\phi_{jk}$  can be introduced, quantum Hall physics can be realized in these systems. Engineering these phase factors, however, is a subtle and challenging problem. I will now detail two superconducting device arrays which could describe a bosonic quantum Hall system.

### 1.3.1 Charge Qubit Lattice

First proposed in this context in 1994 [18, 110], the charge qubit lattice is an array of tiny superconducting grains placed on an insulating substrate, coupled to their neighbors through Josephson contacts so that Cooper pairs can tunnel from grain to grain [28, 131]. Since the regions between the grains are insulating, they do not screen magnetic flux and tunneling Cooper pairs experience an applied magnetic field through the Peierls phases  $\phi_{jk}$  described previously. If the grains are small enough ( $\sim 0.1\mu\text{m}$  in diameter or smaller, corresponding to a net capacitance of  $10^{-15}\text{F}$  or less), the energetic cost of placing additional Cooper pairs on a grain becomes substantial, and the Hamiltonian is given by a Bose Hubbard model,

$$H = -\frac{E_J}{2} \sum_{jk} (a_j^\dagger a_k e^{i\phi_{jk}} + \text{H.C.}) + 4E_C \sum_i (n_i - O_i)^2. \quad (1.17)$$

Here,  $E_J$  is the Josephson energy which couples the grains through Cooper pair tunneling, the charging energy  $E_C = e^2/2C$ , where  $C$  is the self-capacitance of a grain, and  $O_i$  is a normalized charge offset term. Historically, it was precisely this system (without the magnetic field) which the Bose Hubbard model was

created to describe [30]. The offsets  $O_i$  represent the sum of intrinsic effects (trapped charges on the insulating substrate, deformations in the grains, and charged impurities) and externally applied potentials.

There are a number of potential advantages to the charge qubit lattice. First, the energy scales  $E_J$  and  $E_C$  can be large, with  $E_J$  taking values up to 2K and  $E_C \sim 10$ K or higher. Using the gaps calculated in chapter 4, this leads to many-body quantum Hall gaps of around 1K in the clean limit at  $\nu = 1/2$  or 1, larger than the gap at  $\nu = 5/2$  in the best 2DEG systems [82]. Further, assuming a  $1.5\mu\text{m}$  spacing between grains, the magnetic field required for a flux density of  $\Phi_0/4$  per plaquette is  $220\mu\text{T}$ , far smaller than the 2 – 10T fields used in 2DEG experiments. Finally, the discrete nature of the grains makes it possible to independently tune the offset potential  $O_i$  at every site, offering unprecedented control for the braiding and manipulation of quasiholes.

These advantages come with a serious drawback, however, in the form of charge noise. Prior to tuning, the offsets  $O_i$  will take random values between  $-1/2$  and  $1/2$  at every site, since even with perfect fabrication methods there will always be stray charges on the substrate and local chemical potential shifts in the superconducting grains. While the classical fluctuations in  $O_i$  are slow (five or more orders of magnitude slower than the hopping frequency [20]), they are large, and so in absence of local tuning the lattice will be extremely disordered. Since the strength of this disorder scales with  $E_C$ , quantum Hall states will never form unless the  $O_i$  are rapidly and individually tuned to a uniform value when the system is initialized. The local measuring and tuning of hundreds of gates at mK temperatures is an extremely challenging technical problem, making it unlikely that bosonic quantum Hall states will be realized in charge qubit lattices

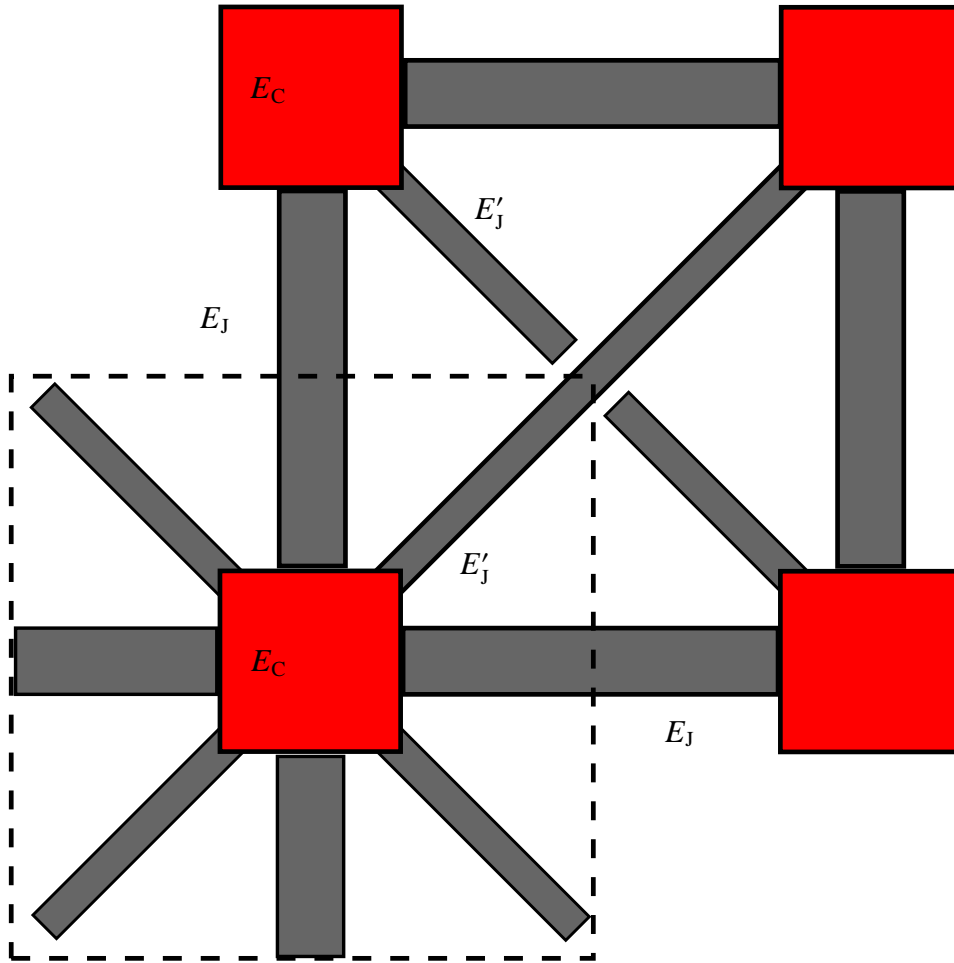


Figure 1.2: Unit cell for a charge qubit array. The superconducting grains (red) are small enough that their charging energy  $E_C$  is larger than the Josephson coupling energies  $E_J$  and  $E'_J$ . If this is the case, fluctuations in the Cooper pair density  $n_i$  are strongly suppressed, and occupation at each site is restricted to  $n$  and  $n + 1$  Cooper pairs. Since the states created and annihilated by  $a_i^\dagger$  and  $a_i$  are real Cooper pairs, the system's conductivity can be measured directly through standard methods.

in the near term.

### 1.3.2 Flux Qubits

An alternative to the charge qubit lattice is to use a lattice of flux qubits [79, 86], superconducting rings interrupted by three Josephson junctions whose eigenstates are distributions of circulating currents in the presence of a frustrating magnetic field. These circulating currents have a nonzero magnetic dipole moment, and through physics analogous to the Aharonov-Casher effect (the dual of the Aharonov-Bohm effect for a magnetic dipole moving in an electric field) [3], they can hop from ring to ring with phase factors that mimic a nontrivial gauge field. The use of flux qubits in this manner is my own idea and new to this work, and forms the fifth chapter of the dissertation. Flux qubits are not sensitive to charge offsets, eliminating the charge noise problem described in the previous paragraphs. I believe that this method offers a real chance of robustly simulating bosonic quantum Hall physics with current technology, and I provide detailed calculations to support this claim later in this work.

## 1.4 Outline of this Dissertation

This dissertation is organized into five further chapters. The first, chapter 2, reproduces my paper “Parent Hamiltonian for the Quantum Hall States in a Lattice” [60], which shows that appropriately choosing the hopping matrix elements  $J_{jk}$  in a Bose Hubbard model can exactly reproduce the lowest Landau level and degeneracy of the continuum problem, providing a direct link between the two systems. The next chapter reproduces my paper “Non Abelian Braiding of Lattice Bosons” [59], where I built on the lattice LLL result to show that the braiding of anyons with realistic potentials could be simulated numer-

ically to determine the anyonic statistics of the quantum Hall states in that model. Following that, I include a new paper, “Equation of State for Quantum Hall Bosons in a Lattice” where I calculate the gaps and robustness of the various FQH plateaus in lattice bosons and provide an outlook for observing them in cold atoms experiments. This paper is currently in preparation for publication. In chapter 5, “A Vector Potential for Flux Qubits,” I propose an entirely new circuit architecture by which flux qubits– which are insensitive to charge noise and the most robust qubit currently realized– could act like a Bose Hubbard model in a nontrivial gauge field. Finally, in the conclusion, I summarize my research and speculate about future directions and topological quantum computing.

CHAPTER 2  
 PARENT HAMILTONIAN FOR THE QUANTUM HALL STATES IN A  
 LATTICE

This work was done in collaboration with Erich Mueller, and was published in Physical Review Letters. [60]

The interplay between periodic potentials and magnetic fields is an important topic [47, 108, 89, 78, 21]. In the tight binding limit, the lattice broadens the Landau levels into a series of finite bandwidth “Hofstadter bands” which can be represented as a self-similar fractal. Since the original band-gaps persist, the integer quantum Hall effects are robust against the lattice. The split degeneracy, however, invalidates many of the analytic arguments used to explain the fractional quantum Hall effect [66, 44, 92, 141], and questions remain about the nature of the interacting system. Here, by adding longer range hoppings to a Hubbard model, we produce a Hamiltonian for which several Hofstadter bands coalesce into a single degenerate manifold. Adding local repulsion between the particles, we show that at appropriate filling factors the Laughlin wavefunction becomes an exact ground-state.

In a uniform magnetic field, the most general hopping Hamiltonian on a two-dimensional square lattice is

$$H = \sum_{j \neq k} J(z_j, z_k) a_j^\dagger a_k; \quad J(z_j, z_k) = W(z) e^{(\pi/2)(z_j z_k^* - z_j^* z_k) \phi}, \quad (2.1)$$

where the position of the  $j$ 'th lattice site is written in complex notation as  $z_j = x_j + iy_j$ , and the complex displacement between the two sites is  $z = z_k - z_j$ . The operators  $a_j$  annihilate an atom at site  $j$ . The phase factor  $(z_j z_k^* - z_j^* z_k) \phi = 2i(x_j y_k - y_j x_k) \phi$ , corresponds to a uniform magnetic field in the symmetric gauge,

with flux  $\phi$  through each plaquette. This flux is only defined modulo 1, and having a full flux quantum through each plaquette is gauge equivalent to no flux. We will explicitly assume  $0 \leq \phi \leq 1$ , and take  $\phi = p/q$  to be the ratio of two relatively prime integers. If one chooses  $W$  to be  $-t$  for nearest neighbors and zero otherwise, one reproduces the Hofstadter spectrum [47]. We show that if instead we choose

$$\begin{aligned} W(z) &= t \times G(z) e^{-\frac{\phi}{2}[(1-\phi)|z|^2]} \\ G(z) &\equiv (-1)^{x+y+xy}, \end{aligned} \tag{2.2}$$

the lowest  $p$  Hofstadter bands collapses to a single fully degenerate Landau level. Although we work in the symmetric gauge  $\mathbf{A} = (B/2)(x\hat{\mathbf{y}} - y\hat{\mathbf{x}})$ , converting our results to other gauges is trivial: under a gauge transformation  $\mathbf{A}(\mathbf{r}) \rightarrow \mathbf{A}(\mathbf{r}) + \nabla\Lambda(\mathbf{r})$ , the field operator transforms as  $c_j \rightarrow c_j e^{i\Lambda(\mathbf{r}_j)}$ . The flux is measured in units of  $\phi_0 = h/e$ , where  $h$  is Planck's constant, and  $e$  is the electric charge. Our derivation of this Hamiltonian is similar to one used by Laughlin [67] and subsequently corrected/extended in [103, 123]. The paradigm of creating a parent Hamiltonian for which a desired quantum state is an exact eigenstate has been fruitful in a number of other spin models [6, 2, 139]. We will work in units where  $t = 1$ .

Our model is relevant to many broader studies of quantum Hall physics. The analytic nature of our proof expands our understanding of quantum Hall eigenstates, and since we have defined a lattice model with the same ground state structure as the continuum problem, our theory could prove to be a valuable starting point for computational studies of the quantum Hall systems. Further, it is likely [78] that interesting Quantum Hall ground states may exist on the lattice that have no direct continuum analog, and the analytic lowest Landau

level (LLL) of our model should make it much easier to search for them.

The most promising experimental realization of our model is in optical lattices [10]. Optical lattice experiments can study both bosonic and fermionic quantum Hall states, and allow us in principle to study much larger fluxes (such as  $\phi = 1/3$  or more) than can be achieved with real magnetic fields. The gauge potential in the optical lattice system can be created in a number of ways: time-varying hopping elements [108], lattices with multiple sets of minima [81], coherent Raman scattering [109] and rotation [43, 100, 120, 136, 21, 71]. Further, optical lattice systems allow us to directly tune the hopping amplitudes between nearby sites. Long range hopping is difficult to arrange, but  $J$  falls off as a Gaussian, and in the limit of small  $\phi$  it suffices to include only nearest and next-nearest neighbor hopping. The ratio of the nearest and next-nearest neighbor hopping matrix elements can be controlled in an experiment by adjusting the shapes of the barriers between those sites. One practical scheme would involve adding an additional array of shallow wells displaced by half a lattice spacing in both the  $x$  and  $y$  directions. Integrating out these shallow sites will renormalize the nearest and next-nearest neighbor hoppings. A second scheme would be to divide the original lattice into two sublattices. Separating the sublattices in the  $z$ -direction will attenuate the nearest neighbor tunnelling while leaving the next-nearest neighbor matrix element largely unchanged. Figure 2.1 compares the energies of the single particle eigenstates of Eq. (2.1), using the  $W$  in Eq. (2.2), as well as truncating to only nearest neighbors or next-nearest neighbors. As one can see, even for  $\phi = 1/3$ , the next-nearest neighbor hopping already reduces the bandwidth to  $0.1t$ .

Not only does this Hamiltonian produce a macroscopically degenerate manifold of single particle ground states, but this manifold is spanned by wavefunctions of the form

$$\psi_n(z_j) = \langle j|\psi_n\rangle = z_j^n \exp\left(-\frac{\pi\phi}{2}|z_j|^2\right), \quad (2.3)$$

all with energy  $\epsilon = -1$ . Remarkably, this is the same structure as the continuum problem, where the LLL is characterized by the same degenerate set of single particle states. To prove this result, we write

$$\frac{\langle j|H|\psi_n\rangle}{\langle j|\psi_n\rangle} = \sum_{z \neq 0} G(z) \frac{(z_j + z)^n}{z_j^n} e^{-\frac{\pi}{2}|z|^2 - \pi\phi z_j^* z}. \quad (2.4)$$

We then appeal to the singlet sum rule [91, 67],

$$k(c) \equiv \sum_z e^{cz} G(z) e^{-\frac{\pi}{2}|z|^2} = 0 \quad \forall c, \quad (2.5)$$

where the sum is over all  $z = n + im$  with integer  $n$  and  $m$ . By taking any number of derivatives with respect to  $c$  one finds

$$\sum_z f(z) G(z) e^{-\frac{\pi}{2}|z|^2} = 0, \quad (2.6)$$

for any *entire* function  $f(z)$  that diverges sufficiently slowly as  $|z| \rightarrow \infty$ <sup>1</sup>. Since we do not include the  $z = 0$  term in Eq. (2.4), one immediately finds that the right hand side is simply -1, proving that the LLL wavefunctions (2.3) are degenerate eigenstates. No analogous argument works for the higher Landau level wavefunctions, which involve powers of both  $z^*$  and  $z$ .

Given that the wavefunctions in (2.3) are identical to those of the continuum problem, the total number of degenerate states per unit area is the same as in

---

<sup>1</sup>If  $f$  diverges faster than  $e^{\pi|z|^2/2}/z^2$ , the the sum will *not* be absolutely convergent; we thus can't reorder terms from the Taylor series over  $n$  with those from the sum on  $z$ , invalidating the cancellation order by order in  $z$ .

the continuum. In our units, where the lattice spacing is unity, this results in  $\phi N_s$  LLL wavefunctions in a region containing  $N_s$  lattice sites. Thus  $\phi$  is the fraction of all single particle states which reside in the LLL. Taking  $\phi = p/q$ , the standard Hofstadter problem yields  $q$  distinct bands. Thus, as we confirm numerically, our LLL must be made from the lowest  $p$  of these. This  $p$ -fold collapse is consistent with the relationship between the Chern numbers of the Hofstadter bands, and that of the LLL [64].

For  $\phi > 1/2$  it is natural to also consider the Hamiltonian formed if one replaces  $\phi$  in Eq. (2) with  $1 - \phi$  and leaves equation (1) unchanged. Due to the periodicity in  $\phi$  of lattice models, this gives a Hamiltonian with the same absolute flux per plaquette, however it is clearly a distinct Hamiltonian, with shorter range hopping. This alternative Hamiltonian yields states analogous to (2.3), but with  $z$  replaced by  $z^*$ , and a degeneracy of  $(1 - \phi)N_s$  in a region of  $N_s$  lattice sites.

The massive ground state degeneracy of our system can be lifted by interactions. Since our model reproduces the continuum lowest Landau level, we can simply use those results. On-site repulsion in the lattice is equivalent to point interactions in the continuum. Consider for example the interacting Hamiltonian

$$H = \sum_{j \neq k, \sigma} J(z_j, z_k) a_{j\sigma}^\dagger a_{k\sigma} + \frac{U}{2} \sum_{j, \sigma} a_{j\sigma}^\dagger a_{j\sigma}^\dagger a_{j\sigma} a_{j\sigma}, \quad (2.7)$$

Any LLL wavefunction which vanishes when two particles coincide is a ground state of this Hamiltonian. Due to the structure of the LLL, there is a maximal atomic density for which this occurs. For bosons the highest density ground state is the  $\nu = 1/2$  Laughlin state, while for 2-component fermions it is the ferromagnetic “111” state. At fixed density, these states are unique up to topological

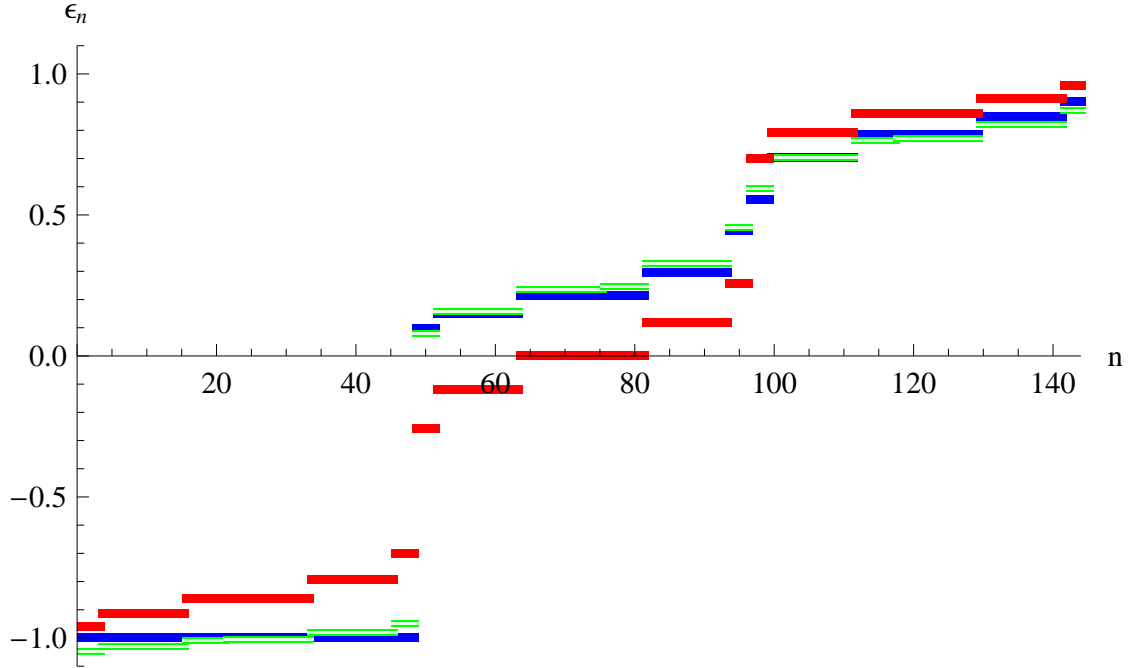


Figure 2.1: (Color Online) All single particle eigenvalues for the hopping Hamiltonian in Eq. (2.1) with  $\phi = 1/3$  on a  $12 \times 12$  lattice with periodic boundary conditions. The index  $n$  labels eigenvalues from smallest to largest. The dark blue points use hopping matrix elements given by Eq. (2.2), the light green points are the same model with only nearest and next nearest neighbor hopping, and the medium red points have only nearest neighbor hopping (the Hofstadter Hamiltonian). Energies are all measured in units of  $t$ . The blue and green points are nearly indistinguishable. The lowest  $1/3$  of the dark blue points are all degenerate.

degeneracies. The other Laughlin states and more exotic quantum Hall states are also ground states if  $\nu \leq 1/2$ , however they are not unique if all interactions are local.

Longer ranged interactions [5, 43], on the other hand, will typically lift the degeneracy entirely, but we shall not treat them in any detail here. Long range interactions can be realized in an optical lattice through dipolar gases. Such

interactions also make analytic results more difficult to obtain. However, since our model has the same ground state manifold as the continuum problem, any arguments based on the analytic structure of the LLL states will hold in our lattice theory.

Our argument is readily extended to a finite system with magneto-periodic boundary conditions,

$$\psi(z + nL + imL) = \psi(z) e^{i\pi\phi L(ny - mx)}. \quad (2.8)$$

There one replaces the polynomials in Eq. (2.3) with appropriate products of Gaussians and Jacobi theta functions [45, 1]. One also replaces  $J(z_j, z)$  in Eq. (2.1) by its magneto-periodic extension

$$J_L(z_j, z) = \sum_R J(z_j, z + R) \exp\left(\frac{\pi}{2}(z_j R^* - z_j^* R)\phi\right), \quad (2.9)$$

where the sum is over all  $R = nL + imL$  for integer  $n, m$ . This finite system is amenable to numerical calculations. To invoke the singlet sum rule in a periodic geometry, one must simply merge the sums on  $z$  and  $R$  into a single sum over all  $z \neq 0$ . The phase factors from the magnetoperiodicity of  $\psi(z)$  and  $J$  cancel each other.

In the finite system with magneto-periodic boundary conditions, one re-places defines the periodic analog of the Laughlin wavefunction

$$\begin{aligned} \Psi(\{z_n\}) &= \Psi_{\text{cm}} \times \prod_{k < j}^M \chi_{jk}^p \prod_{j=1}^M e^{\pi \frac{pM}{2L^2} (z_j^2 - |z_j|^2)} \\ \Psi_{\text{cm}} &= \prod_{i=1}^p \theta_1\left(\frac{\pi}{L} (Z - Z_i)\right). \end{aligned} \quad (2.10)$$

The center of mass coordinate is  $Z = \sum_j z_j$ , and  $\chi_{jk} = \theta_1(\pi(z_j - z_k)/L)$ , with  $\theta_1(z) = \sum_n (-1)^{n-1/2} e^{-\pi(n+1/2)^2} e^{iz(2n+1)}$ . There are  $p$  parameters  $Z_i$  which represent the location of the center of mass zeros. In the continuum system there is a symmetry

which causes the energy to be independent of how these are chosen. The space of degenerate states is spanned by  $p$  orthogonal wavefunctions. In most lattice models this symmetry is broken, and the degeneracy is lifted. Since Eq. (2.10) is made up of lowest Landau wavefunctions, in our model the degeneracy persists. In Fig. 2.2 we confirm this degeneracy via an exact diagonalization calculation for 4 bosons on a  $4 \times 4$  lattice with  $p = 2$  and hard-core repulsion. We find similar results on  $3 \times 3$  lattices.

Our results gives some insight into recent calculations of Sorensen et al. [108, 43]. They investigated the standard Bose-Hubbard model with nearest neighbor hopping and a uniform magnetic field. Fixing the filling factor at  $\nu = 1/2$ , they found that when  $\phi$  became of order 0.2 the overlap between the exact ground state and the  $p = 2$  Laughlin state (2.10) begins to rapidly decrease. The characteristic range of hoppings in our model increases with  $\phi$  – and near  $\phi = 0.2$  the next nearest neighbor matrix element starts to become significant.

One may well ask how fractional quantum Hall physics would manifest itself in cold atoms. Although most difficult, the most exciting observations would be ones which investigated the braiding properties of the excitations [117, 142]. These states also have definite signatures in Bragg spectroscopy [89]. The most robust probe, however, is an analog of the vanishing longitudinal resistance seen in solid state systems – namely the incompressibility of the fractional quantum Hall states [128, 21]. This incompressibility is readily observed in trapped systems, where the chemical potential (and hence the filling factor) varies slowly in space. As is caricatured in Fig. 2.3, the equation of state  $n(\mu)$  has a series of plateaus corresponding to the filling factor taking on integer fractions. Within the local density (Thomas-Fermi) approximation, the density profile of

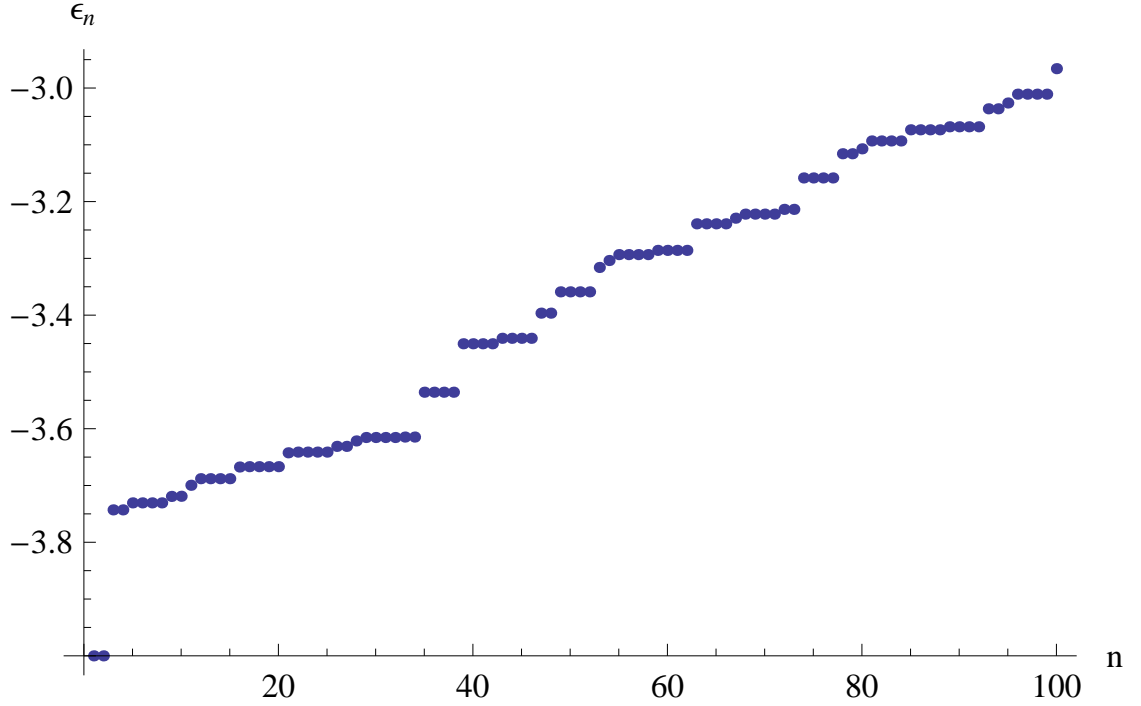


Figure 2.2: First 100 eigenvalues for 4 particles on a  $4 \times 4$  lattice with periodic boundary conditions,  $\phi = 1/2$ , and hard core repulsion. The two states at  $\epsilon = -4$  are Laughlin states (2.10); the degeneracy stems from the toroidal geometry. There is a distinct energy gap of  $0.566t_{nn}$  to the lowest excited states, where  $t_{nn}$  is the nearest neighbor hopping amplitude.

the trapped cloud will display these same plateaus. The width of these plateaus is set by the gap to single particle excitations in the fractional quantum Hall states. As shown in figure 2.2, in the hard core limit the gap in a  $4 \times 4$  lattice at  $\nu = 1/2$  and  $\phi = 1/2$  is 0.566 times the nearest-neighbor tunnelling strength  $t_{nn}$ . This should be compared to the bandwidth  $V \approx 4t_{nn}$ . As  $\mu$  goes from 0 to  $V$  the density goes from zero to one. One therefore expects that the  $\nu = 1/2$  plateau will occupy roughly 1/8 of the cloud. More involved estimates will be given in chapter 4.

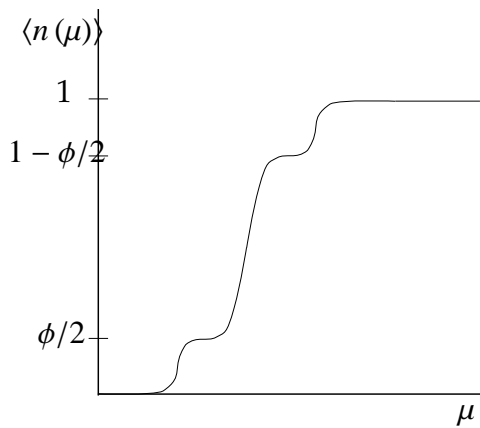


Figure 2.3: Schematic plot of  $\langle n \rangle$  vs.  $\mu$ , for lattice bosons described by the model given in Eqs. (2.1,2.2), with hard core interactions added. The steps correspond to incompressible fractional quantum Hall states commensurate to  $\nu = 1/2$ . This structure will be visible in the density profile of a trapped gas. In the presence of finite (but large) local repulsion this same structure will repeat between each of the Mott plateaus. Similar structure will be seen with Fermions, but with plateaus at fillings with odd denominators.

CHAPTER 3  
NON-ABELIAN BRAIDING OF LATTICE BOSONS

This work was done with Paul Ginsparg and Erich Mueller, and was published in Physical Review Letters. [59]

### 3.1 Introduction

When two identical quantum mechanical particles exchange places, the wavefunction typically acquires a phase:  $\theta = 0$  for bosons, and  $\theta = \pi$  for fermions. Remarkably, there exist 2d systems [66, 44, 92, 141, 134, 133, 103, 123] whose “anyon” excitations display *fractional statistics*, with  $\theta \neq 0, \pi$ . Even more remarkably, there are models in which exchanging quasiparticles not only produces a phase, but also rotates the system between degenerate states [80, 82, 41, 94, 95, 12, 83, 32, 107, 35, 69, 39, 102, 62, 61, 24]. Under these circumstances, exchanges may not commute. Kitaev [61] proposed using such nonabelian quasiparticles for quantum computation, with qubits constructed from the degenerate states. Quantum gates are implemented by “braiding” the quasiparticles: using time-dependent potentials to drag the quasiparticles around one another, switching their positions. The collective nature of the encoded quantum information provides protection against various decoherence mechanisms. Here we start from a microscopic Hamiltonian, and numerically calculate the result of such a braiding experiment. We find that even for surprisingly small systems ( $4 \times 4$  lattices), this procedure can be used to establish non-abelian statistics, and hence to implement quantum gates.

Explicitly calculating the results of a braiding operation for a realistic mi-

microscopic Hamiltonian is difficult. Previous studies have mostly focused on the properties of variational wavefunctions [82, 133, 83, 38, 33, 54, 55, 126, 9, 93, 65, 11]. As in physical experiments, a numerical experiment must contend with finite size effects, mixing of higher bands, the location of unpinned quasiparticles, and uncertainty about both the exact many-body wavefunction and the interaction between a quasiparticle and the applied perturbation. Overcoming these difficulties is well worth the effort, since observing the braiding of two quasiparticles provides a definitive test of exchange statistics. This numerical approach complements more indirect experimental approaches, such as observing shot noise or interference effects in the tunneling of edge states [135].

### 3.2 Model

We choose a model which is both experimentally relevant, and computationally tractable: hard-core bosons hopping on a square lattice, with phases on the hopping matrix elements corresponding to a uniform magnetic field. This model describes Cooper pairs hopping on a Josephson junction array in a magnetic field [131, 28, 116] when the charging energy is large compared to the hopping energy. It also describes cold atoms in a deep optical lattice [10] with an artificial gauge field [109, 71, 136, 21, 72]. Recent developments in cold atom physics [109] suggest that the fractional quantum Hall regime will be attained in the near future.

A general Hamiltonian for lattice bosons is

$$H = - \sum_{jk} \left( J_{jk} e^{i\phi_{jk}} a_j^\dagger a_k + H.C. \right) + \frac{U_2}{2} \sum_j a_j^\dagger a_j^\dagger a_j a_j \quad (3.1)$$

$$+\frac{U_3}{6} \sum_j a_j^\dagger a_j^\dagger a_j^\dagger a_j a_j a_j.$$

$a_k^\dagger/a_k$  creates/annihilates a boson at complex coordinate  $z_k$  on a square lattice with unit lattice spacing. Defining  $z \equiv z_j - z_k = x + iy$  as a complex integer,  $i\phi_{jk} = -\frac{\pi\phi}{2} (z_j z_k^* - z_j^* z_k)$  is the Peierls phase of the  $\mathbf{B}$  field (with  $\phi$  the density of flux quanta per plaquette). The properties of this Hamiltonian depend on the form of  $J_{ij}$ . The simplest model would just include nearest neighbor hopping [47]. As argued in [60], the fractional quantum Hall states are particularly robust if we use a specific gaussian hopping,  $J_{jk} \equiv J(z) = J_0 G(z) \exp\left(-\frac{\pi}{2}(1-\phi)|z|^2\right)$ , where  $G(z) = (-1)^{1+x+y+xy}$  and  $J_0$  is a constant. In all but one case (see caption of table I), we take the hard-core limit of  $U_2 \rightarrow \infty$ . We define  $J_{NN} = J_0 e^{-\pi/4}$  as the energy scale of the problem.  $U_3$  is an artificial three-body repulsion which we introduce in some calculations. The magnetic length in this system,  $l_B = 1/\sqrt{2\pi\phi}$  lattice spacings, is very short for the flux densities studied ( $l_B = 0.56$  for  $\phi = 1/2$ ). We showed in [60] that the single-particle spectrum of (3.1) reproduces the continuum lowest Landau level (LLL) with  $\phi L^2$  degenerate single particle ground states on an  $L \times L$  lattice. As explained in [60], the longer range hoppings can be engineered by appropriately shunting the Josephson junction array, or by appropriately tailoring the optical lattice potential. For  $\phi \lesssim 1/3$  it suffices to include next-nearest-neighbor hopping. Since the lowest Landau level is the ground state manifold of (3.1), a LLL-projected calculation in the continuum would give similar results, at the cost of more complexity in the calculation.

We add to Eq. (3.1) a time-dependent potential  $V_j(t)$  through a Hamiltonian  $H_p = \sum_j V_j(t) a_j^\dagger a_j$ . At time  $t = 0$ , we take  $V$  to be zero except on a few sites, where it is positive. We slowly change  $V$  such that  $V_j(T) = V_j(0)$ , but with two of the potential bumps exchanged. If quasiparticles are pinned to the defects,

this will exchange them. Experimentally, the potential  $V_j$  could be engineered by gates on individual Josephson junctions, or through targeted lasers in an optical lattice. Such addressability was recently demonstrated in [115]. In our numerics, we move our bumps by linearly reducing the amplitude of  $V$  on one site, while linearly increasing it on a neighbor.

Under an adiabatic cyclic change of the Hamiltonian, non-degenerate states will return to themselves with an additional phase factor, while degenerate states can mix:  $e^{-iHT}|\psi_i\rangle = e^{-i\int E dt} \sum_j M_{ij}|\psi_j\rangle$ . Throughout we neglect the  $\int E dt$  term, where  $E(t)$  is the instantaneous energy at time  $t$ . This temporal phase can be experimentally distinguished from the geometric phase by traversing the path at different rates. The unitary matrix  $M_{ij}$  is calculated by integrating the Berry connection:

$$M = P \exp\left(2\pi i \oint d\lambda \gamma\right). \quad (3.2)$$

Here,  $\gamma_{ij} = i\langle\psi_i|\nabla_\lambda|\psi_j\rangle$  is the Berry connection matrix, the  $|\psi_i\rangle$  are a basis of degenerate states,  $\lambda$  parametrizes the path, and  $P$  is the path ordering symbol. While the Berry connection  $\gamma$  is a gauge-dependent quantity, the matrix  $M$  is physical and gauge invariant (up to joint choice of basis at the start and end points).

To numerically calculate Eq. (3.2), we use a method described in [90, 98], breaking the path into many small discrete steps, engineered to maintain the degeneracies of the spectrum. For each point  $\lambda$  on the path, we diagonalize  $H$  to produce a basis  $|\psi_i(\lambda)\rangle$ . This basis is not unique: the phases of  $|\psi_i(\lambda)\rangle$  are arbitrary, and one can form a new basis by taking arbitrary linear superpositions of degenerate states. We fix this arbitrariness by choosing  $\langle\psi_i(\lambda)|\psi_j(\lambda + d\lambda)\rangle =$

$\delta_{ij} + O(d\lambda^2)$ . The Berry matrix is then

$$M_{ij} = \langle \psi_i(\lambda_f) | \psi_j(0) \rangle. \quad (3.3)$$

Following [98], we generate the states  $|\psi_i(\lambda + d\lambda)\rangle = \sum_j (A^{-1})_{ij} |\tilde{\psi}_j(\lambda + d\lambda)\rangle$  by first determining the eigenstates  $|\tilde{\psi}_i(\lambda + d\lambda)\rangle$  using a generic diagonalization algorithm, and then calculating the overlap matrix  $A_{ij} = \langle \psi_i(\lambda) | \tilde{\psi}_j(\lambda + d\lambda) \rangle$ . Since  $A$  will be unitary only up to corrections of order  $d\lambda$ , we perform a Gram-Schmidt orthogonalization at each step.

In Fig. 3.1, we illustrate the initial configurations of the impurities and some of paths over which we move them. We use relatively small systems: between 3 and 9 particles on lattices of up to 24 sites with periodic boundary conditions; with the hard core constraint the largest Hilbert spaces studied contained about 50,000 states. While state-of-the art algorithms on high performance computers would allow us to study larger systems, we find that finite size effects are already sufficiently small on these modest grids, presumably due to the robust nature of the topological effects of interest. Our algorithm was implemented in *Mathematica* on a desktop computer.

### 3.3 Results

The results of our braiding calculations are summarized in table I. In all cases, the applied impurity potentials are strong. We assign each state an effective filling fraction  $\nu_{\text{eff}} = N/N_{\text{LLL}}$ , where  $N_{\text{LLL}}$  is the number of single particle states in the LLL in the presence of the impurities. In every case studied, for  $N_{\text{imp}}$  impurities  $N_{\text{LLL}} = N_\phi - N_{\text{imp}}$  (where  $N_\phi$  is the number of flux quanta), showing that a full quasihole (QH) is pinned at each impurity. Each quasihole is a first order

zero of the many-body wavefunction and binds a single flux quantum. These full QHs will be supplemented by non-abelian fractional QHs at the appropriate filling fractions, though due to the small sizes of our systems and the nearly zero amplitude of the wavefunction near impurities, we cannot be certain of their locations. Our braiding results are consistent with the assumption that any non-abelian fractional QHs track the locations of the impurities. In the thermodynamic limit,  $\nu_{\text{eff}} \rightarrow \nu$ . In the table, each unitary braid matrix  $M$  is denoted by a pair of phases  $(p_1, p_2)$ , where  $e^{i\pi p_1}$  and  $e^{i\pi p_2}$  are the eigenvalues of  $M$ . For cases with more than 2 impurities, we label the exchange of impurities  $i$  and  $j$  (as labeled in Fig. 1) by  $R_{ij}$ .

The simplest case  $\nu_{\text{eff}} = 1/2$  provides an excellent test of the algorithm, since we know (in the absence of a perturbing potential) that both the ground state wavefunction, and its quasihole excitations, are given exactly by Laughlin's variational ansatz [60]. On the torus, the ground state is twofold degenerate [45, 87]. Excitations about these two degenerate ground states require overcoming an energy gap  $\Delta \sim J_{NN}$ . The quasiholes are abelian anyons, and the Berry matrix in the ground state subspace should be the identity times a phase of  $\pm\pi/2$ , depending on the direction of the exchange path [134, 133]. This is consistent with our numerical studies of the path in Fig. 1(a). Since a complete braid of one quasihole around another is equivalent to two exchanges, we find a phase of  $\pi$  for the path 1(c). As expected, when we introduce more impurities, we find that near  $\nu_{\text{eff}} = 1/2$  all braids commute.

A generic potential splits the two-fold degeneracy of the ground state by a small energy  $\epsilon$ . We attribute these splittings to interactions between the quasiparticles when they are moved close to one another. By optimizing the shapes

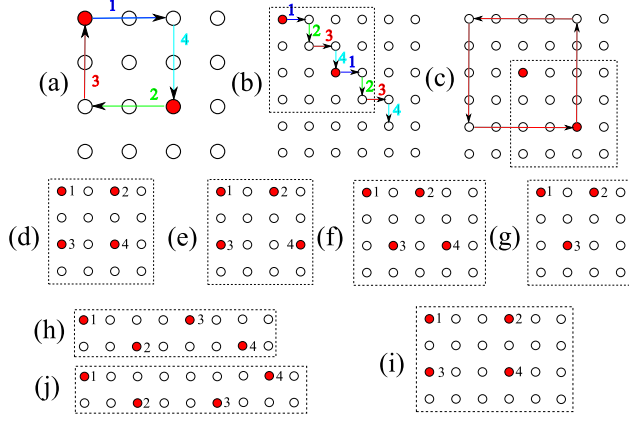


Figure 3.1: (Color online) (a)–(c) Exchange paths used to braid quasiparticles on various lattices. In each path, the impurities (shaded red) are incrementally moved along the segments (1,2,3...) until they return to their starting positions, exchanged. The dashed box represents the periodic lattice boundary. (d)–(i) show the initial configurations of the impurities for the 3- and 4- impurity braids.

of the potential at each time step, we can make  $\epsilon < 0.02\Delta$  for all points in the  $\nu_{\text{eff}} = 1/2$  braid. While largely irrelevant for  $\nu_{\text{eff}} = 1/2$ , this optimization can be crucial for producing sensible results near  $\nu_{\text{eff}} = 1$  or  $3/2$ . If the trajectory is traversed in a time  $T$  such that  $\hbar/\Delta \ll T \ll \hbar/\epsilon$ , these splittings have no physical effect, and we therefore neglect them when calculating  $M$ . The splittings can be further reduced by using larger systems. Detailed graphs of our optimized potentials are shown in the supplemental information [59].

The physics near  $\nu_{\text{eff}} = 1$  and  $3/2$  is richer. At  $\nu_{\text{eff}} = 1$  for  $U_2$  small, all particles are in the lowest Landau level and the ground state  $\Psi_G$  has a large overlap [24] with the Moore-Read (M-R) Pfaffian state  $\Psi_{\text{MR}}$  [82, 80, 41, 94, 83, 32], a state with non-Abelian excitations. We typically perform our calculations using hard-core interactions, for which mixing with excited bands is significant and the overlap is smaller:  $|\langle \Psi_{\text{MR}} | \Psi_G \rangle| < 0.3$ . Despite the small overlaps, the ground state with hard-core interactions is expected to be adiabatically connected to the M-R

Lattice	$N$	$N_\phi$	$N_{\text{imp}}$	GFS	$\nu_{\text{eff}}$	Braid Path/Phases (all $\times\pi$ )
<i>Abelian</i>						
$4 \times 4$	3	8	2	G	1/2	(a) (0.49,0.49), (c) (0.99,0.99)
$4 \times 4$	6	8	2	F	1	(a) (0,0.99), (b) (0,1)
$4 \times 4$	7	8	2	G	7/6	(b) (0,1)
<i>Non-abelian</i>						
$6 \times 4$	4	8	4(i)	S	1	$R_{12}, R_{34} : (0.28, -0.28)$ $R_{24} : (-0.26, -0.75)$ $R_{13} : (0.22, -0.22)$
$4 \times 4$	7	8	3(g)	F	7/5	$R_{13}, R_{23} : (0.08, 0.73)$ $R_{12} : (0.08(1), 0.76(4))$
<i>Ambiguous</i>						
$4 \times 4^*$	4	8	4(d)	F	1	$R_{12}, R_{13}, R_{24}, R_{34} : (0, 1)$
$4 \times 4$	7	10	4(e)	F	7/6	$R_{12}, R_{13}, R_{24}, R_{34} :$ $(0.25(2), -0.25(2))$
$5 \times 4$	4	10	4(f)	G	2/3	$R_{12}, R_{34} : (-0.75, 0.75),$
$8 \times 2$	6	8	4(h)	F	3/2	$R_{12}, R_{34} : (0.32, -0.32)$ $R_{23}, R_{14} : (0, 1)$
$9 \times 2$	9	10	4(j)	F	3/2	$R_{34} : (0.69, -0.69)$

Table 3.1: The results of our numerical braiding studies. Here,  $N$  is the total particle number,  $N_\phi$  is the total number of flux quanta, and  $N_{\text{imp}}$  impurity sites have a repulsive potential applied. ‘‘GFS’’ refers to whether the degenerate pair of eigenstates are the ground (G), first excited (F) or second excited (S) states. The braids are each characterized by a unitary matrix with eigenvalues  $e^{i\pi p_1}, e^{i\pi p_2} \rightarrow (p_1, p_2)$ . The exchange paths are shown in Fig. 1, with  $R_{ij}$  denoting the exchange of impurities  $i$  and  $j$ . The algebras in the non-abelian cases approximate those described in the text [38, 50]; cases labeled as ambiguous contain non-commuting paths but the transformations associated with these paths depended on the details of the path and/or did not match the analytical predictions. Due to finite size splitting, not all paths were accessible on all lattices; only paths which led to a sensible braid and which were stable against small changes in the impurity strength  $V_j$  are quoted here. Hard core interactions ( $U_2 = \infty$ ) were used in all cases except  $4 \times 4^*$ , where we also used ( $U_2 = 0, U_3 = \infty$ ). These two interactions gave nearly identical results.

state, and should share topological invariants such as exchange statistics. The M-R state is the exact ground state [41] of a Hamiltonian with repulsive three body interactions ( $U_2 = 0, U_3 > 0$ ). As we expand on below, we find excellent agreement between calculations using the two- and three-body interactions.

The M-R state is gapped and has two types of fundamental vortex excitations. In addition to the full QHs described earlier, the M-R state has half-quasihole (HQH) excitations, which bind half a flux quantum, partially exclude particles from their location, and are non-abelian Ising anyons [82]. Wavefunctions of the M-R type with  $2n$  HQHs are  $2^{n-1}$ -fold degenerate [83] in the limit that all the HQHs are far apart. Given our strong impurity potentials ( $V_j \geq J_{NN}$ ), we expect each repulsive impurity to bind a full QH and a half quantum vortex. Exchanging two HQHs performs a  $\pi/2$  rotation within the degenerate subspace, and the rotations produced by exchanging different pairs of HQHs do not generally commute. Up to abelian phases, for four HQHs there is a basis [53, 16, 33] in which the braid matrices take the form

$$R_{12} = R_{34} = e^{-i\frac{\pi}{4}\sigma_y}, R_{13} = R_{24} = e^{-i\frac{\pi}{4}\sigma_x}. \quad (3.4)$$

To estimate the overlap of the unitary transformations which result from our braids with the predictions of the analytical theories of Bose quantum Hall states, we use the matrix overlap measure  $(M_1, M_2) \equiv |\text{tr}(M_1 M_2^\dagger)|/2$ . This quantity is insensitive to overall phases or changes to the shared basis of  $M_1$  and  $M_2$ , and we consider two unitary matrices to be equivalent if  $|\text{tr}(M_1 M_2^\dagger)|/2 = 1$ .

For the case of  $N = 4, N_\phi = 8$  and  $N_{\text{imp}} = 4$  on the  $6 \times 4$  lattice (where two impurities need never be nearest or next-nearest neighbors in a braid), our numerical results are in remarkable agreement with eq. (3.4). Labeling the analytical predictions by  $R$  and the numerical matrices  $M$ , we can find a basis where

$$(R_{12}, M_{12}) = (R_{34}, M_{34}) = 0.99, (R_{24}, M_{24}) = 0.98 \text{ and } (R_{13}, M_{13}) = 0.97.$$

When impurities are allowed to approach more closely, however, the numerical results diverge from the analytical predictions, and in many cases, the exchange of two strong impurities produces a rotation by  $\pi$ . We conjecture that this represents the exchange of two pairs of HQHs, which either do not sit directly on the impurities but move with them as they are exchanged, or experience tunneling events when impurities move too close to one another. For the case of a  $4 \times 4$  lattice with  $N = 4$ ,  $N_\phi = 8$  and  $N_{\text{imp}} = 4$ , we obtained identical results when considering the ordinary hard-core two-body or a hard core three-body interaction, where the M-R state is the exact ground state [41]. For  $N = 7$  and  $N_\phi = 10$  on the same lattice (Fig. 3.1e), we consistently obtained rotations by  $(0.5 \pm 0.03)\pi$ , but the matrices which resulted were not straightforwardly related to the analytical predictions in eq. (3.4), and depended strongly on the path by which a pair of impurities were exchanged. These results show that the precise relationship of the non-abelian vortices to the impurities is subtle [125, 52, 93, 111]. Further, they reveal that the Berry matrices can be strongly modified for paths whose impurities come close together. Surprisingly, the degeneracies are not necessarily broken by these close approaches.

Finally, near  $\nu_{\text{eff}} = 3/2$  (fig. 3.1g,h,j), we obtained a result consistent with the predictions for a Fibonacci anyon theory [50], the effective theory of the Read-Rezayi state at  $k = 3$  [95]. Previous numerical studies of continuum bosons in the LLL [24] have found strong evidence for this state, a particularly exciting result since Fibonacci anyons are capable of universal topological quantum computing. Comparing our numerically derived matrices at  $(N = 7, N_\phi = 8$  and  $N_{\text{imp}} = 3)$  with the transformations derived by Hormozi et al. [50], we ob-

tained  $(R_{13}, M_{13}) = 0.99$  and  $(R_{23}, M_{23}) = 0.90$ . However, for the exchange of impurities 1 and 2, we found two sensible paths (a) and (b); in path (a) impurity 3 was allowed to move during the braid and in (b) it was not. We found that  $(R_{12}, M_{12}(a)) = 0.93$ , but  $(R_{12}, M_{12}(b)) = 0.69$  and  $(M_{12}(a), M_{12}(b)) = 0.46$ . As discussed above, this disagreement is likely due to tunneling events when the impurities approached as next-nearest neighbors. For the  $8 \times 2$  and  $9 \times 2$  lattices, we obtained rotations of nearly  $3\pi/5$  as predicted, but the resulting matrices had little overlap with those predicted from the Fibonacci anyon theory.

### 3.4 Summary and Conclusions

In summary, we have numerically studied a realistic model, eq. (3.1), which has anyon excitations at filling fraction  $\nu_{\text{eff}} = 1/2$ , and non-abelian anyons at  $\nu_{\text{eff}} = 1$  and  $3/2$  analogous to those in the Moore-Read and Read-Rezayi states. These results suggest adiabatic continuity between the states of our lattice model with hard-core interactions and those found purely in the LLL [24], to which our model reduces in the limit of weaker on-site interaction. We have also shown that surprisingly small lattices can reproduce infinite-system predictions, without resorting to trial wavefunctions. This robustness is likely related to the topologically protected nature of the states, and is encouraging for future experiments.

The most intriguing implication of our result is in quantum computation. In recent years, a wealth of theory [82, 16, 13, 33, 38] has shown that the M-R state of electrons at  $\nu = 5/2$  could be used to construct topologically protected quantum memory and quantum computing operations, and has described potential

implementations. While non-abelian statistics in the  $\nu = 5/2$  state have not yet been confirmed experimentally, the fact that the  $\nu = 1$  M-R state and the  $\nu = 5/2$  M-R state are in the same universality class implies that the theory for manipulating quasiholes in the  $\nu = 5/2$  electron gas can be applied directly to our lattice boson system. Our  $\nu = 3/2$  results are even more exciting since the Read-Rezayi states can be used to construct a universal set of quantum gates. Implementing our model in a Josephson junction array would open a new area of physics to study topological noise protection and non-abelian statistics, since for  $\phi \leq 1/4$  three non-abelian plateaux ( $\nu = 1, 3/2,$  and  $2$ ) could be studied in the same experiment. The ability to individually address any lattice site would provide an unprecedented ability to manipulate quasiholes [33], potentially creating a truly universal “quantum loom.”

### 3.5 Acknowledgments

We thank Chetan Nayak, Andrei Bernevig, Chris Laumann and Chris Henley for useful discussions. This work was supported by an Army Research Office grant with funding from the DARPA OLE program, by NSF grant PHY-1068165 and by the Department of Defense (DoD) through the National Defense Science and Engineering Graduate (NDSEG) program.

## CHAPTER 4

### EQUATION OF STATE OF QUANTUM HALL BOSONS IN A LATTICE

This work was done in collaboration with Erich Mueller, and is in preparation for publication.

#### 4.1 Introduction

Recent experimental advances have made the study of exotic quantum Hall states in bosons increasingly relevant [25]. While the quantum Hall effect in fermions has been the subject of an enormous body of theoretical and experimental studies in two dimensional electron gases [92, 141], the bosonic equivalent has been less studied. The most promising systems for experimentally studying Bose quantum Hall physics include arrays of superconducting qubits (where two states of the qubit can act the presence or absence of a hard core boson) [131, 28, 85], “photon lattices” of coupled optical waveguides [42, 127] and neutral cold atoms [10], where an effective magnetic field may be introduced through rotation [24, 100, 21, 120, 136, 36] or more exotic means [81, 43, 71, 109, 72, 22, 4, 25]. While experimental challenges (noise and defects in superconducting arrays [28, 20], weak effective interactions in waveguides, heating and weak effective fields in cold atoms [10, 21, 77]) have thus far prevented the realization of bosons in the quantum Hall regime [41, 97, 23, 43, 108, 78, 60, 114, 57, 59], tremendous progress has been made in recent years and we expect that this physics will be demonstrated in the near future. Here we study systems of strongly interacting lattice bosons in an effective gauge field. By explicitly computing the equation of state we demonstrate how fractional quantum Hall states can be observed in cold atoms through *in*

*situ* density imaging.

We study lattice bosons for a number of reasons. First, lattice bosons display all of the physics of continuum bosons, as well as additional phenomena not seen in the continuum [47, 64, 5, 43, 89, 108, 142, 129, 60, 128, 49]. Second, some of the most promising ideas for creating analogs of magnetic fields in cold atoms rely on a lattice, where the effective gauge field manifests itself through Pierels-like phases in the hopping matrix elements. *Staggered* fields strong enough to reach the lowest Landau level regime have been already been demonstrated [4]; effective gauge fields of this magnitude are extremely difficult to produce in the continuum. Third, the most plausible solid state realizations of bosonic quantum Hall states are in lattices. Fourth, lattice systems are more amenable to numerical simulation than continuum systems. They require a smaller computational basis than the continuum, removing the need for approximations such as projection into the lowest Landau level. Finally, in a recent work [60] we showed that adding longer ranged hopping terms to a Bose Hubbard model can exactly reproduce the continuum lowest Landau level, providing a bridge between the two systems.

To study these bosons, we numerically diagonalize the full many-body Hamiltonian on small lattices and average over twisted boundary conditions to minimize finite size effects. Defining the filling fraction  $\nu$  to be the ratio of particle density to flux density, our results show the unambiguous existence of gapped states at filling fraction  $\nu = 1/2$  (corresponding to a Laughlin state), [43, 108, 60] and at  $\nu = 1$  (a paired state with non-Abelian excitations) [80, 32, 82, 117, 59], as well as additional plateaus at other interesting filling fractions. The existence of gaps at these filling fractions leads to a staircase of

incompressible states, which could be observed in an optical lattice experiment as plateaus in the radial density distribution  $n(\mathbf{r})$  [138, 31, 37, 36]. By directly calculating the gaps and examining the resulting finite-temperature density profiles, we can place upper limits on the temperatures at which these effects could be observed. In addition, some of the filling fractions where we observe gaps are anomalous, suggesting a rich array of exotic quantum Hall or charge density wave states in the interacting lattice boson system worthy of further experimental and theoretical study.

We also study the role of hopping range on the stability of FQH states. We recently showed that the addition of specially chosen longer-ranged hopping amplitudes to a lattice model can yield a massively degenerate single-particle manifold of ground state wavefunctions which are identical to the lowest Landau level (LLL) wavefunctions of the continuum limit [60]. In addition to this Gaussian hopping model, we study models with nearest neighbor (Hofstadter) and nearest (NN) and next nearest neighbor (NNN) hoppings. In the latter case we choose the ratio of the hopping matrix elements to coincide with the Gaussian model. We find that the equation of state is very sensitive to this choice of hopping. In particular, both the next nearest neighbor and Gaussian models possess significantly more robust fractional quantum Hall (FQH) states, which are visible at much higher temperatures. Engineering challenges associated with adding NNN hopping seem to be well worth attempting.

The remainder of this paper is organized as follows. In the next section, we review the Gaussian hopping model and describe our numerical methods for calculating the system's partition function. We then present our results, discussing the structure of the series of incompressible states and providing an es-

timate of their gaps and associated observability temperatures. We take care to illustrate the effect of short- and long-ranged hopping amplitudes on the quantum hall states, and provide an outlook for observing them in future experiments.

## 4.2 Methods and Hamiltonian

### 4.2.1 System Hamiltonian

Throughout this work, we study the Bose-Hubbard Hamiltonian

$$H_u = - \sum_{jk} \left( J_{jk} e^{i\phi_{jk}} a_j^\dagger a_k + H.C. \right) + \frac{U}{2} \sum_j n_j (n_j - 1). \quad (4.1)$$

Here,  $j$  and  $k$  denote lattice sites on a two-dimensional square lattice,  $J_{jk}$  is a real hopping amplitude, and  $U$  is a local repulsion term. The subscript  $u$  in  $H_u$  denotes that this is the uniform system Hamiltonian. We work in the hard core limit of  $U \rightarrow \infty$  to reduce the size of our computational basis by forbidding double occupancy of any lattice sites. The Peirels phase  $\phi_{jk}$  is best defined by introducing a complex representation of the sites:  $z_j = x_j + iy_j$ , with  $x_j$  and  $y_j$  integers. In the symmetric gauge, the Pierels phases  $e^{i\phi_{jk}}$  are

$$i\phi_{jk} = -\frac{\pi\phi}{2} \left[ -z_j z_k^* + z_j^* z_k \right]. \quad (4.2)$$

This Hamiltonian is an excellent description of atoms in an optical lattice with an artificial gauge field, and can accurately describe the behavior of Cooper pairs in a Josephson junction array if  $U$  is large compared to  $J$ .

To better approximate a larger system, we perform our calculation in twisted, magnetoperiodic boundary conditions defined by twist angles  $\{k_x, k_y\}$ ,

so that

$$\begin{aligned} \Psi(z_j + nL_x + imL_y) = \\ e^{i(nk_x L_x + mk_y L_y) + \frac{\pi}{2}(z_j R^* - z_j^* R)\phi} \Psi(z_j), \end{aligned} \quad (4.3)$$

where  $R = nL_x + imL_y$ , when a single particle is translated by one entire lattice period. For a single particle, all the eigenvalues of (3.1) on an arbitrarily large lattice may be found by simply diagonalizing the Hamiltonian on a smaller lattice for a sufficiently large number of twist angle pairs. While this equality does not hold for multiparticle states, twist angle averaging is an (uncontrolled) way to reduce boundary effects. One imagines that a fraction of the finite size effects will average to zero for a suitably large number of twist angle pairs. The data presented here are computed on lattices averaged over twenty five randomly chosen pairs of  $\{k_x, k_y\}$ , always including  $\{0, 0\}$ .

In a previous work, we demonstrated that, on an infinite lattice, if  $J_{jk}$  in (3.1) takes the form

$$\begin{aligned} J_{jk} &\equiv J(z_j - z_k) = J(z), \\ J(z) &= J_0 G(z) \exp\left(-\frac{\pi}{2}(1-\phi)|z|^2\right), \\ G(z) &= (-1)^{1+x+y+xy} \end{aligned} \quad (4.4)$$

(where  $J_0$  is a constant energy scale) the lowest  $\phi L^2$  single particle eigenstates collapse to a single massively degenerate band [91, 67, 60, 40]. This degeneracy is related to the fact that these states are precisely the exact lowest Landau level eigenstates of the continuum problem, which in the infinite  $L$  limit are

$$\psi_n(z_j) = (z_j)^n e^{-\frac{\pi\phi}{2}|z_j|^2}. \quad (4.5)$$

Here,  $n$  is an integer with  $0 \leq n \leq N_\phi$ , where  $N_\phi$  is the total number of magnetic flux quanta in the system. In a finite lattice with magnetoperiodic bound-

ary conditions, the eigenstates are instead described by the Jacobi elliptic theta functions [1, 45, 133, 134], and the hopping amplitudes are replaced by their sum over lattice periods,

$$J(z_j, z) \rightarrow \sum_R J(z_j, z + R) \exp\left(\frac{\pi}{2}(z_j R^* - z_j^* R)\phi\right). \quad (4.6)$$

The degeneracy and ground state energy are unchanged. A plot of the distribution of eigenvalues vs  $\phi$  is shown in fig. 4.1. For any value of  $\phi$ , the ground state band gap (defined to be average energetic spacing between the states in the lowest and first excited Hofstadter bands) is increased by the longer-ranged hopping terms, an effect that is most pronounced as  $\phi$  approaches 1/2, where the Hofstadter spectrum [47] becomes gapless while the Gaussian hopping model's gap is large. Since the nearest neighbor hopping value varies with  $\phi$  in this model, for the remainder of this work we will express all energy scales in terms of the nearest neighbor hopping parameter  $J_{NN} = J_0 \exp -\frac{\pi}{2}(1 - \phi)$ . For examples of similar lattice models with a nonzero Chern number and a (nearly) flat ground state band, see [112, 113, 132, 84, 96].

## 4.2.2 Local Density Approximation

Since the primary focus of this work is on cold atom systems, we need to account for the fact that real experiments will be performed on clouds held in a harmonic trap. To implement the trap potential, we add to the uniform system Hamiltonian  $H_u$  a position dependent chemical potential  $-\sum_j \mu_j n_j$ . In an optical lattice, the Hamiltonian becomes

$$H = H_u + \frac{m\omega_t^2}{2} \sum_j n_j \mathbf{r}_j^2. \quad (4.7)$$

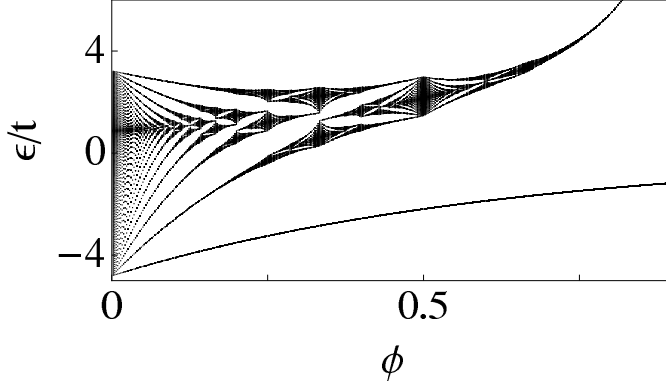


Figure 4.1: Eigenvalues of the Gaussian hopping model (4.4) as a function of  $\phi$  for  $J_{NN} = t$ . The energies diverge as  $\phi$  approaches 1 since the hopping amplitudes become infinite-ranged in this limit. The lower band is an exactly degenerate LLL and contains  $\phi L_x L_y$  degenerate states on an  $L_x \times L_y$  lattice. The excited bands are qualitatively similar to the fractal bands of the nearest neighbor (Hofstadter) model, and are analogous to the excited Landau levels of the continuum problem, albeit without the exact degeneracy of the continuum Landau levels. The gap from the lowest Landau level to the first excited band scales linearly with  $\phi$  for small  $\phi$ , but by  $\phi = 1/4$  it is approximately constant, increasing by only  $\sim 14\%$  from  $\phi = 1/4$  to  $\phi = 1/2$ . Beyond  $\phi = 1/2$ , it increases and eventually diverges as the hopping becomes infinite ranged.

We shall assume that this potential is slowly varying over the magnetic length scale, which in units of the lattice spacing  $a$  is

$$l_B/a = \frac{1}{\sqrt{2\pi\phi}}. \quad (4.8)$$

Under this constraint we can treat the system in the local density approximation (LDA), under which the properties of the system near  $\mathbf{r}$  can be calculated from the partition function of a uniform system with  $\mu = \mu(\mathbf{r})$ . For the fluxes considered ( $1/4 \leq \phi \leq 1/2$ ), the magnetic length is less than a lattice spacing; note that in relative terms these fluxes are orders of magnitude larger than the real magnetic flux in a typical 2DEG experiment, when compared to the spacing of the atomic crystal lattice. Corrections to the LDA should scale as powers

of  $m\omega_i^2 ra/J_{NN}$ , and for appropriately shallow traps these effects should only become significant at the cloud edges, where the density vanishes and we do not expect FQH physics.

One important caveat to our study is that we are unable to calculate  $\mu(n)$  for arbitrary  $n$ , since we cannot diagonalize states with non-integer numbers of particles. This means, for example, that the plateau for  $\nu = 3/4$  seen in the  $4 \times 4$  lattice with flux density  $\phi = 1/2$  is not present in the density profile computed for the same flux density on a  $5 \times 4$  lattice, since  $\nu = 3/4$  describes a state with 7.5 particles on that lattice. Our calculation may therefore fail to predict states which would arise in larger systems; however, the large range of lattices and flux densities studied here will partially compensate for this.

### 4.2.3 Many-Body States

The central purpose of this work is to investigate the density signatures of the exotic correlated states which are found at rational filling fractions. In this section we review the properties of some of these states. Non-interacting fermions exhibit a staircase of incompressible states whenever a Landau level is filled ( $\nu$  integer); these states are magnetic band insulators with a gap equal to the Landau level spacing. Non-interacting bosons, on the other hand, cannot fill a Landau level due to Bose statistics, and simply form a condensate of LLL states [46] at zero temperature. A gapped state of bosons at any filling fraction must therefore be driven by interactions and indicates exotic physics. The simplest such state on a lattice is the Laughlin state [66, 45] at  $\nu = 1/2$ ,

$$\Psi_L(\{z_j\}) = \prod_{i<j} (z_i - z_j)^2 \prod_i e^{-\frac{\pi\phi}{2}|z_i|^2}, \quad (4.9)$$

where the  $z_i$  are complex coordinates on the square lattice. This wavefunction is the product of Gaussians and a symmetric polynomial (called a Jastrow factor) which vanishes quadratically as two particles approach each other, and therefore minimizes the contact interaction in (3.1). The highest power of  $z$  allowed in a LLL state (4.5) is  $N_\phi - 1$ , so the wavefunction of the above state with one more particle added at  $z_{N+1}$  must either allow for double occupancy ( $\Psi$  nonvanishing as one or more  $z_i$ 's approach  $z_{N+1}$ ) or promote particles into the first excited band, increasing the energy of the state in either case. This finite energy cost ensures that the system is gapped at  $\nu = 1/2$ . The  $\nu = 1/2$  state is unique up to a topological degeneracy dependent on the system's boundary conditions. For a system of LLL bosons with contact interactions only, all states with  $\nu < 1/2$  are compressible, since they can be written as the product of any symmetric polynomial of appropriate degree with (4.9), and therefore a large degeneracy persists. In our Gaussian hopping model the Laughlin state is the exact ground state, and even for nearest neighbor hopping it is still a good description of the ground state at  $\nu = 1/2$  for low flux densities [43, 108].

More interesting are the states with odd-denominator filling fractions, such as  $\nu = 1$ , which are believed to be bosonic analogues of the  $\nu = 5/2$  Moore-Read state in 2DEGs [80, 32, 94, 95, 82]. The Moore-Read state of bosons at  $\nu = 1$  is

$$\Psi_{Pf}(\{z_j\}) = \text{Pf} \left[ \frac{1}{z_i - z_j} \right] \prod_{i < j} (z_i - z_j) \prod_i e^{-\frac{\pi\phi}{2}|z_i|^2}. \quad (4.10)$$

The additional factor is given by the Pfaffian of an antisymmetric matrix with entries  $M_{ij} = (z_i - z_j)^{-1}$ . It can alternately be written as an antisymmetrized sum over all the ways the  $z_N$  particles can be paired.

The Pfaffian wavefunction (4.10) no longer vanishes as any pair of particles approach each other; however, within the limit of the LLL projection (where  $\omega_{LL}$

is large compared to the product of  $U$  with the particle density squared) and restricted to two-body contact interactions, it is a very good description of the ground state. We performed a Monte Carlo evaluation of its interaction energy for up to  $N = 64$  particles at various particle densities and obtained an average energy of  $E_{Pf} = 0.08UN$  at  $\phi = 1/2$ , a savings of better than a factor of three compared to an uncorrelated state (note that the Pfaffian wavefunction does vanish when *three* or more particles coincide). In the  $U \rightarrow \infty$  limit, the Pfaffian wavefunction (4.10) is no longer a good description of the ground state since it does not screen double occupancy. However, for  $\phi = 1/2$ , (4.10) has a lower ground state energy than the numerically calculated  $U \rightarrow \infty$  ground state of the Gaussian hopping model for  $U < 4.5J_{NN}$  (note that this is approximately equal to the total bandwidth). Above this value there will be some promotion to higher bands within the true ground state, although the important physical properties (including the degeneracy and braid properties of the low-lying excitations) are unchanged in the large  $U$  limit, a fact confirmed by our numerical studies of impurity braiding [59] and topological entanglement entropy (unpublished).

Finally, in addition to these gapped quantum Hall fluids, which also occur in the Jain sequence of composite fermion states [97], at the appropriate particle and flux densities the system can also stabilize charge density wave states, analogous to the Wigner crystal phase of 2d electrons. These states can have a ground state energy gap and can be difficult to distinguish from the quantum Hall states through exact diagonalization, since the small size of the lattice makes it impossible to distinguish long-ranged order from short ranged antiferromagnetic density correlations. For example, we find an anomalously large gap in the Hofstadter model for  $\nu = 1$  on a  $6 \times 3$  lattice with  $N_\phi = 6$ , which could indicate a competing charge density wave state, since the CDW would

be commensurate on this lattice. While beyond the scope of this work, quantum Hall states can be identified through numerical calculation of the system's Chern number [108], topological entanglement entropy [63, 68, 29, 144, 70, 26] or quasiparticle braiding statistics. Further, in a real experiment, the gapped plateaus may be dozens of sites wide, making it possible to use real-space imaging to extract the long-ranged order parameter of the density wave states.

## 4.3 Results and Discussion

### 4.3.1 Equation of State

We computed the equation of state for various flux densities on  $4 \times 4$ ,  $5 \times 4$  and  $6 \times 3$  lattices with magnetoperiodic boundary conditions. Sample density profiles are plotted in figures 4.2 and 4.3 as a function of chemical potential  $\mu$ . These profiles can be mapped onto in-trap density profiles through the local density approximation  $\mu \rightarrow \mu_0 - m\omega_t^2 \mathbf{r}^2 / 2$ .

Of primary concern are the widths of the plateaus as a function of  $\mu$ , since wider plateaus are both easier to resolve in density imaging and more robust at finite temperature. In fig. 4.4(a,b), we present the scaling of the widths of  $\nu = 1/2$  and  $\nu = 1$  plateaus with the flux density  $\phi$ , where  $W$  is the width of the range in  $\mu$  at a specific filling fraction across which the compressibility  $\partial n / \partial \mu$  vanishes in the limit of  $T \rightarrow 0$ . In fig. 4.4(c), we present a scatter plot of the all plateau widths  $W$  derived in our calculations as a function of filling fraction  $\nu$ . To be observed in a real experiment, a plateau must be large compared to both the lattice spacing and the imaging resolution, so the energetic widths plotted

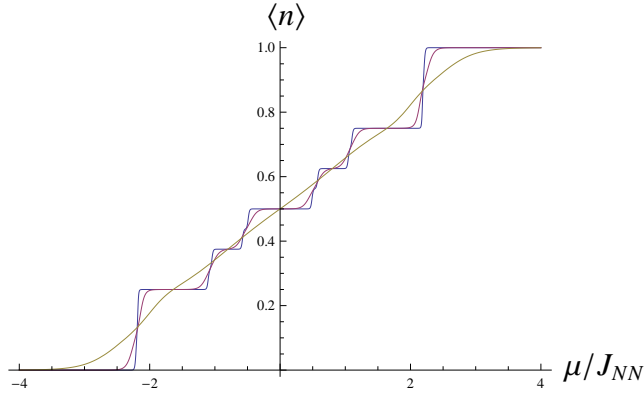


Figure 4.2: (Color online) The effect of temperature on the equation of state for a  $4 \times 4$  lattice with 8 fluxes using Gaussian hopping parameters. The curves for the  $4 \times 4$  lattice were calculated for the Gaussian hopping model for  $T = \{0.01, 0.05, 0.25\} J_{NN}$  (blue, purple, gold) and demonstrate the effect of temperature on the observability of the plateaus in  $\partial \langle n \rangle / \partial \mu$ . While the signatures of the plateaus at  $T = 0.25 J_{NN}$  are difficult to discern by eye, traces of the  $\nu = 1/2$  plateaus are visible as weak local minima in  $\partial n / \partial \mu$ .

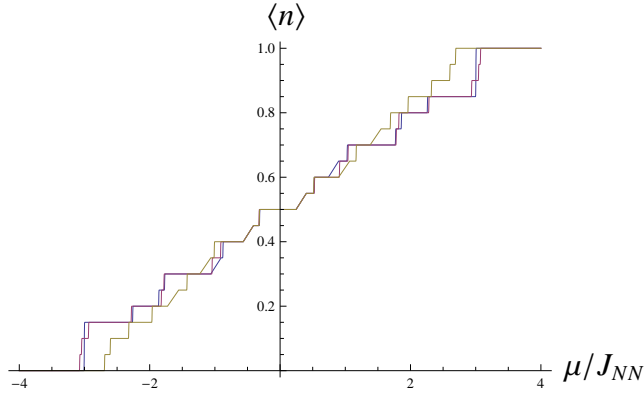


Figure 4.3: (Color online) The effect of hopping parameter choices on the equation of state, demonstrated in a  $5 \times 4$  lattice with 6 fluxes for  $T \rightarrow 0$ . The three choices of hopping parameters are Gaussian (blue), NN and NNN (purple), and NN only (gold). The increased plateau width for longer-ranged hopping is clearly apparent. For larger fluxes ( $\phi \sim 1/2$ ) additional terms beyond NNN hopping must be included to match the Gaussian model results.

in fig. 4.4 can be used to estimate the requisite shallowness of the trap in order to observe the quantum Hall plateaus. We caution that, for the system sizes studied, finite size effects are large and likely dominated by commensurability, which tended to increase the plateau width relative to incommensurate cases at similar flux densities.

In the vast majority of cases, longer ranged hopping enhances the plateau width  $W$  compared to the nearest neighbor (Hofstadter) case. While at high fluxes near  $\phi = 1/2$  the full long ranged model must be considered to dramatically increase  $W$ , at low flux densities such as  $\phi = 1/3$  or  $\phi = 1/4$  the next nearest neighbor term is sufficient to reproduce the results of the exact model to within a few percent. In these cases, next nearest neighbor hopping increases the gaps and observability temperatures by up to a factor of 2, which could be the difference between confirming the existence of incompressible states or not, since we expect the nearest neighbor hopping term to be on the order of a few nK in the large  $U$  limit. An unweighted average of all particle and flux densities studied on the  $4 \times 4$ ,  $6 \times 3$  and  $5 \times 4$  lattices gives  $W_{\nu=1/2}/J_{NN} = \{0.79, 0.65, 0.38\}$  for the Gaussian model, NN and NNN hopping, and the Hofstadter model, respectively. Similarly,  $W_{\nu=1}/J_{NN} = \{0.54, 0.45, 0.41\}$  for these choices of hopping amplitudes. On average, the plateau width at  $\nu = 1/2$  increased by 66% with the addition of next nearest neighbor hopping, whereas the plateau at  $\nu = 1$  is increased by about 10%.

From these plots and calculated plateau widths, we can estimate approximate temperature scales below which the Bose quantum Hall states can be observed. These states have no local order parameters; rather, they are distinguished by topological quantities, such as the existence of anyon excitations or

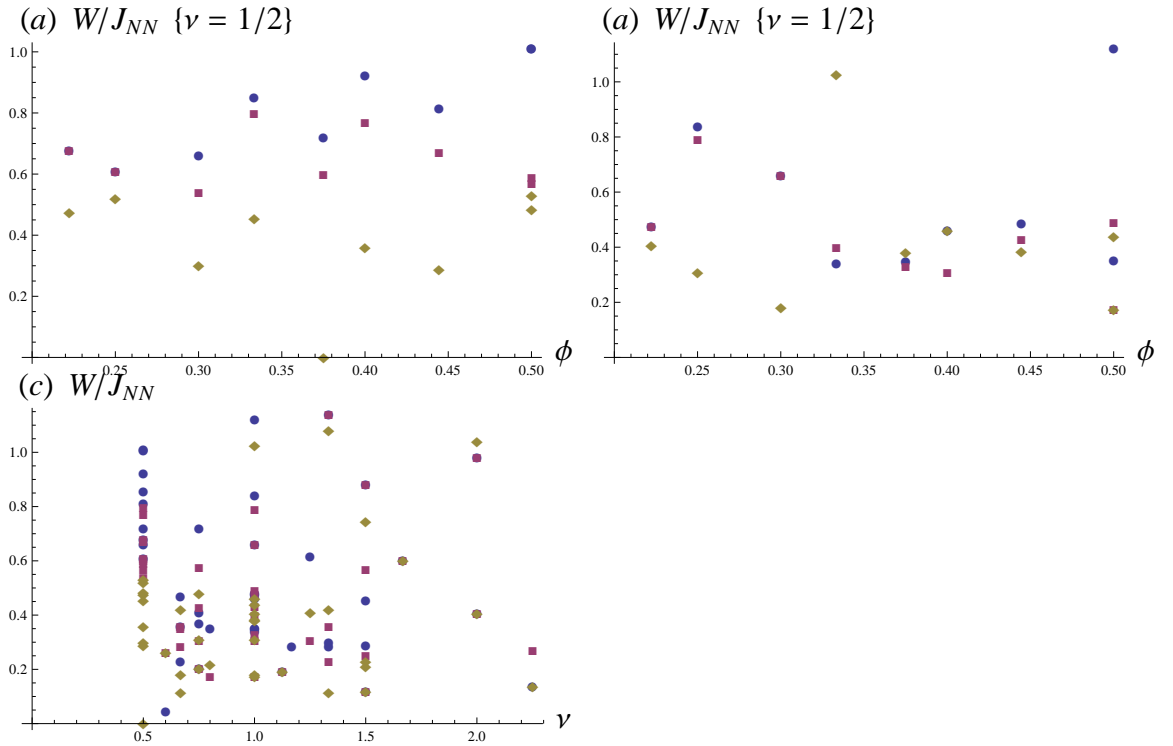


Figure 4.4: (Color online) (a,b) Plateau widths vs  $\phi$  at  $\nu = 1/2$  (a) and  $\nu = 1$  (b) vs  $N_\phi$  for various lattice sizes. Blue circles correspond to the Gaussian hopping model, purple squares to NN and NNN hopping, and gold diamonds to the Hofstadter model. These widths are extracted by finding the width in  $\mu$  for which  $\partial n/\partial \mu$  vanishes as  $T \rightarrow 0$ . Anomalously large gaps at  $\nu = 1$  occurred when the flux was commensurate and could indicate competition from charge density wave order. Due to the small system sizes studied, density correlations are insufficient to separate charge density wave states with long-range order from fractional quantum Hall liquids with short-ranged antiferromagnetic correlations. Longer ranged hopping increases  $W$  in every case at  $\nu = 1/2$  and in most cases at  $\nu = 1$ . At lower fluxes, the NNN and Gaussian results were nearly identical. (c) Scatter plot of all plateaus observed in our calculations, as a function of  $\nu$ . Gaps tend to decrease with increasing  $\nu$ . Most of the filling fractions shown (such as  $\nu = 3/4$  or  $5/4$ ) are likely to be abelian composite fermion states [97]; the states at  $\nu = 1$  and  $3/2$  are likely to be non-abelian.

a finite Chern number. There is no finite-temperature phase transition from a compressible to an incompressible state (and no associated  $T_c$ ). Instead, as the temperature is lowered below the excitation gap  $\Delta$  the population of excitations becomes exponentially suppressed, causing a reduction in the compressibility  $\kappa = \partial n / \partial \mu$ , which vanishes exponentially for  $T \ll \Delta$ . We can therefore identify FQH plateaus at finite temperature by finding regions where  $\partial n / \partial \mu$  has a local minimum for  $n$  proportional to the flux density by a rational fraction. Note that it is difficult to determine a criteria for the observability of a plateau, as inhomogeneities in the optical potential, incomplete equilibration, finite size effects beyond the LDA and finite resolution uncertainties in measuring  $n$  and  $\partial n / \partial r$  are all factors complicating a real measurement, and not accounted for in our numerical simulations. With that caveat, local minima in  $\partial n / \partial \mu$  are typically visible until  $T \sim W/2$  in our study. Plateaus nearest to the particle-hole symmetry point  $\langle n \rangle = 1/2$  are typically more visible relative to their width than ones closer to  $\langle n \rangle = 0$  or 1.

While longer ranged hopping does enhance the stability of the FQH states, in the absence of the artificial gauge field, the next nearest neighbor hopping term in a square optical lattice is zero by symmetry since the optical potential is separable in the  $x$  and  $y$  directions. In most cases, the gauge field source violates this separability (for example, in light-assisted hopping setups such as the one realized by the Bloch group [4], particle tunneling amplitudes are highly anisotropic before the Raman lasers are turned on), and so we expect that the artificial gauge field source itself will generate next nearest neighbor hopping terms. Given an optical potential, the next nearest neighbor tunneling amplitudes can be calculated through a tight-binding model or an analysis of neighboring Wannier functions [10].

### 4.3.2 Total Entropy of the Trapped System

In studying trapped cold atomic systems, it is frequently more useful to consider the entropy per particle than the system temperature, which is difficult to measure [143]. For example, in the method developed by the Harvard group [7], selective tuning of on-site orbital excitation energies is used to engineer extremely high fidelity ( $S \simeq 0.01k_B$  per particle) Mott insulating regions in an optical lattice of bosons with extremely high fidelity. The system can then be tuned to experience phase transitions into different states, and if the rates for which the unit filling constraint is removed and the artificial gauge field is turned on are sufficiently slow, then the process is approximately adiabatic and the entropy will only increase at quantum phase transition points, such as the transition from a gapless superfluid to the Laughlin state at  $\nu = 1/2$ . By calculating  $S(T)$ , we can obtain an “observability entropy” from the observability temperatures ( $T \sim W/2$ ) described above. Since the total entropy will increase in the transition from a trapped BEC to the “wedding cake” structure of Mott insulator and quantum Hall states, the observability entropy provides an upper bound on the required entropy of the initial BEC to observe the quantum Hall plateaus after the system has re-equilibrated.

We calculate the entropy  $S = \partial_T (k_B T \log Z)$  as a function of  $T$  and local  $\mu$ , and then divide by  $L_x L_y$  to obtain an average entropy density per site, just as we obtained the particle density  $\langle n \rangle$ . We then set  $\mu(\mathbf{r}) = \mu_0 - m\omega_l^2 \mathbf{r}^2$  and integrate the calculated  $S$  and  $\langle n \rangle$  over  $\mathbf{r}$  to obtain the total entropy and total particle number, the ratio of which is the entropy per particle. We choose  $\mu_0$  and  $m\omega_l^2$  such that the cloud has a radius of approximately 50 lattice spacings and contains  $\sim 4000$  particles. Example  $S$  vs.  $T$  curves for various lattice and flux densities

are plotted in Fig 4.5.

From the average plateau widths described above, we can define an average target entropy by finding the average entropy per particle  $S/N$  for which  $T = W/2$ . For the Gaussian model in the trap potential described above,  $\langle S_{T=W/2} \rangle = 0.472k_B$  per particle for observing the  $\nu = 1/2$  plateau and 0.415 for observing the  $\nu = 1$  plateau. Similarly, for NN and NNN hopping these entropies are 0.446 and 0.377, and for the Hofstadter model they are both equal to 0.338. These entropies exceed the lowest values of  $S/N$  achieved through conventional cooling means (the record to our knowledge being  $S/N \sim 0.1k_B$  for bosons in an optical lattice [77]), though those experiments were performed in the weakly interacting regime without an artificial gauge field, which may itself be a significant heating source [25]. As mentioned earlier, far lower entropies have been achieved in Mott insulating regions, but absent an extremely difficult calculation of equilibration dynamics in the strongly interacting regime with an artificial gauge field, we cannot predict how much entropy will be gained in the phase transitions from the Mott insulator to the staircase of quantum Hall states.

Another concern is the equilibration time for the quantum Hall states to form. If the intrinsic timescale of the system is set by the inverse of the gap, then assuming  $J_{NN} = 5\text{nK} \simeq 108\text{Hz}$ , letting the gap be  $\Delta = J_{NN}/2$  gives a system timescale of  $\sim 19\text{ms}$ . Given that hold times in the trap are typically at most a few seconds, incomplete equilibration of the system could be a significant barrier to observing quantum Hall physics.

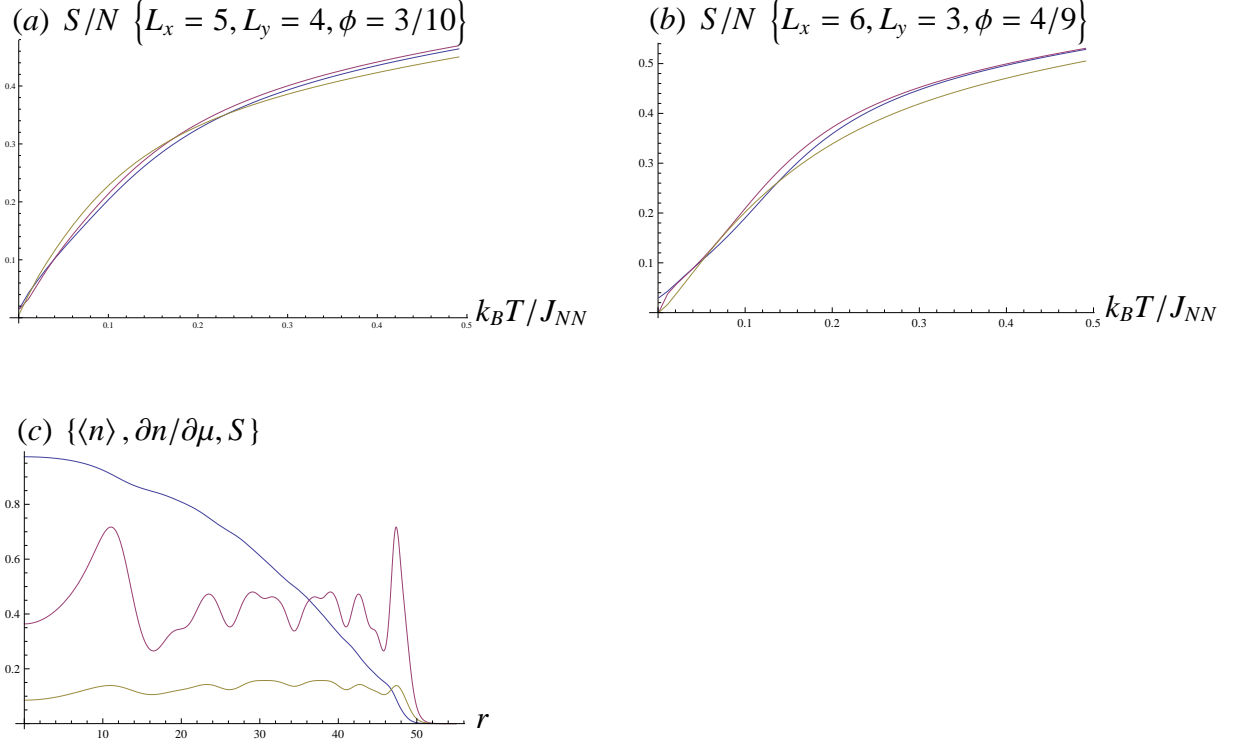


Figure 4.5: (Color online) (a,b) Trap-averaged entropy per particle as a function of  $k_B T$  for  $\phi = 3/10$  (a, calculated on a  $5 \times 4$  lattice) and  $\phi = 4/9$  (b, calculated on a  $6 \times 3$  lattice). The blue curve corresponds to the Gaussian hopping model, the purple to NN and NNN hopping, and the gold to the Hofstadter model. (c) Radial density (blue), compressibility ( $\partial n / \partial \mu$ , purple) and entropy density (gold) as a function of radial coordinate  $r$  for the Gaussian hopping model with  $\mu(r) = (3.3 - 0.0028r^2) J_{NN}$  and  $k_B T = 0.15 J_{NN}$ . Due to the finite system temperature,  $\partial n / \partial \mu$  does not vanish, but it does exhibit local minima at the appropriate rational filling fractions.

## 4.4 Conclusions and Outlook

Using numerical exact diagonalization, we computed the equation of state for strongly interacting quantum bosons in a lattice in an effective magnetic field. Our results suggest that incompressible bosonic quantum Hall states can be observed in cold gases through *in situ* density imaging in the near future. In particular, the zero temperature width of the plateau in  $\nu = 1/2$  Laughlin state is in the range of  $W \sim 0.5 - 1J_{NN}$  (depending on flux density and choice of hopping parameters), with an excitation gap and associated observability temperature both approximately equal to  $W/2$ . Temperatures  $k_B T < J_{NN}$  have been reliably achieved in prior experiments on bosons in deep optical lattices, and while we expect the artificial gauge field to be an additional heating source, next generation cooling techniques may be able to offset it. Further, our trap-averaged entropy calculations show that local minima in the compressibility (which approach incompressibility as the temperature is lowered) can be observed at achievable values of  $S/N$ , again assuming that heating from the artificial gauge field does not dramatically change the system entropy compared to bosons in an ordinary deep optical lattice. Longer ranged hopping can dramatically increase the widths of the quantum Hall plateaus, especially for the Laughlin state at  $\nu = 1/2$ , and optical lattice configurations which naturally produce these hopping terms could make quantum Hall physics much easier to observe through density imaging.

## 4.5 Acknowledgments

We would like to thank Stefan Natu for useful discussions related to this work. This work was supported by the National Science foundation and by the DARPA OLE program.

## CHAPTER 5

### A VECTOR POTENTIAL FOR FLUX QUBITS

This work was done in collaboration with Erich Mueller, and is in preparation for publication.

#### 5.1 Introduction

The realization of a quantum Hall state of bosons— a state of charged, strongly interacting bosons confined to a 2d plane in a transverse magnetic field— would be a tremendous development in condensed matter physics. Beyond the academic interest in such a system and its important differences from the more familiar fermionic states in 2d electron gases (2DEGs, [66, 92, 141]), previous studies [24, 43, 108, 21, 78, 49, 114, 57] suggest that quantum Hall bosons can exhibit ground states with various types of abelian and non-abelian anyon statistics. This property makes these systems a candidate for topological quantum computing, which promises far greater noise tolerance than current approaches [61, 82].

There are significant technical obstacles to constructing such a system: nature does not provide any obvious candidates for a 2d fluid of charged bosons in an (unscreened) magnetic field. One promising proposal is to simulate the magnetic vector potential artificially in neutral cold atoms [25, 10]. However, there is no obvious way to measure conductivity in cold atoms, so the simplest and most dramatic signature of quantum Hall physics— quantized transverse conductance— cannot be directly measured, though other features of quantum Hall physics, such as the gap, could be observed through other methods. An al-

ternative scheme is to use lattices of tiny superconducting grains (charge qubits, [18, 110, 28, 131, 75, 20]) connected through Josephson junctions. Conductivity can be directly measured in this system and suitably low temperatures can be reached in a dilution refrigerator, but the random charge noise (which scales linearly with the interaction strength) characteristic to these grains would prevent the quantum Hall regime from being reached without significant local tuning of the potentials on hundreds or thousands of lattice sites. Other proposals include superconducting Jaynes-Cummings lattices [85] and “photon lattices” of coupled optical waveguides [42, 127].

We here propose a new system which avoids many of these obstacles. Our scheme is to construct a square lattice of “flux qubits”—mesoscopic superconducting rings interrupted by three Josephson junctions, placed in a magnetic field [79, 86, 17, 73, 74, 118, 76, 58, 15, 56]—operated in the regime where the two lowest eigenstates carry distinct nonzero values of the average circulating current and therefore magnetic flux (henceforth called fluxons). By capacitively coupling the rings to their neighbors through superconducting transformers, fluxons can tunnel from site to site, and due to phase accumulation analogous but not identical to the Aharonov-Casher effect [3], with appropriate voltage offsets they will mimic the physics of charged particles moving in a magnetic field. These qubits are operated in a regime where charge noise can be safely ignored, so they do not require the level of local tuning necessary in a charge qubit lattice. In addition, the fluxons naturally experience strong local repulsive interactions, and they can be manipulated with external electromagnetic fields.

## 5.2 Three-Junction Flux Qubits

The basic elements of our system are three-junction flux qubits, originally proposed by Mooij *et al* [79, 86] and widely adopted in the superconducting device community. The circuit diagram of this type of qubit is shown in figure 5.1. Adopting the standard notation in the literature, the qubit consists of a ring interrupted by three Josephson junctions, two with Josephson energy  $E_J$  and junction capacitance  $C$  and one with Josephson energy  $\alpha E_J$  and capacitance  $\alpha C$ . The ring is placed in an ambient magnetic field which points into the page and has a magnitude such that the total flux through the ring is  $f\Phi_0$ , where  $\Phi_0 = h/2e$  is the magnetic flux quantum. There are capacitances  $\gamma C$  and  $\kappa C$  connected to external voltage sources. The capacitances  $\gamma C$  represent the capacitive coupling of the ring to stray charges on the substrate, and since  $\gamma \sim 10^{-2}$  in a typical flux qubit we will neglect them in our calculations. On the other hand, the capacitances  $\kappa C$  are not necessarily small compared to  $C$  and are connected to a real constant voltage source  $V_E$ . The rings are interrupted by shunted transformers  $M$  connected to capacitors  $gC$  as shown in fig. 5.3, where  $g \ll 1$ . If  $g$  and the self inductance  $L$  of the inner ring side of the transformer are both small, these circuit elements only weakly perturb the single-ring Hamiltonian, and will only be of importance when considering interactions between neighboring rings. The transformers could simply be parallel wires as shown in fig. 5.3b. We assume that the mutual inductance  $M$  in the transformer is much larger than the self-inductances of the wires, and we further assume that the voltage drop  $\Delta V_{j2}$  across the interior (ring) side of each transformer is small compared to the dynamical part of voltage drop across the Josephson junction below it (ignoring the constant shifts  $V_E$  and  $V_0$ ; this condition works out to  $\Delta V_{j2} \ll 2e/C$ ).

The bottom of the ring is held at constant voltage  $V_0$ , and we choose it to have superconducting phase  $\phi = 0$ . With these conventions, the ring Hamiltonian is:

$$\begin{aligned}
H = & \frac{C}{2} \left[ (V_1 - V_0)^2 + (V_2 - V_0)^2 + \alpha (V_1 - V_2)^2 \right. \\
& \left. + \kappa (V_1 - V_E)^2 + \kappa (V_2 - V_E)^2 \right] + O(g) \\
& - E_J [\cos(\phi_1) + \cos(\phi_2) + \alpha \cos(2\pi f + \phi_1 - \phi_2)].
\end{aligned} \tag{5.1}$$

$V_1$  and  $V_2$  are the voltages at the segments labeled by (1) and (2) in fig. 5.1. To quantize the Hamiltonian, we want to write the voltages  $V_i$  in terms of the charges  $Q_1$  and  $Q_2$ , which are the sums of all the charges on the capacitor faces connected to the associated regions. Explicitly,

$$\begin{aligned}
Q_1 &= C(\kappa(V_1 - V_E) + \alpha(V_1 - V_2) + V_1 - V_0), \\
Q_2 &= C(\kappa(V_2 - V_E) + \alpha(V_2 - V_1) + V_2 - V_0).
\end{aligned} \tag{5.2}$$

These relations can be inverted to obtain

$$\begin{aligned}
V_1 &= \frac{(1 + \alpha + \kappa) Q_1 + \alpha Q_2}{(1 + 2\alpha + \kappa)(1 + \kappa)C} + \frac{V_0 + \kappa V_E}{1 + \kappa}, \\
V_2 &= \frac{(1 + \alpha + \kappa) Q_2 + \alpha Q_1}{(1 + 2\alpha + \kappa)(1 + \kappa)C} + \frac{V_0 + \kappa V_E}{1 + \kappa}.
\end{aligned} \tag{5.3}$$

Inserting these relations into (5.1), the ring Hamiltonian becomes

$$\begin{aligned}
H = & \frac{(1 + \alpha + \kappa)(Q_1^2 + Q_2^2) + 2\alpha Q_1 Q_2}{2(1 + 2\alpha + \kappa)(1 + \kappa)C} + H_c \\
& - E_J [\cos(\phi_1) + \cos(\phi_2) + \alpha \cos(2\pi f + \phi_1 - \phi_2)].
\end{aligned} \tag{5.4}$$

Here,  $H_c$  is an irrelevant constant term. Upon quantizing the Hamiltonian,  $Q_j = (2e/i)\partial/\partial\phi_j$  and  $\phi_j$  are the charges and phases on regions (1) and (2) of the ring as indicated in figure 5.3. The qubit is typically operated in the regime where  $f \sim 1/2$ ,  $\alpha \sim 3/4$  and  $E_J \geq 30E_C$ , where  $E_C = e^2/2C$ . We will require  $f \neq 1/2$  in order to obtain complex hopping matrix elements.

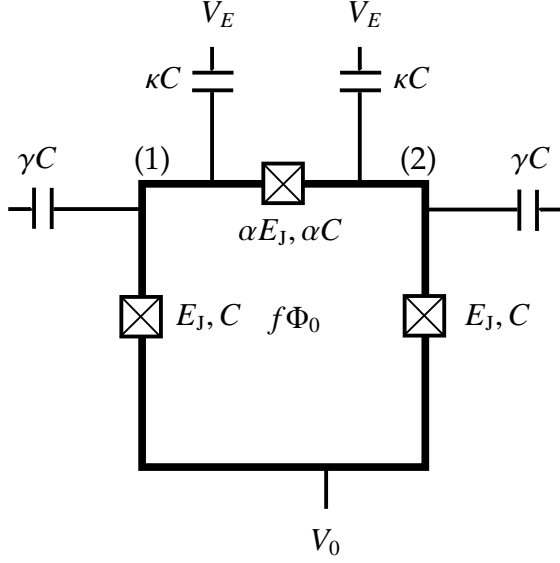


Figure 5.1: Single flux qubit, without any circuitry to connect it to its neighbors. The center Josephson junction has its Josephson energy and capacitance scaled by the parameter  $\alpha$  relative to the equivalent parameters in the other two junctions;  $\alpha$  is typically in the range of 0.6-0.8. The capacitances  $\kappa C$  are used to apply an external voltage  $V_E$  to generate phases when the rings are coupled, and  $\kappa$  is  $O(1)$ . The capacitances  $\gamma C$ , on the other hand, represent the passive coupling to stray charge noise in the environment, and in a typical flux qubit,  $\gamma \sim 10^{-2}$ . Since  $\gamma \ll \kappa$  we neglect these terms in our calculations. A magnetic flux  $f\Phi_0$  penetrates the ring, and if  $f \neq 1/2$  or zero time-reversal symmetry is broken. The phases  $\phi_1$  and  $\phi_2$  of the superconducting regions (1) and (2) are the two degrees of freedom of the qubit, and the bottom of the ring is chosen to be  $\phi = 0$  and held at voltage  $V_0$ .

The eigenstates of this Hamiltonian can be computed numerically, and depend strongly on  $f$  and  $\alpha$ . Examples of these states are plotted in fig. 5.2. For  $f$  near  $1/2$  and  $\alpha > 1/2$ , the potential has two minima at  $\phi_1 = -\phi_2 = \pm\phi^*$ , corresponding to states with net circulating current. If  $f \neq 1/2$ , the potential is no longer symmetric along the  $\phi_- = (\phi_1 - \phi_2)/2$  direction, leading to differing expectation values of  $\phi_-$  between the ground and first excited states. This situation persists even if  $f$  is large enough that the potential no longer has two local

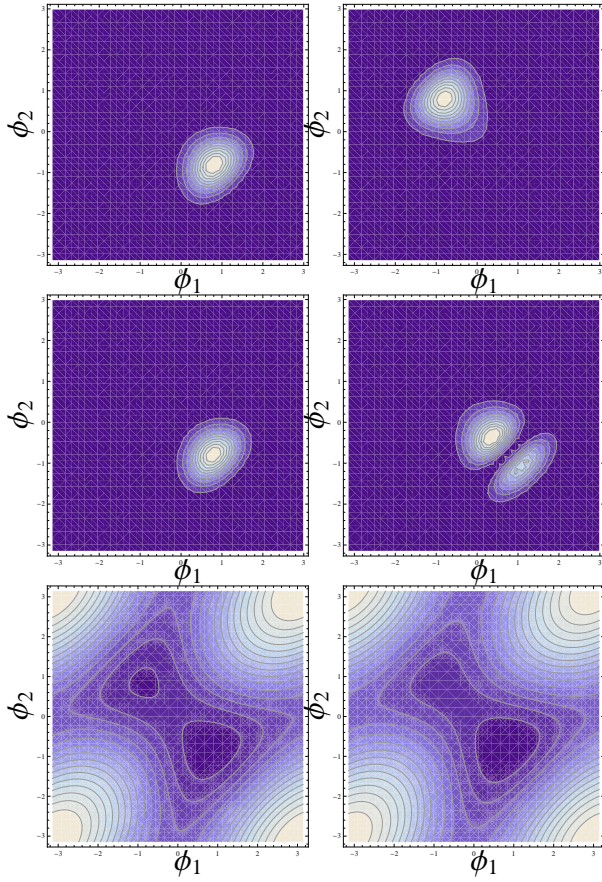


Figure 5.2: Eigenstates of (5.4), with plots of the potential in the bottom row. In the top row,  $|\psi(\phi_1, \phi_2)|^2$  is plotted for the ground state  $|0\rangle$  (left) and the first excited state  $|1\rangle$  (right) for  $E_J = 40E_C$ ,  $\alpha = 0.75$ ,  $\kappa = 1$  and  $f = 0.515$ . In this regime the potential has two minima (with different energies, since  $f \neq 1/2$ ), and  $|0\rangle$  and  $|1\rangle$  are concentrated in them with little overlap. Due to the large potential barrier separating them, the tunneling matrix elements in this regime are exponentially suppressed with  $J_{jk} \propto \exp -c \sqrt{E_J/E_C}$  for some  $c$  dependent on  $f$  and  $\alpha$ . In contrast, in the middle row the same quantities are plotted for  $|0\rangle$  and  $|1\rangle$  when  $f = 0.54$  and the potential has a single (asymmetric) minimum and the overlap in  $|\psi(\phi_1, \phi_2)|^2$  between the wavefunctions is appreciable.  $J_{jk}$  is no longer exponentially suppressed and is 2 orders of magnitude larger in this regime, but it is difficult to measure the state of the qubit by measuring the current  $I_c \sin \phi_1$ . On the bottom row, the potential terms in (5.4) are plotted for  $f = 0.515$  on the left and  $f = 0.54$  on the right.

minima, and while previous studies of flux qubits have all been in the double minimum regime, for the purposes of this proposal we only require that the two lowest eigenstates  $|0\rangle$  and  $|1\rangle$  have nonzero expectation values in  $\langle\phi_-\rangle$ , though neither  $|0\rangle$  nor  $|1\rangle$  (the fluxon state) carries a definite circulating current. Example ground and first excited state wavefunctions are plotted in fig. 5.2 for the two regimes. Note that in absolute terms, the difference between the two states corresponds to a net flux through the loop which is far less than a flux quantum—typically  $\sim 10^{-3}\Phi_0$  in previous experiments.

Before proceeding, it is useful to state a few facts about the low-lying eigenstates. We write  $\phi_{\pm} = (\phi_1 \pm \phi_2)/2$ . Throughout this work, we will make frequent use of the following relations

$$\begin{aligned}\langle a|\phi_+|b\rangle &= \langle a|\frac{\partial}{\partial\phi_+}|b\rangle = 0, \\ \langle a|\phi_-|b\rangle &= c_{ab}, \\ \langle a|\frac{i\partial}{\partial\phi_-}|b\rangle &= -\langle b|\frac{i\partial}{\partial\phi_-}|a\rangle = d_{ab}.\end{aligned}\tag{5.5}$$

Here  $a$  and  $b$  are each 0 or 1. The first line of (5.5) holds even if  $f = 1/2$ , as both  $|0\rangle$  and  $|1\rangle$  are even about  $\phi_+ = 0$  and have no net momentum along  $\phi_{\pm}$ . Generally,  $c_{ab}$  is nonzero if  $f \neq 1/2$  and  $d_{ab}$  nonzero if  $a \neq b$  and  $f \neq 1/2$ . These relations do not always hold for the higher excited states.

We will now consider the many-ring problem, where the rings are coupled so that a fluxon in a given ring can tunnel to one of the neighboring rings if that ring is unoccupied. With external voltages applied appropriately, the tunneling matrix element will pickup a nontrivial phase analogous to the Aharonov-Bohm phase  $q \int \mathbf{A} \cdot d\mathbf{l}$  that a charged particle experiences when tunneling in a magnetic field. We will derive this result and then compute the amplitudes and phases of the hopping matrix elements  $J_{jk}$  for realistic device parameters.

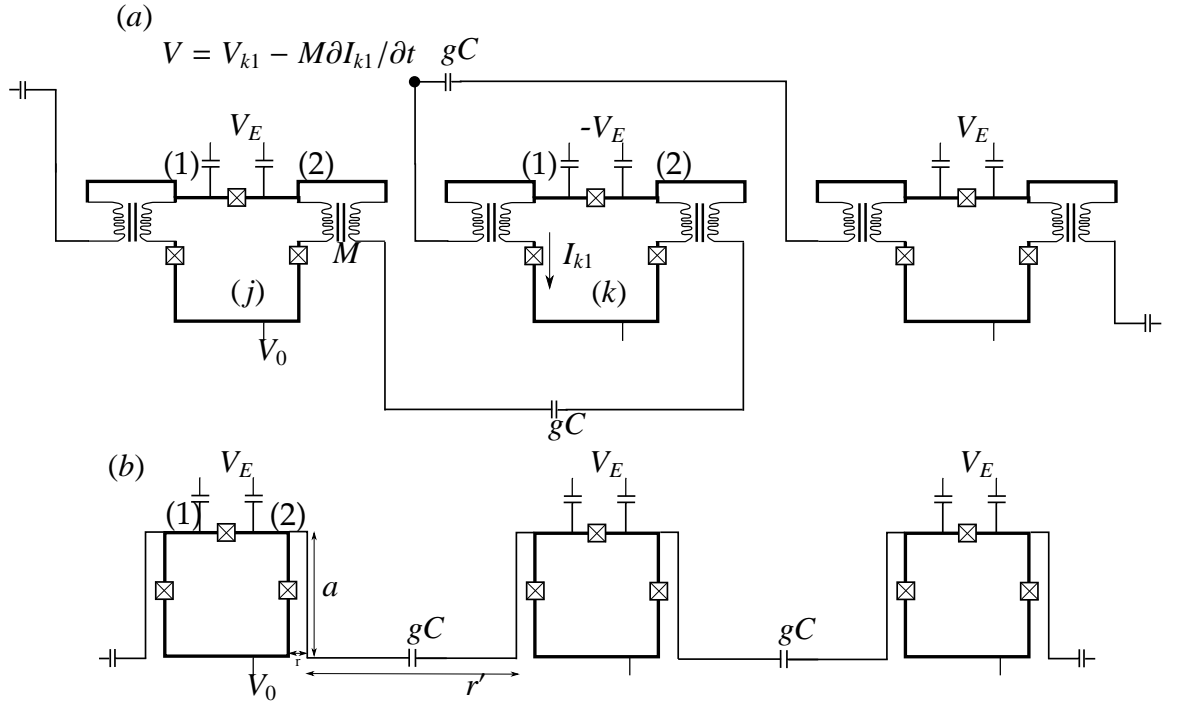


Figure 5.3: Flux qubit array. (a) Schematic circuit diagram. The lattice unit cell consists of a single superconducting ring interrupted by three Josephson junctions, with  $E_J$  and  $C$  labeled in the figure. The phases of regions in (1) and (2) are taken to be the two degrees of freedom in each ring, and each is broken up by a transformer  $M$ , which is shorted across the top so the voltage at the coupling capacitors  $gC$  is given by  $V_i - M \partial I_i / \partial t$ , where  $I_i$  is the current through the Josephson junction to the bottom half of the ring. The applied voltages  $V_E$  alternate down the array. The rings discussed in the text are labeled  $j$  and  $k$ . (b) One possible arrangement of wires which realizes the transformer-capacitor coupling. This scheme can be generalized to 2d arrays as well, provided that the voltages and geometries of the contacts are chosen appropriately. If  $r \ll a$  and  $r \ll r'$ , the mutual inductance  $M$  is given by  $M = (\mu_0/2\pi) \left( r - \sqrt{a^2 + r^2} + a \tanh^{-1} \frac{a}{\sqrt{a^2 + r^2}} \right)$ . The phase generated in this arrangement will be  $\varphi + \pi$  as detailed in table 5.1.

## 5.3 Many-Ring Hamiltonian

### 5.3.1 Transformer-Capacitor Coupling

We couple these qubits to each other so that a fluxon (state  $|1\rangle$ ) on one qubit can be transferred to one of its neighbors (in state  $|0\rangle$ ) by quantum tunneling. We will show how the use of superconducting transformers, which pick up voltage shifts from the rate of change of the currents flowing through the sides of each ring, can lead to complex hopping matrix elements if the ends of the transformers are coupled capacitively to each other. The coupling of two qubits using only capacitors or only inductive elements will lead to real-valued hopping terms, and it is the subtle interplay of the two types of circuit elements with offset voltages and the ring geometry that leads to complex hopping.

Consider a pair of flux qubits coupled capacitively to each other as shown in fig. 5.3a with capacitances  $gC$ , with  $g \ll 1$ . We will focus on the left and center qubits in fig. 5.3a this derivation. We choose  $C, E_J, f$  and  $g$  so that the following conditions hold: (i)  $E_J \gg E_C$  (so that charge noise from stray offset charges on the substrate can be ignored; previous designs have been in the range  $30 < E_J/E_C < 80$ ), (ii) the relative nonlinearities of the spectrum, characterized by  $|E_i - \omega|/\omega$ , where  $\omega = E_1 - E_0$  is the fundamental excitation energy, to all be significantly distinct from unity (this requirement will be formalized below), and finally (iii)  $f \neq 1/2$  so that  $\langle \phi_1 \rangle = -\langle \phi_2 \rangle$  is nonzero in both the ground and excited states. If these requirements are met, we can restrict our attention only to the lowest lying excited states  $|1\rangle$  and  $|0\rangle$ . Note that  $f = 1/2$  the Hamiltonian is symmetric under the interchange of  $\phi_1$  and  $\phi_2$ , so there will be no average circulating current. We want the nonlinearities to be far from unity so that pro-

cesses involving higher excited states, such as one where two  $|1\rangle$  states combine to form a  $|2\rangle$  and a  $|0\rangle$ , are forbidden by energy conservation.

We will now explicitly derive the hopping coupling between the two neighboring rings  $j$  and  $k$  shown in fig. 5.3a,

$$J_{jk} \equiv \langle 0_j 1_k | H_{jk} | 1_j 0_k \rangle, \quad (5.6)$$

which is the matrix element for transferring a fluxon from one ring to its neighbor. Region (2) in ring  $j$  is connected to region (2) in ring  $k$ . Using the equivalent circuit in fig. 5.3a, the coupling term in the Hamiltonian is

$$H_{jk} = \frac{gC}{2} \left( (V_{j2} - V_{j,\text{ind}}) - (V_{k2} - V_{k,\text{ind}}) \right)^2. \quad (5.7)$$

Here, the induced voltage is the contribution from the transformer, which is equal to  $M\partial I_{j2}/\partial t$ . We compute this induced voltage using the Josephson current and phase relations  $I = I_c \sin \phi$  and  $\delta V = h\dot{\phi}/(2e)$ :

$$V_{j,\text{ind}} = -\frac{2I_c M e}{h} (V_{j2} - V_0) \cos \phi_{j2}. \quad (5.8)$$

We now plug in (5.3) for  $V_{j2}$ , making the assumption that  $\kappa C (V_{jE} - V_0) \gg 2e$ . If this is the case, we can neglect the charge terms  $Q_i$  and obtain:

$$V_{j,\text{ind}} = -\frac{2I_c M e \kappa}{h(1 + \kappa)} (V_{jE} - V_0) \cos \phi_{j2} \quad (5.9)$$

The equation for  $V_{k,\text{ind}}$  is identical up to the replacement of  $\phi_{j2}$  with  $\phi_{k2}$  and  $V_{jE}$  with  $V_{kE}$ . Using the relations (5.5),  $H_{jk}$  (to lowest order in  $g$ ) becomes

$$\begin{aligned} H_{jk} &= \frac{8gE_C(1 + \kappa)^2}{(1 + 2\alpha + \kappa)^2} \times \\ &\quad \left( \frac{\partial}{\partial \phi_{j2}} - iG_j \cos \phi_{j2} \right) \left( \frac{\partial}{\partial \phi_{k2}} - iG_k \cos \phi_{k2} \right), \\ G_j &= C \frac{I_c M \kappa (1 + 2\alpha + \kappa)}{h(1 + \kappa)} (V_{jE} - V_0). \end{aligned} \quad (5.10)$$

We have neglected terms which only act on single rings, since if  $g$  is small they will simply make a small correction to the “kinetic” terms of the Hamiltonian (5.4). If the wires are arranged as in fig 5.3b,  $M = (\mu_0/2\pi) \left( r - \sqrt{a^2 + r^2} + a \tanh^{-1} \frac{a}{\sqrt{a^2 + r^2}} \right)$ .

We now demonstrate that  $J_{jk} = \langle 0_j 1_k | H_{jk} | 1_j 0_k \rangle$  will be complex and have a phase controlled by  $V_{jE}$  and  $V_{kE}$ . Since the single-ring Hamiltonian is real, we can choose  $|0\rangle$  and  $|1\rangle$  to be real valued vectors in the phase basis:

$$|i\rangle = \int d\phi_1 d\phi_2 \psi_i(\phi_1, \phi_2) |\phi_1, \phi_2\rangle, \quad (5.11)$$

where  $\psi_i(\phi_1, \phi_2)$  is a real-valued function. Let  $G_j = -G_k = G$ . We define

$$H_{jk} \equiv \frac{8gE_C(1+\kappa)^2}{(1+2\alpha+\kappa)^2} \Gamma_{2j} \Gamma_{2k}. \quad (5.12)$$

The matrix element is then given by:

$$\begin{aligned} J_{jk} &= \frac{8gE_C(1+\kappa)^2}{(1+2\alpha+\kappa)^2} \langle 1 | \Gamma_{2j} | 0 \rangle \langle 0 | \Gamma_{2k} | 1 \rangle, \\ &= \frac{8gE_C}{(1+2\alpha+\kappa)^2} \left[ \langle 1 | \frac{\partial}{\partial \phi_{2j}} | 0 \rangle \langle 0 | \frac{\partial}{\partial \phi_{1k}} | 1 \rangle \right. \\ &\quad + G^2 \langle 1 | \cos \phi_{2j} | 0 \rangle \langle 0 | \cos \phi_{2k} | 1 \rangle \\ &\quad + iG \langle 1 | \frac{\partial}{\partial \phi_{2j}} | 0 \rangle \langle 0 | \cos \phi_{2k} | 1 \rangle \\ &\quad \left. - iG \langle 0 | \frac{\partial}{\partial \phi_{2k}} | 1 \rangle \langle 1 | \cos \phi_{2j} | 0 \rangle \right]. \end{aligned} \quad (5.13)$$

Since  $f_0(\phi_1, \phi_2)$  and  $f_1(\phi_1, \phi_2)$  are real, the first two terms in (5.13) are real and the last two are purely imaginary. We note that, since the symmetry between  $\phi_1$  and  $\phi_2$  is broken, the imaginary part of (5.13) would change sign if it were region (1) connected to region (1) instead of region (2) connected to region (2). Because of this, the phase  $\varphi$  for tunneling from the leftmost ring in fig. 5.3a to the center ring is identical to the phase for tunneling from the center ring to the rightmost ring. If  $G_j = G_k = 0$ , the hopping matrix element is real and negative.

Note also that if we had connected region (2) of ring  $j$  to region (1) of ring  $k$  and set  $G_k = G$  instead of  $-G$ , we would have obtained a phase of  $\varphi + \pi$ , since  $\langle 0 | \partial / \partial \phi_1 | 1 \rangle = - \langle 0 | \partial / \partial \phi_2 | 1 \rangle$ . This allows for tremendous flexibility in setting the phases of the hopping matrix elements, since even with all offset voltages set to zero (or with the transformers absent or routed around in the wiring) the signs of the hopping matrix elements can be controlled simply by the geometry of the wirings. A list of possible connections and voltages with their resulting phases is shown in table 5.1.

We have numerically computed the magnitude of  $J$  vs. the parameters  $f$  and  $\alpha$  in (5.4), with  $G = 0.8\pi$  chosen so that the phase accumulated in tunneling across one lattice spacing was approximately  $\pi/4$ . The matrix elements were calculated by evaluating (5.13) with  $g = 0.1$ . The results of this parameter search are plotted in fig. 5.4; for  $E_J = 200\text{GHz}$  hopping parameters up to  $2.5\text{GHz}$  are possible in this approach. The optimum parameter space (given the nonlinearity requirements described earlier) is  $\alpha \sim 3/4$  and  $0.525 < f < 0.55$ . Note that in this regime the potential only has a single minimum, and the ground and first excited state wavefunctions are analogous to deformed versions of the ground and first excited harmonic oscillator states along  $\phi_-$  (and symmetric about  $\phi_+$ ). In the double minimum regime, the current distributions of the two states are well separated from each other, but as a consequence  $J_{jk}$  is exponentially suppressed and is 2-3 orders of magnitude lower than in the single minimum regime.

### 5.3.2 Interactions

The coupling  $H_{jk}$  also generates a nearest neighbor potential interaction between fluxons. Noting that  $\langle i | \partial / \partial \phi_1 | i \rangle = 0$  but  $\langle i | \cos \phi_1 | i \rangle = \langle i | \cos \phi_2 | i \rangle \neq 0$ , evaluating  $\langle lm | H_{jk} | lm \rangle$  for  $l, m$  0 or 1 leads to the nearest neighbor interaction:

$$\widehat{U}_{jk} = -\frac{8gE_C(1+\kappa)^2}{(1+2\alpha+\kappa)^2}G_jG_k \times \langle n_j | \cos \phi_1 | n_j \rangle \langle n_k | \cos \phi_1 | n_k \rangle. \quad (5.14)$$

Here,  $n_{j/k} = 0$  or  $1$ . For  $f \neq 1/2$ ,  $(\langle 1 | \cos \phi_1 | 1 \rangle - \langle 0 | \cos \phi_1 | 0 \rangle) \neq 0$ , and since the signs of  $G_j$  and  $G_k$  depend on the offset voltages  $V_{jE}$  and  $V_{kE}$  the interaction can be either attractive or repulsive. This dependence can be used to engineer position-dependent interactions and on-site potential shifts. The relative magnitude of this term compared to  $J_{jk}$  depends on  $f$ ,  $G$ , and  $\alpha$  and is plotted in fig. 5.4. Longer ranged interactions will arise when qubits beyond nearest neighbors are connected to each other.

It is also possible to tune the nearest neighbor interactions independently from the hopping term. Consider the arrangement shown in fig. 5.6. Additional transformers have been inserted *below* the Josephson junctions; even though the lower region is held at constant voltage  $V_0$ , the time-varying current flowing through the junction to the constant voltage source from the capacitively coupled source  $V_E$  will create voltage shifts in the transformers. The orientation of the transformers determines whether the voltage shift from them will be positive or negative. If the transformers below the Josephson junctions have the same mutual inductance  $M$  and capacitive coupling  $gC$  as those above the junctions, the coupling term  $H'_{jk}$  will be

$$H'_{jk} = \frac{4gE_C(1+\kappa)^2}{(1+2\alpha+\kappa)^2} \quad (5.15)$$

Connection	$\{G_j, G_k\}$	Phase
(1) $\rightarrow$ (1)	$\{G, -G\}$	$\varphi$
(2) $\rightarrow$ (2)	$\{G, -G\}$	$-\varphi$
(2) $\rightarrow$ (2)	$\{-G, G\}$	$\varphi$
(1) $\rightarrow$ (1)	$\{G, G\}$	0
(2) $\rightarrow$ (2)	$\{G, G\}$	0
(2) $\rightarrow$ (1)	$\{G, -G\}$	$\pi$
(2) $\rightarrow$ (1)	$\{G, G\}$	$\varphi + \pi$
(1) $\rightarrow$ (2)	$\{G, G\}$	$-\varphi + \pi$

Table 5.1: Hopping phases for different choices of contacts and offset voltages when a fluxon tunnels from ring  $j$  to ring  $k$  for a given  $|G|$ . The magnitude of each hopping term is identical.  $G$  is linearly proportional to the offset voltage  $V_E$ . A phase of zero corresponds to a hopping matrix element which is real and negative.

$$\times \left( \pm G_j \cos \phi_{1/2,j} \mp G_k \cos \phi_{1/2,k} \right)^2.$$

The relative signs of the two cosine terms depend how the transformers are arranged; for the arrangement shown in the figure, the matrix element from the lower-ring couplings will exactly cancel the interaction potential term (5.14) and alter the hopping matrix element (5.13). Of course, different values of  $M$  and  $g$  will shift the magnitude of this potential contribution, allowing these interaction terms to be tuned independently from the hopping terms.

### 5.3.3 Constraints on $M$

The previous derivation required that the voltage shift on the interior (ring) side of the transformer was small enough to ignore, and could be neglected in the single-ring Hamiltonian. Recalling that  $G_j = C \frac{I_c M \kappa (1+2\alpha+\kappa)}{h(1+\kappa)} V_{jE}$  (for  $V_0 = 0$ ), we can set  $V_E$  by requiring that  $G \sim 1$ . To demonstrate that the voltage shift on the interior of the ring can be ignored, we need to compare the time derivative

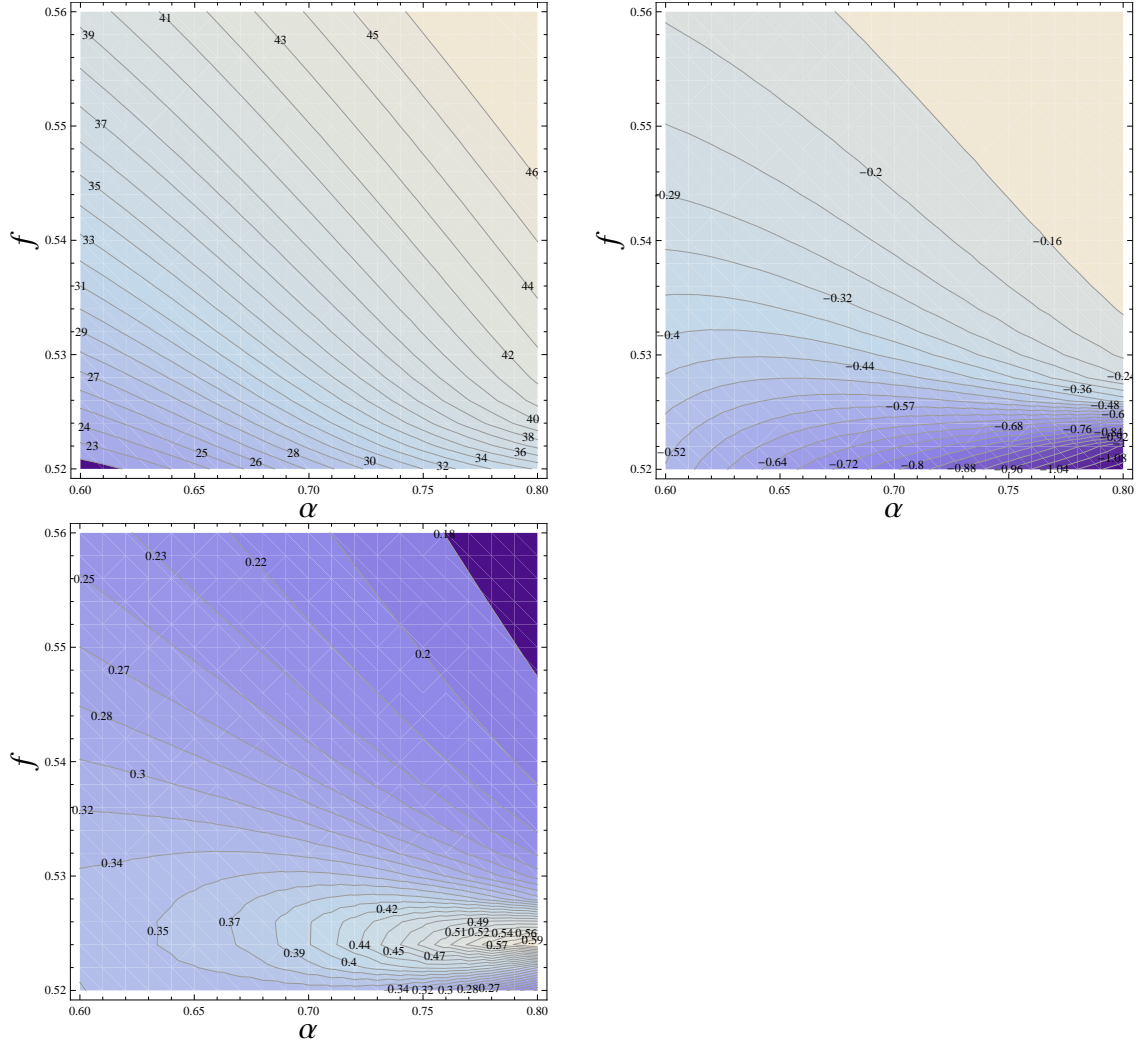


Figure 5.4: Clockwise from top:  $\omega$  in GHz,  $\delta I = \langle 1 | \sin \phi_1 | 1 \rangle - \langle 0 | \sin \phi_1 | 0 \rangle$  and  $\delta\phi^2$  for state  $|1\rangle$ , as functions of  $\alpha$  and  $f$ . These values were calculated for  $E_J = 200\text{GHz}$ ,  $E_C = 5\text{GHz}$  and  $\kappa = 1$ . Note that most of the plot range falls outside of the double minimum regime in the potential.

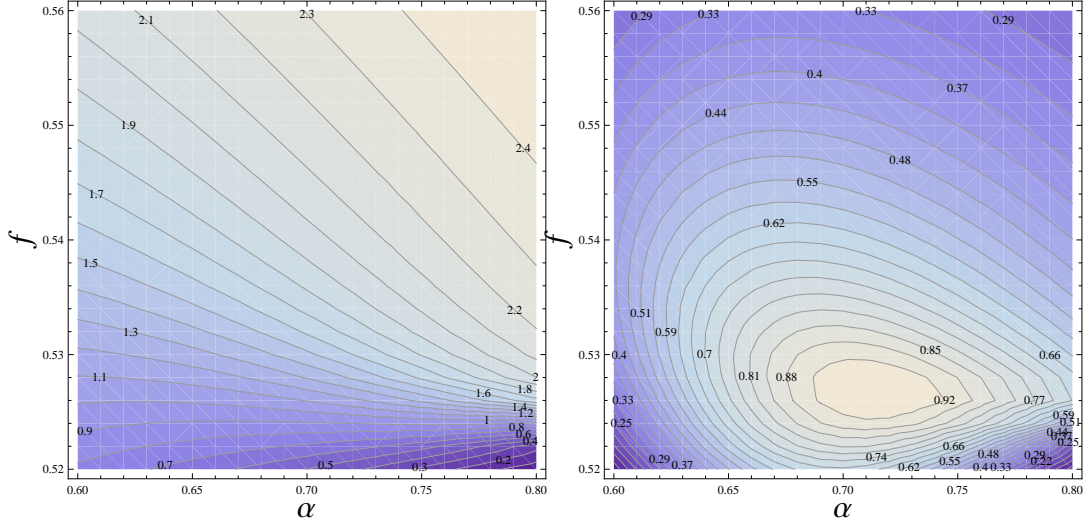


Figure 5.5: Left to right:  $J_{jk}$  and the nearest neighbor energy shift  $U_{jk} = 8gE_C(1+\kappa)^2(1+2\alpha+\kappa)^{-2}G^2 \times \langle 1|\cos\phi_1|1\rangle(\langle 1|\cos\phi_1|1\rangle - \langle 0|\cos\phi_1|0\rangle)$ , both in GHz, as functions of  $f$  and  $\alpha$  for  $G = 0.8\pi$ ,  $g = 0.1$ ,  $E_J = 200\text{GHz}$ ,  $E_C = 5\text{GHz}$  and  $\kappa = 1$ . The hopping phase is approximately  $\pi/4$  for this choice of  $G$ .

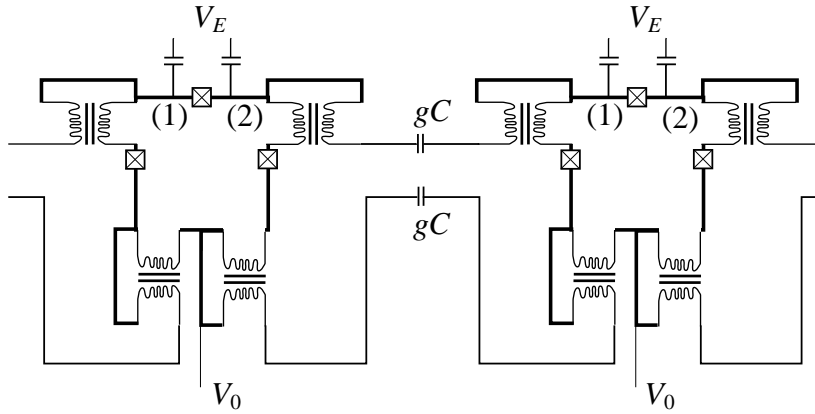


Figure 5.6: Schematic arrangement of additional transformer-capacitor couplings which cancels the interaction term (5.14) generated by the primary coupling. The transformers on the lower right (between region 2 and the constant voltage source  $V_0$ ) side of each ring are reversed relative to the other transformers in each ring, flipping the sign of their voltage shifts. Changing the magnitudes of  $M$  or  $g$  in the lower couplings, or changing the arrangement of the transformers, will produce different nearest neighbor interaction potentials.

of the current through the capacitor  $gC$ ,  $\partial I_{\text{link}}/\partial t$  to the time derivative of the current through the ring  $\partial I_{j_2}/\partial t$ . If  $\partial I_{\text{link}}/\partial t \ll \partial I_{j_2}/\partial t$ , then the induced voltage in the ring can be ignored, since the voltage shift from the transformer in the tunneling leads is  $O(2e/C)$ . We have:

$$\begin{aligned}\partial I_{j_2}/\partial t &\simeq \frac{2I_c e}{h} V_E \cos \phi_{j_2}, \\ \partial I_{\text{link}}/\partial t &\simeq -gC \frac{2I_c M e \kappa}{h(1+\kappa)} V_E \\ &\quad \times (\cos \phi_{j_2} - \cos \phi_{k_2}) \left( \frac{2eV_E}{h} \right)^2.\end{aligned}\tag{5.16}$$

Recall that we also require  $\kappa C V_E \gg 2e$ . If we obtain  $V_E$  by setting  $G = 1$ , requiring that  $\partial I_{\text{link}}/\partial t \ll \partial I_{j_2}/\partial t$  implies that we want to make the product of  $I_c M$  large, but not too large so that  $\kappa C V_E \sim 2e$ . This can be achieved for realistic parameter choices. For example, for  $I_c = 460\text{nA}$  (corresponding to  $E_J = 11\text{K}$ ),  $C = 5\text{fF}$ ,  $g = 0.2$ ,  $\alpha = 0.75$ ,  $\kappa = 2$  and  $M = 5 \times 10^{-11}\text{H}$ ,  $\kappa C V_E \simeq 60e$  and  $\partial I_{j_2}/\partial t \simeq 20 \partial I_{\text{link}}/\partial t$ . Note that the dominant effect of this term is to perturb the single-ring potential. Since  $E_C \ll E_J$ , even if the voltage shift on the inner ring approaches the voltage shift at the connecting capacitors, the deformation of the single-ring potential term will still be small.

### 5.3.4 Charge Noise

In the first section, we noted that stray charges in the environment could produce voltage shifts in the ring through the capacitances  $\gamma C$ . Since  $\gamma$  is two orders of magnitude smaller than  $\kappa$ , we ignored it in calculating the properties of qubits. In the limit of large  $E_J/E_C$ , shifts in the qubit energy levels from offset charges are exponentially suppressed, so there will be no detectable shifts in  $\omega$ . Where these offset charges will manifest themselves, however, is in the

charge-voltage relations (5.2),

$$V_j \rightarrow V_j + \frac{\gamma}{1 + \gamma + \kappa} V_{j0}, \quad (5.17)$$

where  $V_{j0}$  is the voltage from the charge offsets. Inserting this shift into the qubit Hamiltonian (5.4) is equivalent to a simple gauge transformation of the single-ring eigenstates and is of no physical importance, but when we insert it into the coupling term (5.10), it results in a shift of the induced voltage coupling  $G_j$ ,

$$G_j \rightarrow C \frac{I_c M \kappa (1 + 2\alpha + \kappa)}{h (1 + \kappa)} \times \left( V_{jE} + \frac{\gamma (1 + \kappa)}{\kappa (1 + \kappa + \gamma)} V_{j0} - V_0 \right). \quad (5.18)$$

This will lead to a correction to the amplitude and phase of  $J_{jk}$ . However, since we required that  $\kappa C V_E \gg 2e$  and  $\gamma \ll \kappa$ , the correction will be small and we do not expect it to play a significant role in the many body physics.

### 5.3.5 Difference from the Aharonov-Casher Effect

Close examination of (5.13) demonstrates that it is possible to generate nontrivial effective gauge fields for the tunneling fluxons. In the simplest example, consider a large circle of flux qubits, as shown in fig 5.7a with the top Josephson junction always oriented to face the outside of the ring. A single fluxon starting at a given point on the circle, tunneling all the way around the circle and returning to its starting location will accumulate a nonzero phase  $\varphi$ , since it will add a phase  $\varphi'$  with each step to the right and a phase  $-\varphi'$  with each step to the left. This is analogous to the Aharonov-Casher phase accumulated by a moving dipole (fig 5.7b), where a magnetic dipole of moment  $\mathbf{m}$  moving along a closed path picks up a net phase of  $\varphi_{AC} = (1/\hbar c) \int (\mathbf{E} \times \mathbf{m}) \cdot d\mathbf{l}$ .

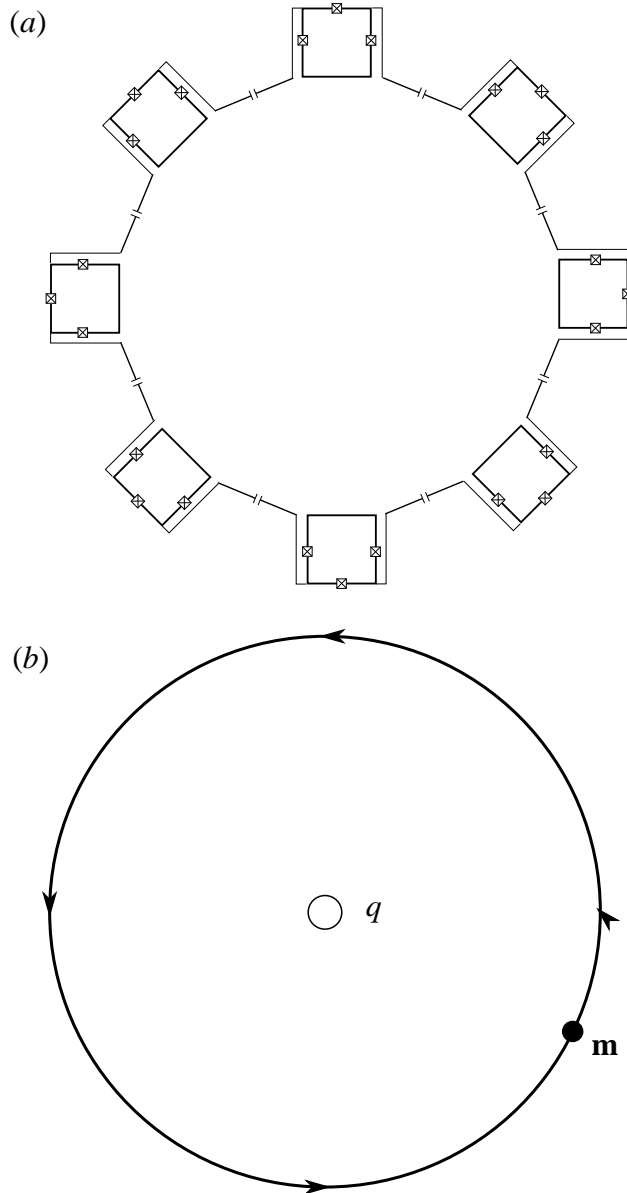


Figure 5.7: Analogy between the artificial vector potential in our flux qubit arrangement and the Aharonov-Casher effect. In (a) the flux qubits are arranged with identical applied voltages  $V_E$  so that tunneling a fluxon around the ring accumulates a nonzero phase  $\varphi$ . The voltage shifts are equivalent to placing a point charge in the center of the ring. In (b), a physical dipole  $\mathbf{m}$  pointing out of the page encircles a point charge  $q$ , also accumulating a phase  $\varphi$  in making a complete loop. It is important to note that, while the hopping phases in (5.13) are structurally similar to the Aharonov-Casher phases, they do not arise from that effect, as detailed in the text.

It is important to note, however, that the phases in (5.13) do not arise from the Aharonov-Casher effect, as the actual A-C phase that would be accumulated tunneling a fluxon around the ring in fig 5.7a is *zero*. This is because, unlike previous studies of Josephson vortex tunneling [27, 34, 119], the “fluxons” we study are not exact, quantized bundles of magnetic flux but rather have wavefunctions describing a spread of different currents with nonzero expectation values. This means that in any tunneling process, there is no definite exchange of circulating current between adjacent flux qubits, so it is not sensible to consider the process as a transfer of a magnetic dipole moment of some quantized magnitude. Rather, it should be viewed as a correlated change in the magnitudes of the dipole moments of a pair of adjacent, immobile dipoles, and since the A-C term in the Lagrangian is proportional to  $\mathbf{v} \cdot (\mathbf{E} \times \mathbf{m})$ , for  $\mathbf{v} = 0$  the Lagrangian is unchanged in this process and the A-C phase is zero. An alternative demonstration of this fact is to consider an electric dipole of moment  $\mathbf{p}$  moving in a circle in the  $xy$  plane around a magnetic dipole of moment  $\mathbf{m}$ , with both  $\mathbf{p}$  and  $\mathbf{m}$  pointed along  $z$ . If a physical dipole is being moved, the Aharonov-Bohm phase is nonzero since the top and bottom charges experience different vector potentials. However, if we replace the moving dipole with a discrete array of dipole moments and increase and decrease the electric dipoles to move a net moment around the ring, the net phase will be zero since the azimuthal component of  $\mathbf{A}_\phi$  does not enter into the equation and all contributions from motion coupling to  $\mathbf{A}_z$  will sum to zero.

### 5.3.6 Two Dimensional Arrays and the Lowest Landau level

By considering a lattice of these rings and ignoring inaccessible higher excited states, we arrive at the final hopping Hamiltonian

$$H = - \sum_{jk} |J_{jk}| (a_j^\dagger a_k e^{i\varphi_{jk}} + \text{H.C.}) + \sum_j \omega n_j + \sum_{jk} U_{jk} n_j n_k. \quad (5.19)$$

A hard-core constraint is enforced. An example configuration which realizes a uniform flux per plaquette is shown in fig. 5.8. Previous studies [47, 64, 5, 43, 89, 108, 142, 129, 60, 128, 49, 59] have shown that the square lattice version of this Hamiltonian is analogous to the lowest Landau level problem of strongly interacting bosons, and realizes abelian and non-abelian fractional ground states at the appropriate fixed densities. We expect that small arrays should be sufficient to observe quantum Hall physics, since the magnetic length  $l_B = a/\sqrt{\varphi}$  (where  $\varphi$  is the gauge-invariant phase accumulated when a fluxon circulates around a plaquette) can be less than a lattice spacing<sup>1</sup>. Connections between flux qubits beyond nearest neighbors can reproduce the exact lowest Landau level of the continuum [60, 59] and lead to more robust fractional quantum Hall states, but they may not be necessary to observe the Laughlin state at  $\nu = 1/2$  [43], where the filling fraction  $\nu$  is the ratio of particle to flux density. A wide range of other possible quantum spin-1/2 models, both with complex phases and without, could be studied in this device architecture; we find quantum Hall systems to be the most intriguing, due to the existence of abelian anyons at  $\nu = 1/2$  and the existence (with tuning) of non-abelian anyons at  $\nu = 1$  and  $3/2$  [82, 59], along with other exotic states at different filling fractions.

---

<sup>1</sup>We calculate the magnetic length by analogy to the mapping to the lowest Landau level in [60]; the coefficient of the Gaussian in the Landau level wavefunctions sets  $l_B$ .

We caution that obtaining uniform gauge fields of arbitrary magnitude is very difficult through this method if the magnitudes of the hopping matrix elements are to be kept constant across the array. When the phase  $\varphi$  becomes large, the shift in the magnitude of  $J_{jk}$  is also large, so the capacitances  $gC$  must be finely tuned to balance this effect. However, when the flux per plaquette is a simple, rational fraction, such as  $1/4, 1/3$ , or  $1/2$  quanta per plaquette, the  $2\pi$  periodicity of  $\varphi$  afforded by the lattice can be exploited to greatly simplify the array engineering process. Appropriate use of the relations in table 5.1 can ensure that phases for each individual hop are near 0 or  $\pi$  and therefore make only small shifts in the magnitudes of the hopping matrix elements. In figure 5.8, an arrangement is shown which produces a uniform flux of  $1/4$  quanta per plaquette. Similar constructions can be employed for lattices with  $1/3$  or  $1/2$  quanta per plaquette and/or next nearest neighbor hopping.

The fluxon loss rate in our array is favorable for observing quantum Hall physics. Given  $J = 2\text{GHz}$ , a (relatively pessimistic) decay rate of the first excited state  $\Gamma_1 = 2\text{MHz}$  [140, 20] and a Landau band spacing of  $\omega_{\text{LLL}} \simeq 3J_{\text{NN}}$ , we have a normalized Landau band spacing of  $3 \times 10^3 \Gamma_1$ . This compares favorably to the equivalent ratio in high-quality GaAs heterostructures [121], where the single-particle scattering rate is  $\Gamma \sim 10\text{GHz}$  and the Landau level spacing at  $B = 10\text{T}$  is  $26.2\text{THz}$ . This ensures that this loss rate by itself will not prevent quantum Hall states from forming in our array, provided that a passive loading mechanism is introduced to balance the decay rate and keep the average fluxon density constant.

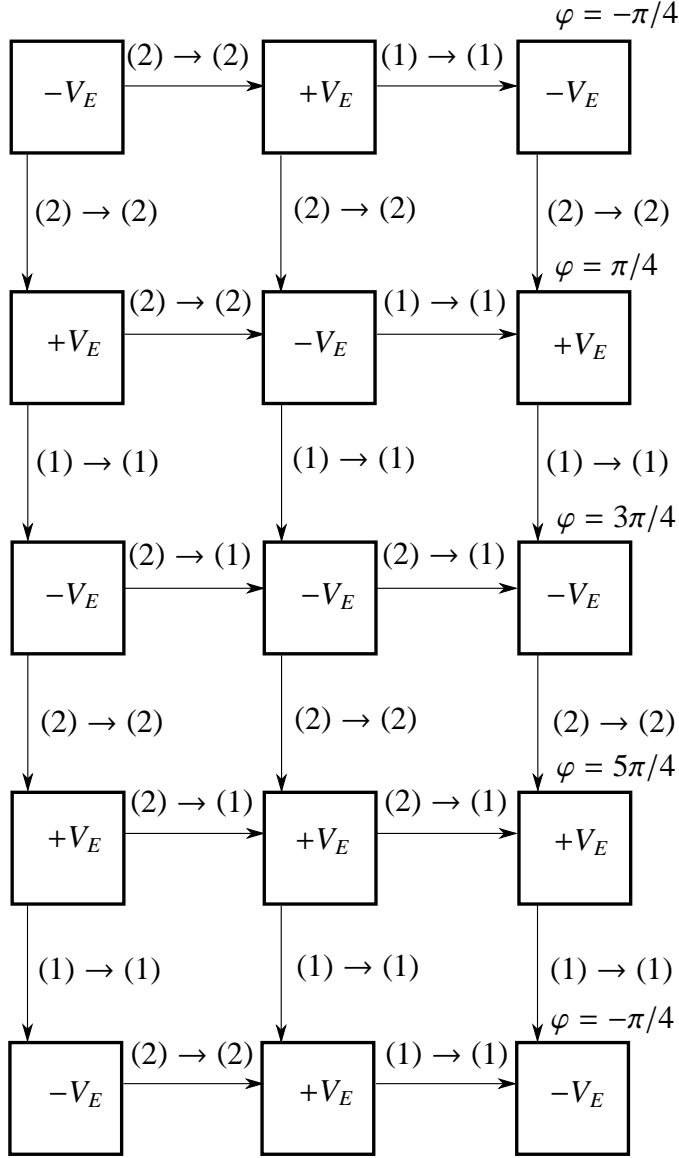


Figure 5.8: A 2d array configuration which would lead to a uniform effective gauge flux of  $1/4$  quanta per plaquette (a net phase of  $\pi/2$  accumulated for encircling a plaquette by moving counterclockwise). The links between rings above or below each other are connected to the inner side of each transformer so pick up no voltage shifts or complex phases. Here  $V_0 = 0$  and the applied voltage  $V_E$  alternates appropriately to ensure that a step to the right yields the phase indicated along the side of each row. By noting that  $\langle \psi | \exp iG \sin \phi_1 | \psi \rangle = \langle \psi | \exp -iG \sin \phi_2 | \psi \rangle$  and  $G \propto V_E$ , we see that  $\varphi = \pi/2$  for motion around any plaquette in this lattice. Next nearest neighbor contacts can also be added, but are not shown here for simplicity.

## 5.4 Conclusion

We have demonstrated a method for realizing a quantum Hall state of bosons using linked flux qubits in an electric field. With appropriate protocols for loading the lattice with fluxons (likely through a microwave source) and performing four-terminal measurements of the fluxon conductivity, we expect that conductivity quantization could be observed on small arrays. The statistics of anyonic collective modes could be determined through similar methods [101, 13, 135, 121]. Beyond this, with suitable methods for manipulating vortices in the fluxon lattice, arrays of flux qubits could be used to construct a topological non-abelian anyon qubit [61, 50, 82], trading information density for topological protection against decoherence. In that sense our proposal is similar to the surface code and cluster state [122] ideas developed in recent years, and provides a new potential mechanism for reducing decoherence in superconducting quantum information devices.

## 5.5 Acknowledgments

We would like to thank Greg Fuchs, Paul Ginsparg, Chris Henley, Matteo Mariantoni, John Martinis and Dan Ralph for useful discussions related to this project. This work was supported by the National Science Foundation.

## CHAPTER 6

### CONCLUSION

In the previous chapters, I covered many aspects of the problem of strongly interacting lattice bosons. In chapter 2, I showed that a lattice model with longer-ranged hopping exactly reproduces the lowest Landau level of the continuum. Thus all of the elegant mathematics (including, potentially, a conformal field theory description of the eigenstates) of the continuum can be applied to this lattice model. In chapter 3, I used realistic impurity potentials to numerically braid anyons on small lattices. This calculation confirmed the anyonic nature of the lattice quantum Hall states. In chapter 4, I studied the equation of state of this system and demonstrated that the ground state energy gaps were large enough to observe bosonic fractional quantum Hall states in near-term experiments. Finally, in chapter 5, I proposed a new architecture for linked superconducting qubits with tunable hopping phases and energies. This architecture avoids the issues of charge noise which have prevented boson quantum Hall physics from being observed in previously studied Josephson junction arrays. I will conclude this thesis with some speculations about using lattice bosons to construct a topological quantum computer, or *Quantum Loom*.

## 6.1 Anyon Qubits

### 6.1.1 Anyon Fusion and Ising Anyons

As described in chapter 3, the topological degeneracies associated with non-abelian anyons can be used to encode quantum information [61, 101, 33, 38,

50, 82]. The two filling fractions of interest for these purposes are  $\nu = 1$  (Ising anyons) and  $\nu = 3/2$  (probable Fibonacci anyons), with dramatically different braiding properties and technical concerns. To understand how anyons can be used to encode quantum information, it is useful to introduce the concepts of topological charges and fusion rules. The details I will present here are taken from the review article by Nayak *et al* [82], which is an excellent introduction to non-abelian anyons and topological quantum computing.

The low-energy degrees of freedom of a non-abelian anyon system can be expressed as a finite set of emergent quasiparticles, which we label as the charges  $\mathbf{q}_i$ . These charges obey four important properties. First, the system contains a trivial charge  $\mathbf{1}$ , which is an unfractionalized abelian particle that describes the underlying particles which create the anyon system— electrons in the 2DEG, fluxons in a lattice of flux qubits, and so forth. In our case, this particle will be a boson. Second, in any process acting on a closed region, the topological charge is conserved, so that the fusion sum (to be defined shortly) of all the topological charges in that region is unchanged by any manipulations of the system which act only on that region. Third, the topological charges obey fusion rules, so that the combination of two charges  $\mathbf{q}_i$  and  $\mathbf{q}_j$  which results from bringing the two charges close together will interact with other anyons which are far away as if it were a single new charge  $\mathbf{q}_k$ . These fusion rules can be expressed by a set of fusion matrices  $F$ , and generically the outcome of the fusion of two non-abelian anyons depends on nonlocal quantum numbers which can be manipulated through braiding and exchanging anyons. Finally, the fourth requirement is that in a closed system, the fusion sum of all charges in the system must be equal to  $\mathbf{1}$ . This requirement can be simply understood as reflecting the fact that the system is made up of real, unfractionalized electrons, cold atoms, Cooper

pairs or fluxons, and while the emergent degrees of freedom may be fractional, the nonexistence of fundamental fractional charges means that the sum of all the emergent quasiparticles must be equivalent to a finite integer number of real particles.

To understand fusion rules, we will consider the Ising anyon theory, discussed in chapter 3, which describes the Pfaffian states of bosons at  $\nu = 1$  and fermions at  $\nu = 5/2$ . In this theory there are three fundamental charges,  $\mathbf{1}$ ,  $\sigma$  and  $\psi$ . The fusion rules of these charges are

$$\begin{aligned}
 \mathbf{1} + X &= X & (6.1) \\
 \sigma + \psi &= \sigma \\
 \psi + \psi &= \mathbf{1} \\
 \sigma + \sigma &= \mathbf{1} + \psi.
 \end{aligned}$$

The symbol  $X$  stands for any of  $\mathbf{1}$ ,  $\sigma$  or  $\psi$ . The first rule simply states that the charge  $\mathbf{1}$  acts as the identity particle. The second and third state that the fusion of a  $\psi$  with a  $\sigma$  or a  $\psi$  with a  $\psi$  has a unique outcome, but the fourth rule states that the fusion of two  $\sigma$  particles can have two possible outcomes, either a trivial particle  $\mathbf{1}$  or a  $\psi$ . The two possible outcomes are referred to as fusion channels, and as will be explained below, these fusion rules require that the system contains degeneracies. In the boson quantum Hall state at  $\nu = 1$ , the  $\sigma$  particles are half-quasiholes (or their conjugates, half-quasiparticles  $\sigma^*$ ) and carry charge  $q/2$  and flux  $\Phi_0/2$ . The charges and fluxes of the  $\mathbf{1}$  and  $\psi$  particles depend on whether  $\sigma$ 's or  $\sigma$  and  $\sigma^*$  particles are fused to create them. A pair of a half quasihole and a half quasiparticle can either annihilate when fused, leaving nothing, or create a neutral  $\psi$  mode.

The minimum degeneracy of a group of non-abelian anyons can be ex-

pressed entirely in terms of its fusion outcomes, which specify the state up to Abelian phases. In the example of Ising anyons,  $2n$   $\sigma$  anyons have a degeneracy of  $2^{n-1}$ . This can be quickly derived by simply grouping the anyons into  $n$  pairs, noting that each pair can fuse to  $\mathbf{1}$  or  $\psi$ . This yields a degeneracy of  $2^n$ , but the requirement that the fusion of all anyons in the system yields  $\mathbf{1}$  gives the constraint that the number of pairs which fuse to  $\psi$  must be even, reducing the total degeneracy by a factor of 2. Exchanging  $\sigma$  particles between different pairs will enact rotations within this degenerate subspace. A basis for these rotation matrices  $R$  was presented in equation (3.4) in chapter 3, along with some discussion of their properties. It is easy to imagine a quantum computer being constructed this way— one pair of anyons for each qubit, with some number of additional pairs left over to manipulate them— and research to this effect is ongoing [101, 38, 33, 82, 121, 56].

The state at  $\nu = 1$  in bosons is in the same universality class as the Pfaffian state believed to be the ground state at  $\nu = 5/2$  in the 2DEG. If the  $\nu = 5/2$  state of electrons is described by a Pfaffian-like wavefunction, it is a state of matter supporting non-abelian anyons. Both numerical studies and quasiparticle interference experiments suggest that this is the case [135, 121]. Up to abelian phases, the braid properties of the bosonic state at  $\nu = 1$  are identical to the theorized Pfaffian state, so previous proposals for quantum computing based on this state can be readily generalized to our lattice bosons.

There is one serious drawback to using Ising anyons for topological quantum computing, however, and it is that the braid group realized by Ising anyons is not large enough to enact any possible unitary transformation, and thus cannot be used to construct a universal set of 1- and 2-qubit gates. To supplement the

gates that one can construct from Ising anyons, one must either use operations which do not have topological protection [16, 88], such as bringing anyons close together for finite times to enact a phase gate from the breaking of the energetic degeneracy, or introduce operations which dynamically change the topology of the system [33]. The former idea would be relatively straightforward to implement, but introduces many additional sources of decoherence or gate errors, and the latter is technologically formidable, requiring the fabrication of three dimensional structures on the nanoscale or exquisite levels of local control of a time-dependent potential. Both of these obstacles might be surmounted in the future, but they present a significant challenge to any practical use of a topological quantum computer based on Ising anyons.

### 6.1.2 Fibonacci Anyons

There is another type of non-abelian anyon which *is* computationally universal, however: Fibonacci anyons. The fusion rules for these anyons are even simpler than in the Ising case: the theory contains only two particles,  $\mathbf{1}$  and  $\tau$ , which fuse according to:

$$\mathbf{1} + \tau = \tau, \tag{6.2}$$

$$\tau + \tau = \mathbf{1} + \tau.$$

The “ $k = 3$  Read-Rezayi” quantum Hall states of fermions at  $\nu = 12/5$  and bosons at  $\nu = 3/2$  may exhibit anyons with these fusion rules, up to a rather complicated array of abelian phases (the theorized state of the 2DEG at  $\nu = 12/5$  has five fundamental charges, but they reduce to  $\mathbf{1}$  and  $\tau$  when abelian phases are factored out). As shown by Hormozi *et al* [50], these phases can be ignored

for the purposes of actual braiding operations, so these states may support truly universal topological quantum computing. It is important to note, however, that there are competing ground states for both of these systems which have other types of braid statistics [99], and there is no firm experimental evidence to support or disprove the existence of Fibonacci anyons at  $\nu = 12/5$  in experiments. Further, the gap at  $\nu = 12/5$  is far smaller than the gap at  $\nu = 5/2$ , reducing the protection against noise and defects.

All that said, let us assume that a  $k = 3$  Read-Rezayi state of bosons at  $\nu = 3/2$  can be stabilized in the lattice quantum Hall model I have described in this dissertation. To my mind, this is an eminently reasonable assumption. The  $k = 3$  R-R state is in close proximity to competing orders (shown in the previously cited studies), and given that the gauge flux density, hopping matrix elements, and nearest neighbor interactions can all be tuned in a flux qubit array, it is very likely that there are ranges of parameter space where the ground state is in the Fibonacci anyon universality class. This state can be used as a universal quantum computer [106, 50, 48, 8], with each qubit constructed from a group of three impurity-pinned quasiholes. Any possible unitary transformation can be implemented using suitably large numbers of braids, and given that the error rate of a given quantum gate decreases exponentially as the number of braids increases *linearly*, the resources required for quantum computing in this state are tractable. In fact, as shown by Baraban *et al* [8], the number of Fibonacci anyons required to factor a 128-bit number using Shor's algorithm [105] is  $\sim 10^3$ , compared to  $10^9$  Ising anyons. Shor's algorithm is the most famous and perhaps the most important example of a problem which is exponentially difficult for a classical computer but can be solved in polynomial time on a quantum computer, and the superiority of Fibonacci anyons to Ising anyons in this case is a stark

demonstration of the potential power of Fibonacci anyon computing.

There is another hidden advantage to the  $\nu = 3/2$  R-R state of bosons compared to  $\nu = 1$  bosons or  $\nu = 5/2$  fermions, one which arises in the measurement of the qubits. To demonstrate this property, I will review the concept of differential conductivity measurement, which is likely the best current proposal for how to measure a non-abelian qubit in a quantum Hall state. After outlining this method, I will cite the explicit results for  $\nu = 1, 5/2$  and  $3/2$ , and show how the  $\nu = 3/2$  state avoids a measurement error which can arise in the other two cases.

### 6.1.3 Measuring a Non-Abelian Anyon Qubit

The most promising method for measuring a non-abelian anyon qubit is differential conductivity interference [101, 13, 51, 14, 135, 121], pictured for an array model in figure 6.1. Schemes to measure conductivity interference take different forms, but they all share the basic feature of one or more quantum point contacts near which quasiparticles have a small probability of tunnel a short distance through the bulk to the other end and thus not traversing part of the sample. This causes the two quasiparticles to experience different unitary transformations due to encircling different collections quasiparticles and magnetic flux in the two paths through the point contacts. The quasiparticles then interfere when the two paths recombine, changing the observed conductivity. For abelian quasiparticles, the unitary transformations are pure phases, but for non-abelian quasiparticles these unitary transformations can take the form of nontrivial rotations which suppress interference independent of any additional

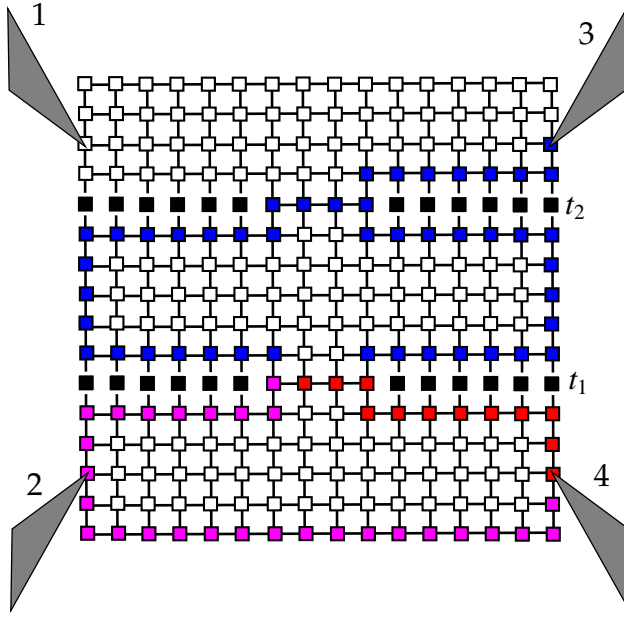


Figure 6.1: Schematic configuration for measuring the statistics of the anyons, adapted from [101, 13, 51, 14, 135, 121]. Particles are forbidden from hopping to the black sites (either due to the sites being physically removed from the array or due to large local repulsive potentials applied at them) and the gray triangles labeled 1-4 are external contacts; in the experiment, a “voltage” (real voltage for electrons and Cooper pairs, a magnetic field shift for fluxons) is applied between contacts 3 and 4 to induce a chiral edge current of quasiparticles from contact 4 to contact 3. The edge quasiparticles are able to tunnel through the narrow constrictions with amplitudes  $t_1$  and  $t_2$ , and as a consequence a voltage is induced between contacts 1 and 2, yielding a finite longitudinal conductivity  $\sigma_{xx}$  (which would be zero were the constrictions absent). The sites shaded red represent the path that ends with tunneling across the  $t_1$  constriction, the sites shaded blue represent the paths which either tunnel through  $t_2$  or exit the system at contact 3, and the sites shaded pink represent the path which includes interfering contributions from the red and blue paths. As argued in the text, one can determine the statistics of the anyons by studying the response of  $\sigma_{xx}$  to changes in the quasiparticle content or flux density of the region between the two constrictions. If the constrictions are removed, the longitudinal conductivity  $\sigma_{xx}$  vanishes and the quantization of the transverse conductivity  $\sigma_{xy}$  can be observed.

abelian phases (such as the Aharonov-Bohm phase from encircling magnetic flux) the quasiparticles may experience. Experiments with two quantum point contacts in 2DEGs have obtained results consistent with non-abelian statistics, and one could easily construct an essentially identical arrangement in our array models<sup>1</sup>. To make contact with these experiments, we will discuss the two-contact geometry first, although single-contact “sack” geometries [51] can also be used to probe the non-abelian character of the quasiparticles.

Consider the pocket geometry in figure 6.1. When the system is in a quantum Hall phase, the bulk will be gapped and all conductivity is carried by gapless chiral edge modes. Due to the bulk gap, the longitudinal conductivity  $\sigma_{xx}$  is zero in a large system, but if the two pinch contacts are narrow enough, edge quasiparticles will acquire a nonzero probability of tunneling through the gapped bulk (given by two tunneling amplitudes  $t_1$  and  $t_2$ ) and yeild a finite  $\sigma_{xx}$ . In the limit of  $t_1$  and  $t_2$  small (so that backscattering and multiple loops can be ignored), the edge conductivity will be proportional to the sum of two quantum amplitudes:

$$\sigma_{xx}(\Psi) \propto |t_1|^2 + |t_2|^2 + 2\text{Re}(t_1^* t_2 f(\Psi)). \quad (6.3)$$

Here,  $t_1$  and  $t_2$  are the tunneling matrix elements for an edge quasiparticle to tunnel across contacts 1 or 2 and  $f(\Psi)$  is a contribution from the quasiparticle exchange statistics which is determined by the state  $\Psi$  of the fluid inside the pocket. The coefficients  $t_1$  and  $t_2$  are non-universal, with amplitudes and relative phase dependent on the microscopic details of the pocket opening and presence of local noise in that region. As a consequence  $t_1$  and  $t_2$  are difficult to

---

<sup>1</sup>To reproduce the specific experiment of Willett *et al*, in which side gates are used to continuously tune the area inside pocket region, one would instead have to tune the magnetic field density, as the area of the pocket cannot be smoothly varied due to the granularity of the lattice and the short magnetic length.

predict *a priori*. We can, however, calculate  $f(\Psi)$ , and therefore the number of possible values of  $\sigma_{xx}(\Psi)$  can be predicted and used to determine the statistics of the quasiparticles. Importantly,  $t_1$  and  $t_2$  should be insensitive to perturbations which are deep in the bulk system or in the pocket, and so long as stray quasiparticles can be kept away from the narrow tunneling regions we can regard them as fixed complex numbers.  $t_1$  and  $t_2$  can be tuned by applying a local gate to the pinch regions, which would raise or lower the potential barrier and change the probability of tunneling through the pinch to avoid traversing the pocket region.

To show how  $\sigma_{xx}$  can be used to measure the state of a qubit, we first consider the Laughlin state at  $\nu = 1/2$ , whose fundamental quasiparticles are abelian anyons with charge  $q/2$ . The total number of anyons in the system must be even, but the total number of anyons in the *center* region is unconstrained. This means that the anyons which pass through the contact  $t_2$  can encircle a different total charge than those which pass through  $t_1$ . Each anyon in the bulk is a full quasihole which binds a single quantum of magnetic flux, so the anyons which encircle it will pick up a phase shift of  $\pi$  relative to those which do not. Equation (6.3) therefore takes two possible values:

$$\sigma_{xx}(\Psi) \propto |t_1|^2 + |t_2|^2 + 2|t_1 t_2| \cos(\beta + n\pi). \quad (6.4)$$

Here  $\beta$  is the combination of the relative phases of  $t_1$  and  $t_2$  and the (constant) Aharonov-Bohm phase accumulated in encircling the center region, and  $n$  is the number of anyons in the region between the two contacts. If this system were instead a Laughlin state of fermions at  $\nu = 1/3$ , the final term would have  $\cos(\beta + 2n\pi/3)$ , since the anyons have charge  $e/3$ . The finite number and spacing of values for  $\sigma_{xx}$  can thus be used to experimentally determine the statistics of the anyons, even if  $t_1$  and  $t_2$  are not known.

Let us now consider the Pfaffian state at  $\nu = 1$ . The fundamental excitations are  $\sigma$  particles, which are fractional quasiholes which carry half a quantum of flux and charge  $q/2$ . As in the previous example, there will be a contribution from the abelian phases, which will give a phase difference of  $\pi$  if the number of  $\sigma$  particles in the center pocket is an even integer modulo 4 (ie, if there are 2, 6, or 10  $\sigma$  particles in the pocket). However, if there are an odd number of  $\sigma$  particles in the center region, then  $f(\Psi)$  is zero, since the act of encircling an odd number of  $\sigma$  particles is equivalent to a NOT gate on the quantum state [16, 14], so the  $\sigma$  particles which traverse the top path are in an orthogonal state to those which traverse the bottom path and the two states do not interfere. Further, if there are an even number of anyons in the central region, they can fuse to either  $\mathbf{1}$  or  $\psi$ . Winding a  $\sigma$  particle around a  $\psi$  produces an additional phase of  $\pi$ . Putting all these phase effects together, if there are  $n$   $\sigma$  anyons enclosed in the center region, the conductivity will be

$$\sigma_{xx}(\Psi) \{\nu = 1\} \propto |t_1|^2 + |t_2|^2 + 2 |t_1 t_2| \cos(\beta + n\pi/2) (-1)^{N_\psi} \frac{1 + (-1)^n}{2}, \quad (6.5)$$

where  $N_\psi = 0$  or  $1$ .

For the Pfaffian state of electrons at  $\nu = 5/2$ , the fundamental quasiholes have charge  $e/4$  and carry half a flux quantum, so there are additional abelian phases, but the result is otherwise the same as the  $\nu = 1$  case. To wit,

$$\sigma_{xx}(\Psi) \{\nu = 5/2\} \propto |t_1|^2 + |t_2|^2 + 2 |t_1 t_2| \cos(\beta + n\pi/4) (-1)^{N_\psi} \frac{1 + (-1)^n}{2}. \quad (6.6)$$

At  $\nu = 3/2$  in bosons, the fundamental quasiholes have charge  $q/2$ , but carry  $1/3$  of a flux quantum rather than the  $1/2$  quantum carried by the anyons at  $\nu = 1$ . These quasiholes have topological charge  $\tau$  and the fusion of two of them can result in either a  $\mathbf{1}$  or a  $\tau$ , up to abelian phases. The quasiparticle interference

result can be generalized from the calculation by Chung and Stone [19]. For bosons at  $\nu = 3/2$  we have:

$$\sigma_{xx}(\Psi) \{ \nu = 3/2 \} \propto |t_1|^2 + |t_2|^2 + 2 |t_1 t_2| \cos(\beta + 2n\pi/3) \left( \frac{2 - \sqrt{5}}{2} \right)^{N_\tau} \quad (6.7)$$

Here  $N_\tau = 1$  if the anyons in the center region fuse to  $\tau$  and 0 if they fuse to  $\mathbf{1}$ .

The fact that these interference patterns all produce a finite range of outcomes which depend on the total topological charge enclosed in a region demonstrates that this method can be used to measure the state of a qubit. Let us now compare these three interference results from this point of view. Assume that  $t_1$  and  $t_2$  are constants which can be determined experimentally. For  $\nu = 1$  and  $\nu = 5/2$ , the sign alternation of the interference term determines whether the qubit is in state  $\mathbf{1}$  or  $\psi$ . However, this phase can equally be the result of the presence of additional quasiholes (2 extra  $\sigma$ 's which fuse to  $\mathbf{1}$  at  $\nu = 1$ , 4 at  $\nu = 5/2$ ), and it is here that a hidden error source enters the system. As mentioned previously, topological charge is conserved, so an error source, such as the scattering of an electron into our out of the well in the 2DEG or the spontaneous decay of a fluxon in the fluxon array, can only create  $\mathbf{1}$  charges, though these may break apart over time into combinations of nontrivial charges which fuse to  $\mathbf{1}$ . While these events are suppressed by the gap, they do occur, and would be equivalent to adding two full quasiholes at  $\nu = 5/2$  or a single full quasihole at  $\nu = 1$ ; this decomposes into 4 or 2  $\sigma$  particles, respectively, in the above counting. In either case, this event produces an additional phase of  $\pi$ , so while it does not change the state of the qubit directly, it changes the *apparent* state of the qubit when measured through differential conductivity. The energy gap does make these events relatively rare, but they are a concern if a prepared state is to be kept for long periods of time.

Fibonacci anyons, on the other hand, do not have this problem, since the amplitude changing factor  $\left(\frac{2-\sqrt{5}}{2}\right)^{N_\tau}$  ensures that even if the abelian phase in the region fluctuates, states where  $N_\tau = 1$  can always be distinguished from cases where  $N_\tau = 0$ . This is true for the Read-Rezayi state of electrons at  $\nu = 12/5$  as well. When combined with the fact that the Fibonacci anyon states are computationally universal where the Ising anyon states are not, it becomes obvious that Fibonacci anyons would be a superior system for topological quantum computation, provided that the technological obstacles to realizing Fibonacci anyons can be overcome.

## 6.2 Towards a *Quantum Loom*

While it is impossible to predict what the ultimate impact of any research will be, I believe that a suitable implementation of the superconducting architecture presented in chapter 5 could stabilize Read-Rezayi states in a real experiment. As shown in chapter 5, the intrinsic decay rate of flux qubits will not be a barrier to this goal, and with good control over the device parameters ( $E_J$ ,  $E_C$ ,  $M$ ,  $gC$  and the magnetic flux density) from ring to ring, scattering from disorder in these parameters should be tractably small. At a flux density of  $1/4$  quanta per plaquette, with just nearest and next nearest neighbor hopping the lowest band is already a nearly exact lowest Landau level, with a bandwidth of only 1.5% of the gap to higher excited bands. At this flux density, the magnetic length is slightly less than a lattice spacing and plateaus at  $\nu = 1/2, 1, 3/2$  and 2 are present. Tuning the nearest neighbor interaction and short-range hopping parameters could ensure that the state at  $\nu = 3/2$  is in the Fibonacci universality class, and given the results of chapter 3 that surprisingly small lattices can ac-

curately reproduce infinite system braiding results, fairly small lattices could be used to demonstrate quantum Hall physics— as a back of the envelope estimate,  $10 \times 10$  or smaller for conductivity quantization, with perhaps four times as many sites for conductivity interference and another factor of two to four beyond that for braiding. To achieve these ends, the following protocols need to be invented for the fluxon lattice:

\* Stabilizing the fluxon population: since the rings have a natural relaxation rate back to their ground state, fluxons added to the system will decay over time until the lattice empties. One way of introducing the fluxons would be to apply resonant microwave pulses at the excitation energy  $\omega$ . The gap in a many-body quantum Hall state may suppress the loss rate but will not cancel it entirely, so some sort of passive “reservoir” source of excitations (or continuous, low-amplitude microwave pumping) will be needed to continually add fluxons to balance the decay rate.

\* Applying and tuning local potentials: in the fluxon lattice, this could be accomplished by tuning the local magnetic field density  $f\Phi_0$ . This will also change the average circulating current at that site and alter the hopping phases, but these shifts are both relatively small.

\* Measuring the conductivity in response to an applied potential: since the fluxons differ from the ground state by an average circulating current in the ring (though this difference may be less than the variance in the wavefunctions), the rate of change of flux in a region could be used to detect the rate at which fluxons are entering or leaving it. Such measurements are possible through SQUID magnetometry, though there may be a better way to measure the current than this.

\* Pinning and braiding quasiholes: as described in chapter 3, the interaction of quasiholes with repulsive impurity potentials is a subtle problem, but one which could be studied directly in a conductivity interference experiment. To have any hope of performing a topological quantum computation, the control over quasihole position needs to be extremely good (thus ensuring that a quasihole does not escape along the way during a braiding operation).

Since the device I am describing does not yet exist, it is of diminishing usefulness to discuss these requirements any further. Tackling any of them in a real experiment would be extremely significant on its own. The qubit architecture I have described is within reach of current technology, and if it functions as predicted, could be scaled to boson quantum Hall physics and beyond. I am certainly *not* claiming that this scheme will be the future of topological quantum computing, nor am I promising that it will be more successful than the numerous other ideas under current consideration. Rather, I am merely stating that it is *possible*, and well worth the attempt at experimental realization.

## BIBLIOGRAPHY

- [1] M. Abramowitz and I. A. Stegun. *Handbook of Mathematical Functions*. National Bureau of Standards, Washington, DC, 1972.
- [2] I. Affleck, T. Kennedy, E. H. Lieb, and H. Tasaki. Rigorous results on valence-bon ground states in antiferromagnets. *Phys. Rev. Lett.* **59**, 799, 1987.
- [3] Y. Aharonov and A. Casher. Topological quantum effects for neutral particles. *Phys. Rev. Lett* **53**, 319, 1984.
- [4] M. Aidelsburger, M. Atala, S. Nascimbène, S. Trotzky, Y.-A. Chen, and I. Bloch. Experimental realization of strong effective magnetic fields in an optical lattice. *Phys. Rev. Lett* **107**, 255301, 2011.
- [5] F. F. Assaad and S. Biskamp. Fractional quantum hall effect on a lattice. *Phys. Rev. B* **51**, 1605, 1995.
- [6] A. Auerbach. *Interacting Electrons and Quantum Magnetism*. Springer-Verlag, 1994.
- [7] W. S. Bakr, P. M. Preiss, M. E. Tai, R. Ma, J. Simon, and M. Greiner. Interaction-induced orbital excitation blockade of ultracold atoms in an optical lattice. *Nature* **480**, 500, 2011.
- [8] M. Baraban, N. E. Bonesteel, and S. H. Simon. Resources required for topological quantum factoring. *Phys. Rev. A* **81**, 062317, 2010.
- [9] M. Baraban, G. Zikos, N. Bonesteel, and S. H. Simon. Numerical analysis of quasiholes of the moore-read wave function. *Phys. Rev. Lett.* **103**, 076801, 2009.
- [10] I. Bloch, J. Dalibard, and W. Zwerger. Many-body physics with ultracold gases. *Rev. Mod. Phys.* **80**, 885, 2008.
- [11] A. T. Bloukbasi and J. Vala. Rigorous calculations of non-abelian statistics in the kitaev honeycomb model. *New Journal of Physics* **14**, 045007, 2012.
- [12] P. Bonderson, V. Gurarie, and C. Nayak. Plasma analogy and non-abelian statistics for ising-type quantum hall states. *Phys. Rev. B* **83**, 075303, 2011.

- [13] P. Bonderson, A. Kitaev, and K. Shtengel. Detecting non-abelian statistics in the  $\nu=5/2$  fractional quantum hall state. *Phys. Rev. Lett.* **96**, 016803, 2006.
- [14] P. Bonderson, K. Shtengel, and J. K. Slingerland. Interferometry of non-abelian anyons. *Annals Phys.* **323**, 2709, 2008.
- [15] J. Bourassa, J. M. Gambetta, A. A. Abdumalikov Jr, O. Astafiev, Y. Nakamura, and A. Blais. Ultrastrong coupling regime of cavity qed with phase-biased flux qubits. *Phys. Rev. A* **80**, 032109, 2009.
- [16] S. Bravyi. Universal quantum computation with the  $\nu=5/2$  fractional quantum hall state. *Phys. Rev. A* **73**, 042313, 2006.
- [17] I. Chiorescu, Y. Nakamura, C.J.P.M. Harmans, and J.E. Mooij. Coherent quantum dynamics of a superconducting flux qubit. *Science* **299**, 1869, 2003.
- [18] M. Y. Choi. Quantum hall effect in ideal superconducting arrays at zero temperature. *Phys. Rev. B* **50**, 10088, 1994.
- [19] S. B. Chung and M. Stone. Proposal for reading out anyon qubits in non-abelian  $\nu = 12/5$  quantum hall state. *Phys. Rev. B* **73**, 245311, 2006.
- [20] J. Clarke and F. K. Wilhelm. Superconducting quantum bits. *Nature* **453**, 1031, 2008.
- [21] N. R. Cooper. Rapidly rotating atomic gases. *Advances in Physics* **57**, 539, 2009.
- [22] N. R. Cooper and J. Dalibard. Optical flux lattices for two-photon dressed states. *Europhysics Lett.* **95**, 66004, 2011.
- [23] N. R. Cooper and E. H. Rezayi. Competing compressible and incompressible phases in rotating atomic bose gases at filling factor  $\nu=2$ . *Phys. Rev. A* **75**, 013627, 2007.
- [24] N. R. Cooper, N. K. Wilkin, and J. M. F. Gunn. Quantum phases of vortices in rotating bose-einstein condensates. *Phys. Rev. Lett.* **87**, 120405, 2002.
- [25] J. Dalibard, F. Gerbier, G. Juzeliunas, and P. Öhberg. *Colloquium: Artificial gauge potentials for neutral atoms.* *Rev. Mod. Phys.* **83**, 1523, 2011.

- [26] J. Dubail, N. Read, and E. H. Rezayi. Real-space entanglement spectrum of quantum hall systems. *Phys. Rev. B* **85**, 115321, 2012.
- [27] W. J. Elion, J. J. Wachtors, L. L. Sohn, and J. E. Mooij. Observation of the aharonov-casher effect for vortices in josephson-junction arrays. *Phys. Rev. Lett.* **71**, 2311, 1993.
- [28] R. Fazio and H. van der Zant. Quantum phase transitions and vortex dynamics in superconducting networks. *Phys. Rep.* **355**, 235, 2001.
- [29] P. Fendley, M. P. A. Fisher, and C. Nayak. Topological entanglement entropy from the holographic partition function. *J. Stat. Phys.* **126**, 1111, 2007.
- [30] M. P. A. Fisher, P. B. Weichman, G. Grinstein, and D. S. Fisher. Bose localization and the superfluid-insulator transition. *Phys. Rev. B* **40**, 546, 1989.
- [31] S. Fölling, A. Widera, T. Müller, F. Gerbier, and I. Bloch. Formation of spatial shell structure in the superfluid to mott insulator transition. *Phys. Rev. Lett.* **97**, 060403, 2006.
- [32] E. Fradkin, C. Nayak, and K. Schoutens. Landau-ginzburg theories for non-abelian quantum hall states. *Nuc. Phys. B* **546**, 711, 1999.
- [33] M. Freedman, C. Nayak, and K. Walker. Towards universal topological quantum computation in the  $\nu=5/2$  fractional quantum hall state. *Phys. Rev. B* **73**, 245307, 2006.
- [34] J. R. Friedman and D. V. Averin. Aharonov-casher-effect suppression of macroscopic tunneling of magnetic flux. *Phys. Rev. Lett.* **88**, 050403, 2002.
- [35] L. Fu and C. L. Kane. Superconducting proximity effect and majorana fermions at the surface of a topological insulator. *Phys. Rev. Lett.* **100**, 096407, 2008.
- [36] N. Gemelke, E. Sarajlic, and S. Chu. Rotating few-body atomic systems in the fractional quantum hall regime. *arXiv:1007.2677v1*, 2010.
- [37] N. Gemelke, X. Zhang, C.-L. Hung, and C. Chin. In situ observation of incompressible mott-insulating domains in ultracold atomic gases. *Nature* **460**, 995, 2009.

- [38] L. S. Georgiev. Topologically protected gates for quantum computation with non-abelian anyons in the pfaffian quantum hall state. *Phys. Rev. B* **74**, 235112, 2006.
- [39] M. Greiter and R. Thomale. Non-abelian statistics in a quantum antiferromagnet. *Phys. Rev. Lett.* **102**, 207203, 2009.
- [40] M. Greiter and R. Thomale. Generalizations of perelomov's identity on the completeness of coherent states. *arXiv:1203.3965*, 2012.
- [41] M. Greiter, X. G. Wen, and F. Wilczek. Paired hall states. *Nuc. Phys. B* **374**, 567, 1992.
- [42] M. Hafezi, E. Demler, M. Lukin, and J. Taylor. Robust optical delay lines via topological protection. *Nature Physics* **7**, 907–912 (2011), 2011.
- [43] M. Hafezi, A. S. Sorensen, E. Demler, and M. D. Lukin. Fractional quantum hall effect in optical lattices. *Phys. Rev. A* **76**, 023613, 2007.
- [44] F. D. M. Haldane. Fractional quantization of the hall effect: A hierarchy of incompressible quantum fluid states. *Phys. Rev. Lett.* **51**, 605, 1983.
- [45] F. D. M. Haldane and E. H. Rezayi. Periodic laughlin-jastrow wave functions for the fractional quantized hall effect. *Phys. Rev. B* **31**, 2529, 1985.
- [46] T.-L. Ho. Bose-einstein condensates with large number of vortices. *Phys. Rev. Lett.* **87**, 060403, 2001.
- [47] D. Hofstadter. Energy levels and wave functions of bloch electrons in rational and irrational magnetic fields. *Phys. Rev. B* **14**, 2239, 1976.
- [48] L. Hormozi, N. E. Bonesteel, and S. H. Simon. Topological quantum computing with read-rezayi states. *Phys. Rev. Lett.* **103**, 160501, 2009.
- [49] L. Hormozi, G. Moller, and S. H. Simon. Fractional quantum hall effect of lattice bosons near commensurate flux. *arXiv:1109.3434*, 2011.
- [50] L. Hormozi, G. Zikos, N. E. Bonesteel, and S. H. Simon. Topological quantum compiling. *Phys. Rev. B* **75**, 165310, 2007.
- [51] C.-Y. Hou and C. Chamon. wormhole geometry for entrapping topologically protected qubits in non-abelian quantum hall states and probing

- them with voltage and noise measurements. *Phys. Rev. Lett.* **97**, 146802, 2006.
- [52] Z.-X. Hu, X. Wan, and P. Schmitteckert. Trapping abelian anyons in fractional quantum hall droplets. *Phys. Rev. B* **77**, 075331, 2008.
- [53] D. A. Ivanov. Non-abelian statistics of half-quantum vortices in p-wave superconductors. *Phys. Rev. Lett.* **86**, 268 (2001), 2001.
- [54] G. S. Jeon, K. L. Graham, and J. K. Jain. Fractional statistics in the fractional quantum hall effect. *Phys. Rev. Lett.* **91**, 036801, 2003.
- [55] G. S. Jeon, K. L. Graham, and J. K. Jain. Berry phases for composite fermions: Effective magnetic field and fractional statistics. *Phys. Rev. B* **70**, 125316, 2004.
- [56] L. Jiang, C. L. Kane, and J. Preskill. Interface between topological and superconducting qubits. *Phys. Rev. Lett.* **106**, 130504, 2011.
- [57] B. Juliá-Díaz, T. Graß, N. Barberán, and M. Lewenstein. Fractional quantum hall states of few bosonic atoms in geometric gauge fields. *New J. Phys.* **14**, 055003, 2012.
- [58] K. Kakuyanagi, T. Meno, S. Saito, H. Nakano, K. Semba, H. Takayanagi, F. Deppe, and A. Shnirman. Dephasing of a superconducting flux qubit. *Phys. Rev. Lett.* **98**, 047004, 2007.
- [59] E. Kapit, P. Ginsparg, and E. Mueller. Non-abelian braiding of lattice bosons. *Phys. Rev. Lett.* **108**, 066802, 2012.
- [60] E. Kapit and E. Mueller. Exact parent hamiltonian for the quantum hall states in a lattice. *Phys. Rev. Lett.* **105**, 215303, 2010.
- [61] A. Kitaev. Fault-tolerant quantum computation by anyons. *Ann. Phys.* **303**, 2, 2003.
- [62] A. Kitaev. Anyons in an exactly solved model and beyond. *Ann. Phys.* **321**, 2, 2006.
- [63] A. Kitaev and J. Preskill. Topological entanglement entropy. *Phys. Rev. Lett.* **96**, 110404, 2006.

- [64] M. Kohmoto. Zero modes and the quantized hall conductance of the two-dimensional lattice in a magnetic field. *Phys. Rev. B* **39**, 11943, 1989.
- [65] V. Lahtinen and J. K. Pachos. Non-abelian statistics as a berry phase in exactly solvable models. *New. J. Phys.* **11**, 093027, 2009.
- [66] R. B. Laughlin. Anomalous quantum hall effect: An incompressible quantum fluid with fractionally charged excitations. *Phys. Rev. Lett.* **50**, 1395, 1983.
- [67] R. B. Laughlin. Spin hamiltonian for which quantum hall wavefunction is exact. *Ann. Phys.* **191**, 163, 1989.
- [68] M. Levin and X.-G. Wen. Detecting topological order in a ground state wavefunction. *Phys. Rev. Lett.* **96**, 110405, 2006.
- [69] M. A. Levin and X.-G. Wen. String-net condensation: A physical mechanism for topological phases. *Phys. Rev. B* **71**, 045110, 2005.
- [70] H. Li and F. D. M. Haldane. Entanglement spectrum as a generaliation of entanglement entropy: Identification of topological order in non-abelian fractional quantum hall effect states. *Phys. Rev. Lett.* **101**, 010504, 2008.
- [71] Y.-J. Lin, R. L. Compton, K. Jiménez-García, J. V. Porto, and I. B. Spielman. Synthetic magnetic fields for ultracold neutral atoms. *Nature* **426**, 628, 2009.
- [72] X.-J. Liu, X. Liu, C. Wu, and J. Sinova. Quantum anomalous hall effect with cold atoms trapped in a square lattice. *Phys. Rev. A* **81**, 033622, 2010.
- [73] A. O. Lyakhov and C. Bruder. Quantum state transfer in arrays of flux qubits. *New. J. Phys.* **7**, 181, 2005.
- [74] J. B. Majer, F. G. Paauw, A. C. J. ter Haar, C. J. P. M. Harmans, and J.E. Mooij. Spectroscopy on two coupled flux qubits. *Phys. Rev. Lett* **94**, 090501, 2005.
- [75] Y. Makhlin, G. Schoen, and A. Shnirman. Quantum state engineering with josephson-junction devices. *Rev. Mod. Phys.* **73**, 357, 2001.
- [76] S. Matsuo, K. Furuta, T. Fujii, K. Nagai, and N. Hatakenaka. Fluxon-based

- gate controls of capacitively coupled flux-based-phase qubits. *Appl. Phys. Lett.* **91**, 093103, 2007.
- [77] D. McKay and B. DeMarco. Cooling in strongly correlated optical lattices: prospects and challenges. *Rep. Prog. Phys.* **74**, 054401, 2011.
- [78] G. Moller and N. R. Cooper. Composite fermion theory for bosonic quantum hall states on lattices. *Phys. Rev. Lett.* **103**, 105303, 2009.
- [79] J. E. Mooij, T. P. Orlando, L. Levitov, L. Tian, C. H. van der Wal, and S. Lloyd. Josephson persistent-current qubit. *Science* **285**, 1036, 2001.
- [80] G. Moore and N. Read. Nonabelions in the fractional quantum hall effect. *Nuc. Phys. B* **360**, 362, 1991.
- [81] E. J. Mueller. Artificial electromagnetism for neutral atoms: Escher staircase and Laughlin liquids. *Phys. Rev. A* **70**, 041603, 2004.
- [82] C. Nayak, S. H. Simon, A. Stern, M. Freedman, and S. Das Sarma. Non-abelian anyons and topological quantum computation. *Rev. Mod. Phys.* **80**, 1083, 2008.
- [83] C. Nayak and F. Wilczek.  $2n$ -quasihole states realize  $2^{n-1}$ -dimensional spinor braiding statistics in paired quantum hall states. *Nuc. Phys. B* **479**, 529, 1996.
- [84] Titus Neupert, Luiz Santos, Claudio Chamon, and Christopher Mudry. Fractional quantum hall states at zero magnetic field. *Phys. Rev. Lett.* **106**, 236804, 2011.
- [85] A. Nunnenkamp, J. Koch, and S. M. Girvin. Synthetic gauge fields and homodyne transmission in Jaynes-Cummings lattices. *New J. Phys.* **13**, 095008, 2011.
- [86] T. P. Orlando, J. E. Mooij, L. Tian, C. H. van der Wal, L. S. Levitov, S. Lloyd, and J. J. Mazo. Superconducting persistent-current qubit. *Phys. Rev. B* **60**, 15398, 1999.
- [87] M. Oshikawa, Y. B. Kim, K. Shtengel, C. Nayak, and S. Tewari. Topological degeneracy of non-abelian states for dummies. *Ann. Phys.* **322**, 1477, 2007.

- [88] C. Nayak P. Bonderson, D. J. Clarke and K. Shtengel. Implementing arbitrary phase gates with ising anyons. *Phys. Rev. Lett.* **104**, 180505, 2010.
- [89] R. N. Palmer, A. Klein, and D. Jaksch. Optical lattice quantum hall effect. *Phys. Rev. A* **78**, 013609 (2008); R. N. Palmer and D. Jaksch, *Phys. Rev. Lett.* **96**, 180407 (2006).
- [90] S. Pancharatnam. Generalized theory of interference, and its applications. part i. coherent pencils. *Proc. Indian Acad. Sci. A* **44**, 247 (1956), 1956.
- [91] A. M. Perelomov. On the completeness of a system of coherent states. *Theoret. Math. Phys.* **6**, 156, 1971.
- [92] R. E. Prange and S. M. Girvin. *The Quantum Hall Effect*. Springer, 1986.
- [93] E. Prodan and F. D. M. Haldane. Mapping the braiding properties of the moore-read state. *Phys. Rev. B* **80**, 115121, 2009.
- [94] N. Read and E. Rezayi. Quasiholes and fermionic zero modes of paired fractional quantum hall states: The mechanism for non-abelian statistics. *Phys. Rev. B* **54**, 16864 (1996), 1996.
- [95] N. Read and E. Rezayi. Beyond paired quantum hall states: Parafermions and incompressible states in the first excited landau level. *Phys. Rev. B* **59**, 8084, 1999.
- [96] N. Regnault and B. A. Bernevig. Fractional chern insulator. *Phys. Rev. X* **1**, 021014, 2011.
- [97] N. Regnault and Th. Jolicoeur. Quantum hall fractions in rotating bose-einstein condensates. *Phys. Rev. Lett.* **91**, 030402, 2003.
- [98] R. Resta. Berry phase in electronic wavefunctions. *Lecture Notes, Università di Trieste*, 1996.
- [99] E. H. Rezayi, N. Read, and N. R. Cooper. Incompressible liquid state of rapidly-rotating bosons at filling factor  $3/2$ . *Phys. Rev. Lett.* **95**, 160404, 2005.
- [100] V. Schweikhard S. Tung and E. A. Cornell. Observation of vortex pinning in bose-einstein condensates. *Phys. Rev. Lett.* **97** 240402, 2006.

- [101] S. Das Sarma, M. Freedman, and C. Nayak. Topologically protected qubits from a possible non-abelian fractional quantum hall state. *Phys. Rev. Lett.* **94**, 166802, 2005.
- [102] B. Scharfenberger, R. Thomale, and M. Greiter. Fractional spin liquid heirarchy for spin  $s$  antiferromagnets. *Phys. Rev. B* **84**, 140404, 2011.
- [103] Darrell F. Schroeter, Eliot Kapit, Ronny Thomale, and Martin Greiter. Spin hamiltonian for which the chiral spin liquid is the exact ground state. *Phys. Rev. Lett.* **99**, 097202, 2007.
- [104] V. Schweikhard, I. Coddington, P. Engels, V. P. Morgendorff, and E. A. Cornell. Rapidly rotating bose-einstein condensates in and near the lowest landau level. *Phys. Rev. Lett.* **92**, 040404, 2004.
- [105] P. Shor. *Proceedings of the 35th Annual Symposium on Foundations of Computer Science*, pg. 124134. IEEE Computer Society, Los Alamitos, CA, USA, 1994.
- [106] S. H. Simon, N. E. Bonesteel, M. H. Freedman, N. Petrovic, and L. Hormozi. Topological quantum computing with only one mobile quasiparticle. *Phys. Rev. Lett.* **96**, 070503, 2006.
- [107] S. H. Simon, E. H. Rezayi, N. R. Cooper, and I. Berdnikov. Construction of a paired wave function for spinless electrons at filling fraction  $\nu=2/5$ . *Phys. Rev. B* **75**, 075317, 2007.
- [108] A. S. Sorensen, E. Demler, and M. D. Lukin. Fractional quantum hall states of atoms in optical lattices. *Phys. Rev. Lett.* **94**, 086803, 2005.
- [109] I. B. Spielman. Raman processes and effective gauge potentials. *Phys. Rev. A* **79** 063613, 2009.
- [110] A. Stern. Quantum hall fluid of vortices in a two-dimensional array of josephson junctions. *Phys. Rev. B* **50**, 10092, 1994.
- [111] M. Storni and R. H. Morf. Localized quasiholes and the majorana fermion in fractional quantum hall state at  $\nu=5/2$  via direct diagonalization. *Phys. Rev. B* **83**, 195306, 2011.
- [112] K. Sun, Z. Gu, H. Katsura, and S. Das Sarma. Nearly flatbands with non-trivial topology. *Phys. Rev. Lett.* **106**, 236803, 2012.

- [113] E. Tang, J.-W. Mei, and X.-G. Wen. High temperature fractional quantum hall states. *Phys. Rev. Lett.* **106**, 236802, 2011.
- [114] B. Juliá-Díaz *et al.* Strongly correlated states of a cold atomic gas from geometric gauge fields. *Phys. Rev. A* **84**, 053605, 2011.
- [115] C. Weitenberg *et al.* Single-spin addressing in an atomic mott insulator. *Nature* **471**, 319, 2011.
- [116] L. B. Ioffe *et al.* Topologically protected quantum bits from josephson junction arrays. *Nature* **415**, 503, 2002.
- [117] L. Jiang *et al.* Anyonic interferometry and protected memories in atomic spin lattices. *Nat. Phys.* **4**, 482, 2008.
- [118] M. Gracjar *et al.* Direct josephson coupling between superconducting flux qubits. *Phys. Rev. B* **72**, 020503, 2005.
- [119] M. König *et al.* Direct observation of the aharonov-casher phase. *Phys. Rev. Lett.* **96**, 076804, 2006.
- [120] R. A. Williams *et al.* Dynamic optical lattices: two-dimensional rotating and accordion lattices for ultracold atoms. *Opt. Express* **16**, 16977, 2008.
- [121] S. An *et al.* Braiding of abelian and non-abelian anyons in the fractional quantum hall effect. *arXiv:1112.3400*, 2011.
- [122] X.-C. Yao *et al.* Experimental demonstration of topological error correction. *Nature* **482**, 489, 2012.
- [123] R. Thomale, E. Kapit, D. F. Schroeter, and M. Greiter. Parent hamiltonian for the chiral spin liquid. *Phys. Rev. B* **80**, 104406, 2009.
- [124] D. J. Thouless. Theory of the quantized hall effect. *Surface Science* **142**, 147, 1984.
- [125] C. Töke, N. Regnault, and J. K. Jain. Nature of excitations of the 5/2 fractional quantum hall effect. *Phys. Rev. Lett.* **98**, 036806, 2007.
- [126] Y. Tserkovnyak and S. H. Simon. Monte carlo evaluation of non-abelian statistics. *Phys. Rev. Lett.* **90**, 016802, 2003.

- [127] R. O. Umucalilar and I. Carusotto. Artificial gauge field for photons in coupled cavity arrays. *Phys. Rev. A* **84**, 043804, 2011.
- [128] R. O. Umucalilar and E. J. Mueller. Fractional quantum hall states in the vicinity of mott plateaus. *Phys. Rev. A* **81**, 053628, 2010.
- [129] R. O. Umucalilar, H. Zhai, and M. Oktel. Trapped fermi gases in rotating optical lattices: Realization and detection of the topological hofstadter insulator. *Phys. Rev. Lett.* **100**, 070402, 2008.
- [130] K. v. Klitzing, G. Dorda, and M. Pepper. New method for high-accuracy determination of the fine-structure constant based on quantized hall resistance. *Phys. Rev. Lett.* **45**, 494, 1980.
- [131] H. S. J. van der Zant, W. J. Elion, L. J. Geerligs, and J. E. Mooij. Quantum phase transitions in two dimensions: Experiments in josephson-junction arrays. *Phys. Rev. B* **54**, 10081, 1996.
- [132] Y.-F. Wang, Z.-G. Gu, C.-D. Gong, and D. N. Sheng. Fractional quantum hall effect of hard-core bosons in topological flat bands. *Phys. Rev. Lett.* **107**, 146803, 2011.
- [133] X. G. Wen, E. Dagotto, and E. Fradkin. Anyons on a torus. *Phys. Rev. B* **42**, 6110, 1990.
- [134] X. G. Wen and Q. Niu. Ground-state degeneracy of the fractional quantum hall states in the presence of a random potential and on high-genus riemann surfaces. *Phys. Rev. B* **41**, 9377, 1990.
- [135] R. L. Willett, L. N. Pfeiffer, and K. W. West. Alternation and interchange of  $e/4$  and  $e/2$  period interference oscillations consistent with filling factor  $5/2$  non-abelian quasiparticles. *Phys. Rev. B* **82**, 205301, 2010.
- [136] R. A. Williams, S. Al-Assam, and C. J. Foot. Observation of vortex nucleation in a rotating two-dimensional lattice of bose-einstein condensates. *Phys. Rev. Lett.* **104**, 050404, 2010.
- [137] D. Xiao, M.-C. Chang, and Q. Niu. Berry phase effects on electronic properties. *Rev. Mod. Phys.* **82**, 1959, 2010.
- [138] A. Yacoby, T. A. Fulton, H. F. Hess, L. N. Pfeiffer, and K. W. West. Compressibility images of the quantum hall state. *Physica E* **9**, 40, 2001.

- [139] H. Yao and S. A. Kivelson. Exact chiral spin liquid with non-abelian anyons. *Phys. Rev. Lett.* **99**, 247203, 2007.
- [140] F. Yoshihara, K. Harrabi, A. O. Niskanen, Y. Nakamura, and J. S. Tsai. Decoherence of flux qubits due to  $1/f$  flux noise. *Phys. Rev. Lett.* **97**, 167001, 2006.
- [141] D. Yoshioka. *The Quantum Hall Effect*. Springer-Verlag, 1998.
- [142] C. Zhang, V. W. Scarola, S. Tewari, and S. Das Sarma. Anyonic braiding in optical lattices. *PNAS* **104**, 18415, 2007.
- [143] Q. Zhou and T.-L. Ho. Universal thermometry for quantum simulation. *Phys. Rev. Lett.* **106**, 225301, 2011.
- [144] O. S. Zozulya, M. Haque, K. Schoutens, and E. H. Rezayi. Bipartite entanglement entropy in fractional quantum hall states. *Phys. Rev. B* **76**, 125310, 2007.